environments

IMPACT FACTOR 3.7

CITESCORE 5.7

Systematic Review

Niobium-Based Catalysts in Advanced Oxidation Processes: A Systematic Review of Mechanisms, Material Engineering, and Environmental Applications

Michel Z. Fidelis, Julia Faria, William Santacruz, Thays S. Lima, Giane G. Lenzi and Artur J. Motheo

Special Issue

Advanced Research on Micropollutants in Water, 2nd Edition

Edited by

Dr. Cátia Graça

MDPI

https://doi.org/10.3390/environments12090311

environments

MDPI

Systematic Review

Niobium-Based Catalysts in Advanced Oxidation Processes: A Systematic Review of Mechanisms, Material Engineering, and Environmental Applications

Michel Z. Fidelis [1,*], Julia Faria [1], William Santacruz [1], Thays S. Lima [1], Giane G. Lenzi [2] and Artur J. Motheo [1]

[1] São Carlos Institute of Chemistry, University of São Paulo (USP), São Carlos CEP 13566-590, SP, Brazil
[2] Department of Chemical Engineering, Federal Technological University of Paraná (UTFPR), Ponta Grossa CEP 84017-220, PR, Brazil
* Correspondence: michelmzzf@usp.br

Abstract

Water contamination by emerging pollutants poses a significant environmental challenge, demanding innovative treatment technologies beyond conventional methods. Advanced oxidation processes (AOPs) utilizing niobium-based catalysts, particularly niobium oxide (Nb_2O_5) and its modified forms, are prominent due to their high chemical stability, effective reactive oxygen species (ROS) generation, and versatility. This review systematically examines recent advancements in Nb_2O_5-based catalysts across various AOPs, including heterogeneous photocatalysis, electrocatalysis, and Fenton-like reactions, highlighting their mechanisms, material modifications, and performance. Following PRISMA and InOrdinatio guidelines, 381 papers were selected for this synthesis. The main findings indicate that niobium incorporation enhances pollutant degradation by extending light absorption, reducing electron–hole recombination, and increasing ROS generation. Structural modifications such as crystalline phase tuning, defect engineering, and the formation of heterostructures further amplify catalytic efficiency and stability. These catalysts demonstrate considerable potential for water treatment, effectively degrading a broad range of persistent contaminants such as dyes, pharmaceuticals, pesticides, and personal care products. This review underscores the environmental benefits and practical relevance of Nb_2O_5-based systems, identifying critical areas for future research to advance sustainable water remediation technologies.

Keywords: niobium; Nb_2O_5; emerging contaminants; pollutant removal; heterostructures

Academic Editor: Cátia Graça

Received: 30 July 2025
Revised: 29 August 2025
Accepted: 1 September 2025
Published: 4 September 2025

Citation: Fidelis, M.Z.; Faria, J.; Santacruz, W.; Lima, T.S.; Lenzi, G.G.; Motheo, A.J. Niobium-Based Catalysts in Advanced Oxidation Processes: A Systematic Review of Mechanisms, Material Engineering, and Environmental Applications. *Environments* **2025**, *12*, 311. https://doi.org/10.3390/environments12090311

1. Introduction

A safe and reliable water supply remains unattainable for a significant segment of the global population. Nearly 30% of humanity lacks access to safely managed drinking-water services, and approximately 1.7 billion people are deprived of basic sanitation facilities [1]. Unsafe water and inadequate sanitation contribute to an estimated 505,000 diarrheal deaths annually, predominantly affecting children under five [2]. Accelerated urbanization and industrialization have driven a 20–25% increase in global water demand since 2000, further stressing limited resources and underscoring the urgent need for advanced treatment technologies [3].

Emerging contaminants such as pharmaceuticals, personal-care products, and industrial chemicals are now routinely detected in surface and groundwater at concentrations

ranging from nanograms to micrograms per liter. More than 900 distinct pharmaceutical compounds, including antibiotics and hormones, have been quantified in aquatic environments, raising concerns over ecological toxicity and antibiotic resistance [4]. Conventional treatment processes typically remove fewer than 45% of these micropollutants, driving rapid growth in the advanced oxidation technologies market, which expanded from USD 5.4 billion in 2025 to a projected USD 7.4 billion by 2032 [5].

Advanced Oxidation Processes (AOPs) generate a broad spectrum of reactive oxygen and chlorine species, such as hydroxyl radicals ($^{\bullet}OH$), superoxide radicals ($O_2^{\bullet-}$), singlet oxygen ($^1O_2$), and ozone (O_3), which mineralize recalcitrant organic compounds and inactivate pathogens in wastewater systems [6,7].

Advanced Oxidation Processes (AOPs) are broadly defined as water treatment technologies based on the in situ generation of highly reactive chemical species, most notably the hydroxyl radical (OH), which mineralize recalcitrant organic compounds and inactivate pathogens in wastewater systems. These processes can be fundamentally categorized into two main groups based on their primary activation mechanism: non-photochemical and photochemical processes. This distinction is crucial as it directly impacts operational requirements, energy consumption, and suitability for specific wastewater matrices.

Non-photochemical AOPs generate radicals through chemical or electrical means without the requirement of light. This category includes processes such as the classic Fenton reaction, which uses ferrous ions (Fe^{2+}) to catalytically decompose hydrogen peroxide (H_2O_2) [8]; ozonation in the absence of light [9]; and electrochemical oxidation [10], where radicals are generated at the surface of high-overpotential anodes. These methods are particularly robust for treating highly turbid or colored effluents where light penetration is a significant barrier.

Photochemical AOPs, conversely, utilize photons from either artificial lamps or solar radiation to initiate or enhance the generation of reactive species. This group encompasses heterogeneous photocatalysis [11], where a semiconductor like Nb_2O_5 is excited by light to produce electron-hole pairs; the photo-Fenton process, which uses light to accelerate the regeneration of the Fe^{2+} catalyst; and UV-driven processes like UV/H_2O_2 or UV/O_3. The degradation efficiency depends on the nature of the pollutant and its reactivity with these oxidative species. AOPs encompass methods such as electrochemical Fenton, and each of them can be tailored to specific applications.

Recent advancements in AOPs have highlighted the role of novel materials in enhancing catalytic efficiency and operational stability [12]. Among these, niobium-based compounds, particularly niobium oxide (Nb_2O_5) and niobium-doped catalysts, have gained increasing attention due to their high chemical stability, efficient light absorption, and tunable electronic properties. Moreover, niobium oxide shares many structural and electronic characteristics with titanium dioxide while exhibiting greater stability under acidic and oxidative conditions, which reduces catalyst deactivation. Brazil holds roughly 95% of the world's known niobium reserves, giving Nb_2O_5 a cost advantage over more scarce or expensive materials. The adjustable band gap and energy-level positions of niobium-doped systems enable visible-light absorption and suppress electron–hole recombination in a manner analogous to TiO_2 modifications [13,14]. These attributes make niobium a versatile material for coupling with AOPs, especially in photocatalytic and electrochemical processes.

While several reviews exist on AOPs and Nb-based materials, the novelty of this work lies in its systematic methodology. By employing Methodi Ordinatio, a multicriteria decision analysis framework, and the PRISMA method, we provide a quantitative ranking of the literature based on scientific impact, offering a structured and prioritized synthesis of the most significant research in the field. The prospects for Nb_2O_5-based catalysts are promising, particularly in the development of solar-driven, sustainable water

treatment systems. Future research is expected to focus on the rational design of advanced heterostructures with tailored electronic properties, the integration of these catalysts into continuous-flow reactors, and the use of computational modeling to accelerate material discovery. This review aims to synthesize the current state of knowledge to guide these future endeavors.

2. Scientometrics

In recent years, the scientific literature has grown exponentially in both volume and diversity, posing significant challenges for researchers in identifying and organizing relevant articles for comprehensive bibliographic reviews. This growth necessitates efficient tools to evaluate the relevance of academic works, particularly in emerging fields such as the application of niobium-based materials in environmental contaminant treatment. To address this need, Methodi Ordinatio, a widely recognized multicriteria decision analysis (MCDA) methodology, was developed to facilitate the selection of articles by considering publication date, citation count, and journal impact metrics. This structured and transparent approach aids in building relevant bibliographic portfolios.

The updated version, Methodi Ordinatio 2.0, offers greater flexibility and precision in calculating the InOrdinatio index, enabling researchers to fine-tune the weights assigned to each criterion according to their relevance to the specific research topic [15]. Figure 1 outlines the seven phases of Methodi Ordinatio, ranging from defining the search strategy to applying the InOrdinatio index for ranking articles by scientific relevance. Furthermore, the tools Finder and RankIn automate data collection and index application, improving reliability while reducing the time required for the process.

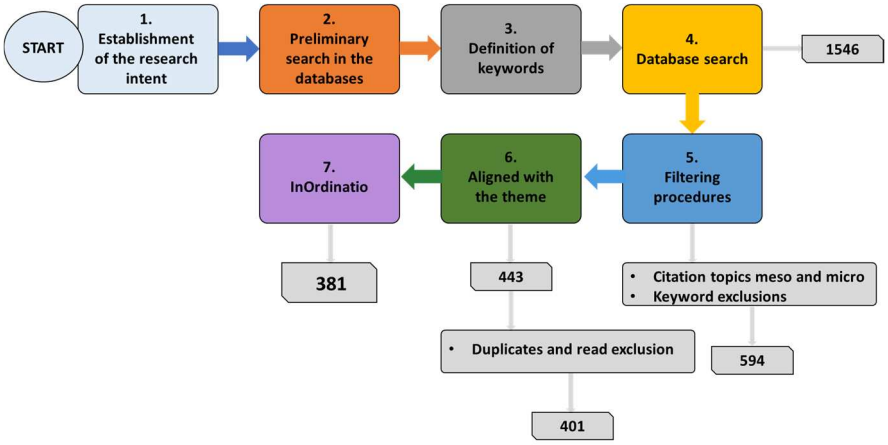

Figure 1. Seven phases of methodi Ordinatio.

Methodi Ordinatio has been extensively discussed in a wide range of journals, solidifying its role as a framework for knowledge review. This approach systematically organizes information according to specific boundaries, thematic insights, and the underlying motivations of researchers, while referencing the contributions of Edward and Ponpandi [16], Zanata et al. [17], da Silva et al. [18], Batista et al. [19], Da Silva et al. [20], Hernández-Contreras et al. [21], Yoshino et al. [22], Zarhri et al. [23], Carvalho et al. [24], Barros et al. [25], Sierdovski et al. [26], Oliveira et al. [27], Regatieri et al. [28], Sarmento et al. [29], Lizot et al. [30], Bail et al. [31], Rosa et al. [32], and Wang et al. [33].

This systematic review was also conducted and reported in accordance with the Preferred Reporting Items for Systematic Reviews and Meta-analyses (PRISMA) 2020 statement, as can be seen in Supplementary File S1, in order to adhere to the guidelines of transparency and validity [34]. The review protocol was not registered in a public repository.

Systematic Search Methodology

Step 1—Establishing Research Intent

This study aimed to construct a bibliographic portfolio from scientific articles focused on the application of niobium in the degradation or removal of emerging contaminants through AOPs.

Steps 2, 3, and 4—Database Selection and Initial Search

A comprehensive search was conducted across three major academic databases: ScienceDirect, Web of Science (WoS), and Scopus. The WoS was selected as the primary source due to its extensive collection of publications relevant to the keywords used, its capability to filter by meso and micro topics (facilitating article selection), and the consistency of its search results. Additionally, most articles retrieved from WoS were also present in the other databases. The exclusion of "nitrobenzene" was necessary due to multiple occurrences of the abbreviation "nb" being misinterpreted in the search results. This query yielded a total of 1546 articles.

For the final search in WoS, the advanced search system was employed using the query builder with the following input:

"((niobi OR nb2o5) AND (removal OR degradation OR AOP) NOT (nitrobenzene))—Articles"*

Steps 5 and 6—Filtering Procedures

The retrieved articles underwent filtering using the following criteria:

"((niobi OR nb2o5) AND (removal OR degradation OR AOP) NOT (nitrobenzene))—Articles—Citation topics Meso 2.74 Photocatalysts 2.90 Water Treatment 2.62 Electrochemistry 2.41 Catalysts—Citation topics micro EXLCUDE Oxigen reduction reaction Supercapacitor Electrochromism Litium-ion Battery Litium-sulfur Batteries Adsorption"*

This systematic approach facilitated the selection of the most recent and impactful studies within the researched themes, focusing on AOPs and excluding unrelated applications. Despite this, the dataset still contained several duplicates and irrelevant articles. A secondary filtering step was performed to remove duplicates and exclude articles misaligned with the study's objectives.

The publication period considered was all years. After these filtering procedures, the dataset was reduced to 401 articles.

Step 7—Application of the InOrdinatio Index

The filtered articles were ranked based on their scientific relevance using the InOrdinatio index, calculated as per Equation (1) proposed by [34]. This methodology integrates factors such as journal impact factor (*IF*), citation count, and publication year, enabling a systematic ranking of articles according to scientific criteria.

$$InOrdinatio = \{(\Delta^* IF) - [\lambda^* (ResearchYear - PubYear)/HalfLlife] + \Omega^* \sum Ci/[(ResearchYear + 1) - PubYear] \quad (1)$$

where

- *IF* is the impact factor (or estimated CiteScore if *IF* is unavailable);
- Δ is the weight (0–10) assigned to the importance of *IF*;
- λ is the weight (0–10) assigned to the relevance of publication year;
- Ω is the weight (0–10) assigned to the annual average citation count;
- *ResearchYear* is the year of analysis;
- *PubYear* is the year of publication;
- *HalfLife* is the journal's cited half-life;
- C_i is the total number of citations retrieved from Google Scholar.

For this systematic review, the selected values were $\Delta = 4$, $\lambda = 9$, and $\Omega = 6$, reflecting the novelty of the research topic. Greater emphasis was placed on publication year to account for the emerging nature of the field, while *IF* was weighted moderately to prevent

excessive disparities in scores. Articles with negative InOrdinatio scores were excluded, resulting in a final selection of 381 articles.

To facilitate the visualization of the articles excluded during the filtering steps, the PRISMAflow diagram [34] was used (Figure 2). The diagram demonstrates that the PRISMA filtering procedures were similar to those employed in the InOrdinatio method. To uphold reliability and align with PRISMA guidelines, all authors actively engaged in every phase of the process of evaluating the selected articles.

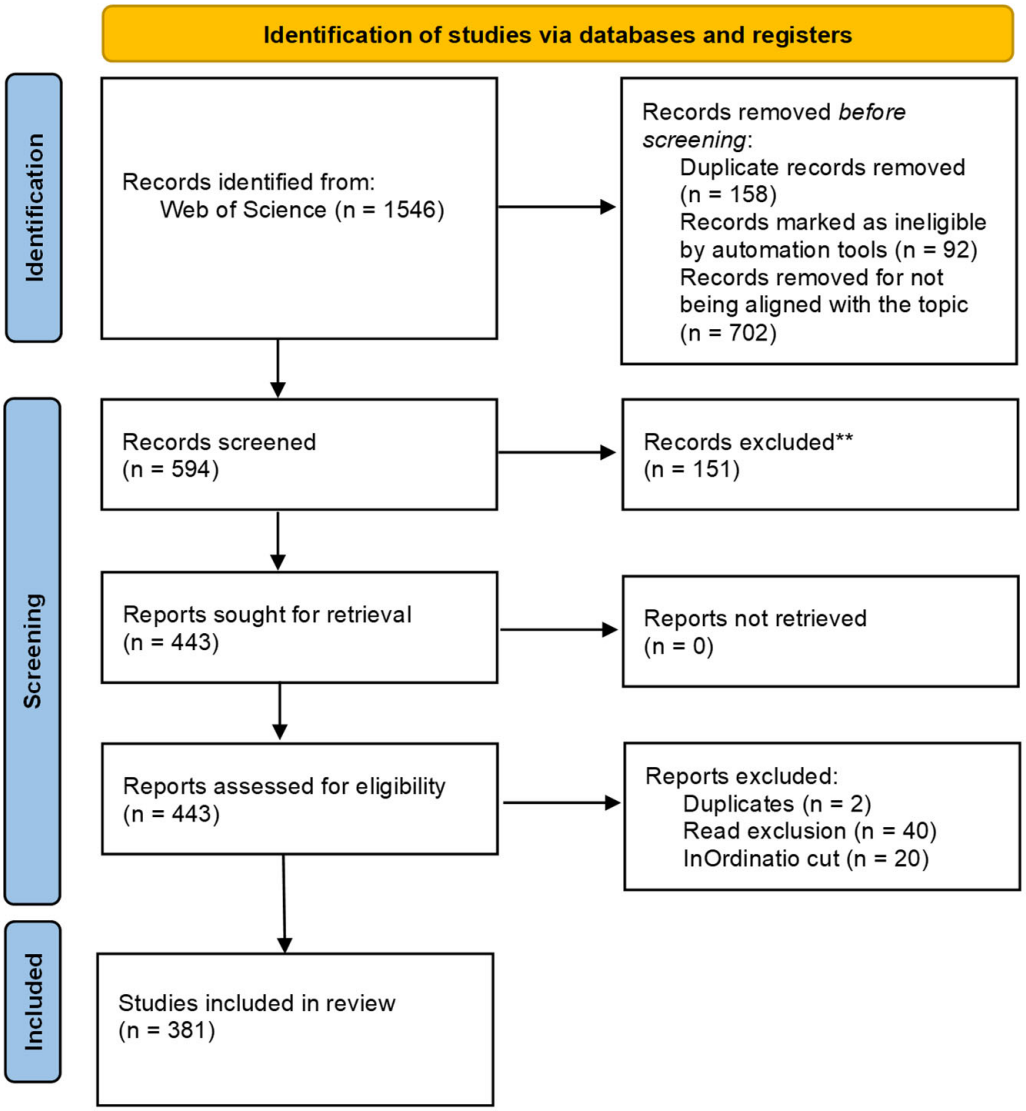

Figure 2. PRISMA flow diagram for niobium in the degradation or removal of emerging contaminants through AOPs' filtering process. ** Records excluded after manual verification due to lack of alignment with the topic.

2.1. Statistical Analysis and Visualization

Based on the bibliographic search results, the software tools CiteSpace (CiteSpace Basic) and VOSviewer (version 1.4.0) were used for visual analysis with 1-year increments. The flowchart of this bibliometric analysis is shown in Figure 3.

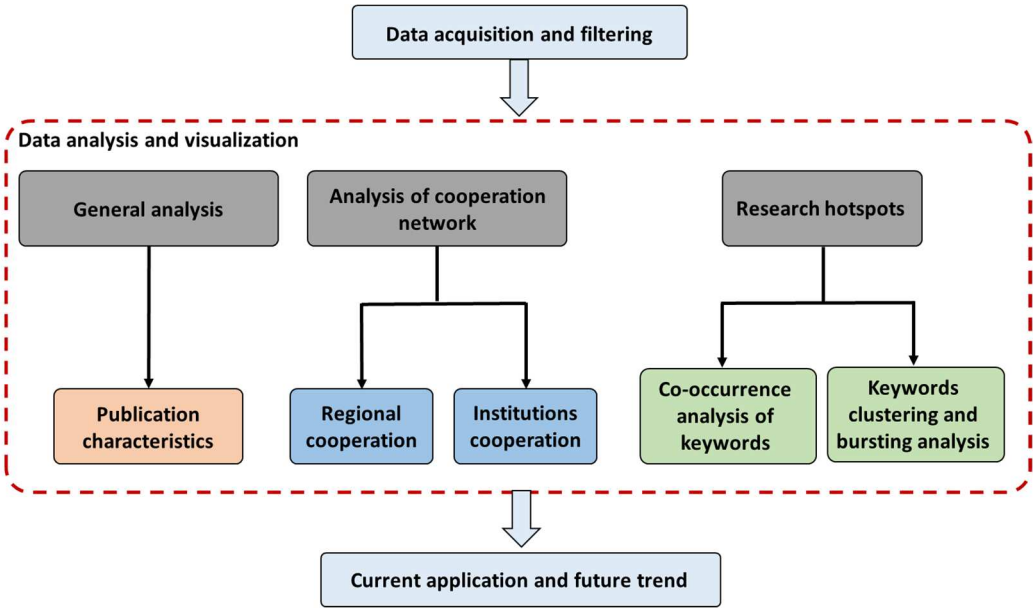

Figure 3. Flowchart of bibliometric analysis.

2.1.1. Publication Characteristics

The annual publication count provides a valuable indicator for evaluating the scientific development and visibility of a given research area. As shown in Figure 4, research activity regarding niobium applications in AOPs for emerging contaminant degradation has grown steadily from 1996 to 2023. This trend suggests a gradual consolidation of this topic within the environmental catalysis field. However, the absence of an exponential growth phase, typical in fast-developing technologies, may reflect the specialized nature of niobium chemistry, the relatively limited number of research groups dedicated to this material, or challenges in its processing and integration into catalytic systems.

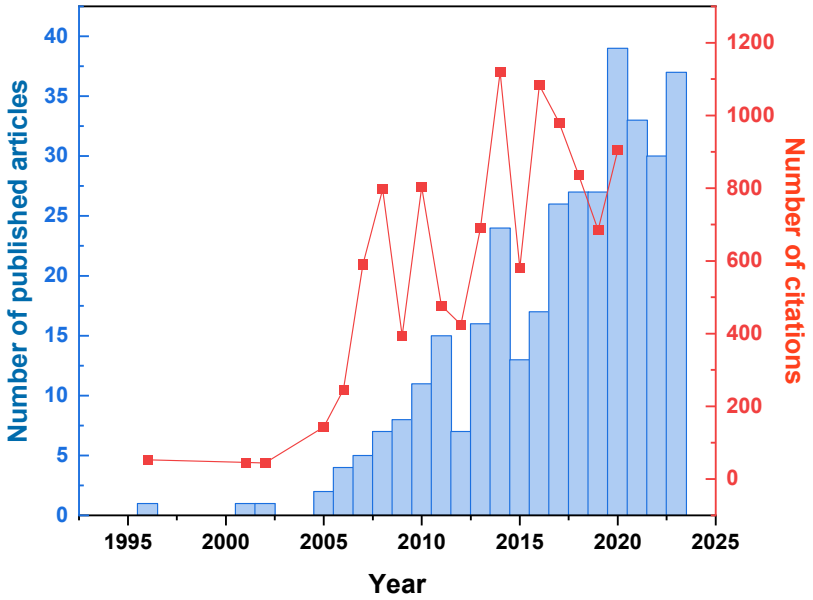

Figure 4. Number of publications on niobium application in advanced oxidation processes for the degradation of emerging contaminants per year from 1996 to 2023.

This pattern may reflect both the emerging status of niobium-based materials and certain structural barriers in the field. While niobium offers compelling properties such as stability in acidic media, tunable electronic structure, and compatibility with visible-

light-active semiconductors, its use remains predominantly confined to academic research. This could be partially attributed to the lack of standardized methodologies for synthesis and testing, which makes it difficult to compare catalytic performance across studies or to define clear design criteria for material optimization.

In addition, the citation profile of the literature remains relatively modest when compared to more established AOP themes, such as those involving TiO_2 or Fenton-based systems. The limited number of internationally visible review papers and collaborative networks may contribute to this dynamic. Despite this, the steady growth in both publications and citations over recent years suggests that niobium-based research is gaining traction and could benefit from coordinated strategies to enhance its scientific impact.

Figure 5 presents a statistical graph of the top ten subject areas or research directions related to the study topic, based on the WoS search results. The number of articles published within each subject area is indicated. It is evident that the research topic has been predominantly explored in the fields of Physical Chemistry (112 articles), Multidisciplinary Materials Science (88 articles), and Multidisciplinary Chemistry (45 articles). Additionally, a notable cluster comprising Environmental Engineering, Chemistry, and Environmental Sciences accounts for a significant portion of the research, with 104 articles.

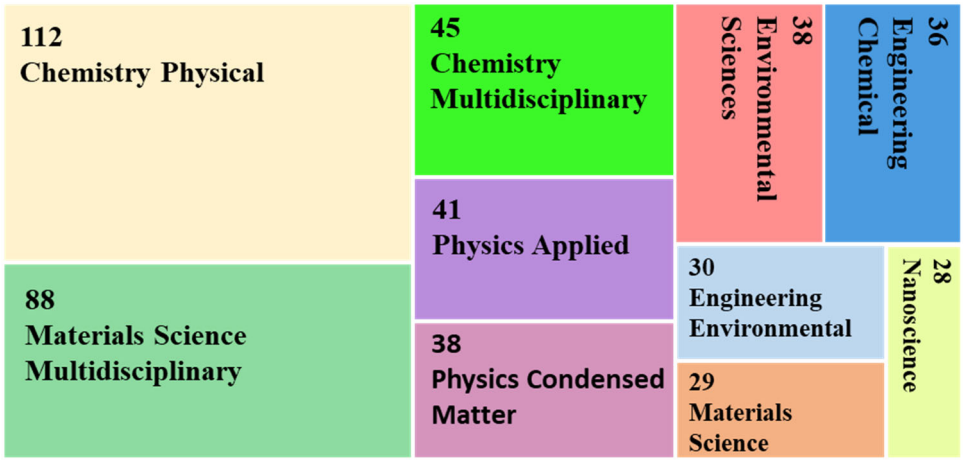

Figure 5. Number of publications on niobium application in AOPs for the degradation of emerging contaminants in top ten subject areas.

Within these fields, four key topics stand out, representing over 95% of the research base, as illustrated in Figure 6. These topics include Photocatalysis (~70%), Catalysts (~16%), Water Treatment (~12%), and Electrochemistry (~1%).

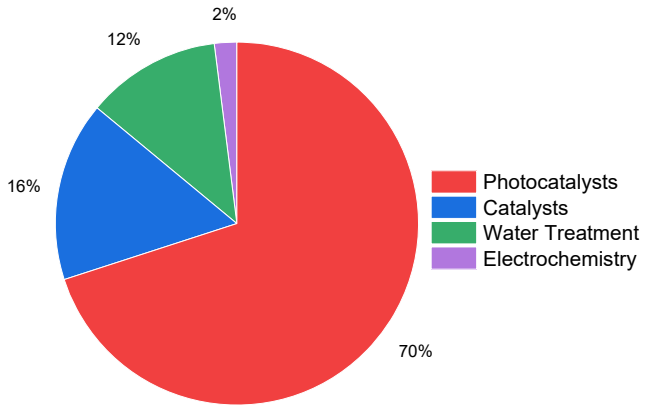

Figure 6. Key topics of the research base.

2.1.2. Analysis of Cooperation Network

Through the analysis of the cooperation network, it is possible to trace the communication trajectory of scientific research activities, including interactions within and between countries, regions, institutions, and research groups. This approach highlights collaborative trends and provides an overview of knowledge dissemination patterns.

Research Contributions from Different Countries and Regions

By performing a statistical analysis of research articles published across different countries and regions, it becomes possible to evaluate the scientific investment and academic influence of each location in specific research fields. The results are shown in Figure 7, which identifies 20 nodes and 75 connections in the regional cooperation network diagram. This indicates that 20 countries or regions have contributed to the field.

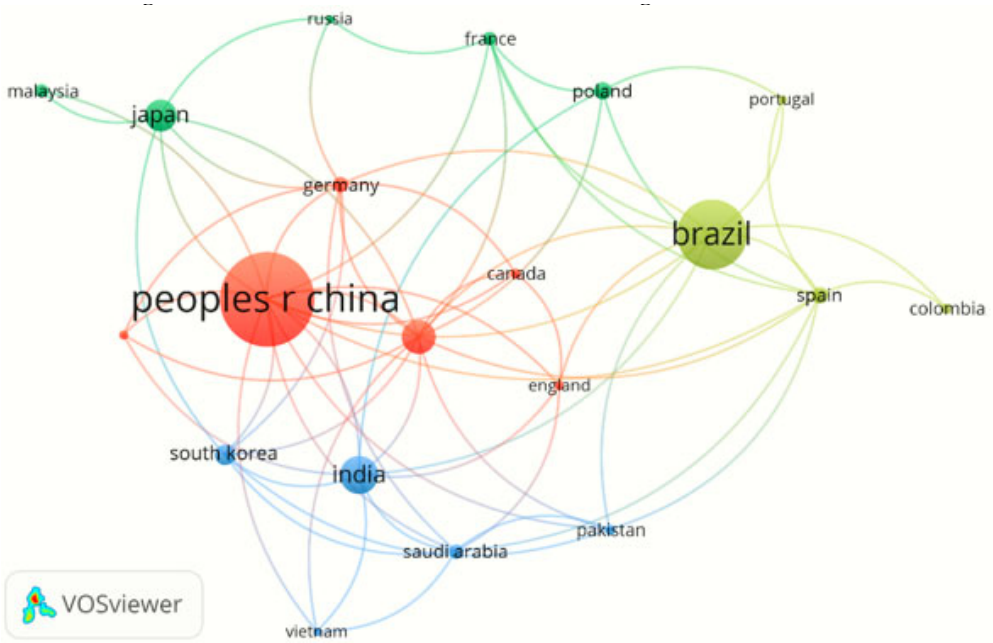

Figure 7. Network map of national cooperation focusing on AOPs with niobium for decontamination.

The publication statistics are summarized in Table 1, revealing that China leads with 201 articles, reflecting substantial global recognition and impact in this field. Despite being an emerging economy, Brazil follows in second place with 132 publications, a noteworthy position that appears to be closely tied to the country's significant niobium reserves and the growing interest in discovering new applications for this metal. Brazil is home to some of the largest niobium deposits worldwide, contributing approximately 90% of global production and holding 95% of known reserves. Its principal Nb producer, Companhia Brasileira de Metalurgia e Mineração (CBMM), has prioritized research partnerships with universities and research institutes, fostering innovative studies and accelerating scientific output.

The leading positions of China and Brazil in publications regarding niobium-based catalysts highlight the global strategic importance of this resource, particularly considering that Brazil holds approximately 95% of the world's known niobium reserves. Enhanced scientific collaboration between these two nations could significantly advance the development of sustainable technologies through technical/scientific knowledge exchange, joint researcher training initiatives, and cooperative development of innovative and practical solutions for global environmental challenges.

Table 1. Statistics on the number of national and regional publications and citations in the field.

Countries/Regions	Number of Publications	%
China	201	33.8
Brazil	132	22.2
India	56	9.4
USA	50	8.4
Japan	46	7.7
South Korea	25	4.2
Poland	19	3.1
Spain	18	3.0
Germany	17	2.8
Saudi Arabia	15	2.5

Additional contributors include India (56 articles), the USA (50 articles), and Japan (46 articles). Although they publish fewer articles overall, many of these nations also demonstrate strong citation metrics, indicating the relevance of their research. However, Brazil's early involvement and strategic collaborations have propelled it to a leading position in both the volume and impact of publications on niobium-based materials.

Institution Cooperation

Table 2 presents the bibliometric analysis of institutional collaboration in research on the use of niobium for the treatment of emerging contaminants. For this bibliometric analysis, the 25 institutions with the highest number of publications were considered based on the results of the InOrdinatio method.

Table 2. Institutions with more publications in the field.

Affiliations	Publication Count
Universidade Estadual De Maringa (Brazil)	25
Chinese Academy Of Sciences (China)	23
Universidade De Sao Paulo (Brazil)	23
Universidade Tecnologica Federal Do Parana (Brazil)	19
Universidade Federal De Sao Carlos (Brazil)	16
Universidade Federal De Minas Gerais (Brazil)	15
Centre National De La Recherche Scientifique (France)	13
Adam Mickiewicz University (Poland)	11
Nanjing University (China)	11
Universidade Estadual Paulista (Brazil)	11
Universidade Federal De Lavras (Brazil)	11
National Institute For Materials Science (Japan)	10
Empresa Brasileira De Pesquisa Agropecuaria (Brazil)	9
Jiangsu University (China)	9
Jilin University (China)	9
United States Department Of Energy (DOE) (USA)	9
Universidade Federal De Pelotas (Brazil)	9
Universidade Federal Do Rio Grande Do Norte (Brazil)	9
Consejo Superior De Investigaciones Cientificas (Spain)	8
Universidade Federal Do Rio Grande Do Sul (Brazil)	8
Wuhan University Of Technology (China)	8
Zhengzhou University (China)	8
East China University Of Science Technology (China)	7
Universidade De Brasilia (Brazil)	7
Universidade Estadual De Campinas (Brazil)	7

The Figure 8 reveals distinct patterns of interaction. Brazilian institutions demonstrate a significant level of cohesion, marked by consistent collaborations among national universities and research centers. This synergy reflects a coordinated national effort to advance scientific and technological progress in the application of niobium in environmental technologies. Similarly, Chinese and Japanese institutions stand out as hubs of strong internal integration, indicating a strategic focus on research and development in this area. This structure highlights the priority given by these institutions to the study of niobium, particularly regarding its application in the treatment of emerging contaminants.

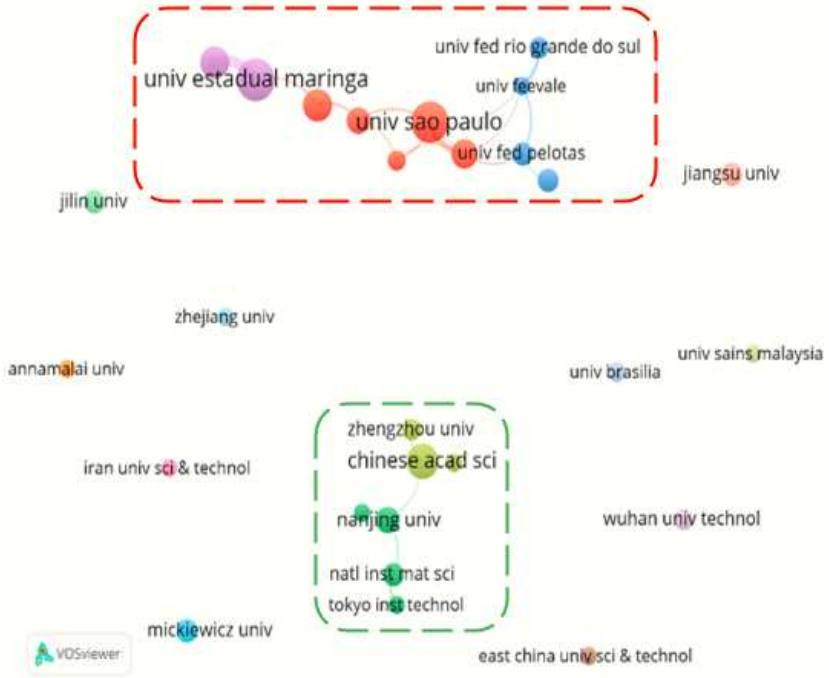

Figure 8. Cooperation relationships regarding AOPs with niobium for water decontamination. The universities enclosed by the red and green lines correspond to Brazilian and Chinese institutions, respectively.

However, unlike other widely investigated topics and more established materials, international collaborations in this field remain scarce. The analysis reveals limited interconnectivity among institutions from different countries, suggesting that transnational interactions are underexplored. This lack of global research networks may constrain scientific advancement in the field, while also presenting a significant opportunity to foster international collaborations. Promoting initiatives that integrate different regions and global institutions could accelerate the development of niobium-based technologies, driving innovative solutions for emerging contaminant treatment.

Co-Occurrence Analysis of Keywords and Research Hotspots

Figure 9 presents the co-occurrence network of keywords extracted from Web of Science publications on Nb_2O_5-based AOPs. Each node in the map represents a keyword, with node size proportional to its frequency and link thickness indicating co-occurrence strength. The most frequently occurring terms, such as photocatalysis, advanced oxidation processes, heterostructures, and nanostructures, highlight the community's foundational interest in charge-carrier dynamics, reactive oxygen species generation, and material design strategies aimed at improving catalytic efficiency.

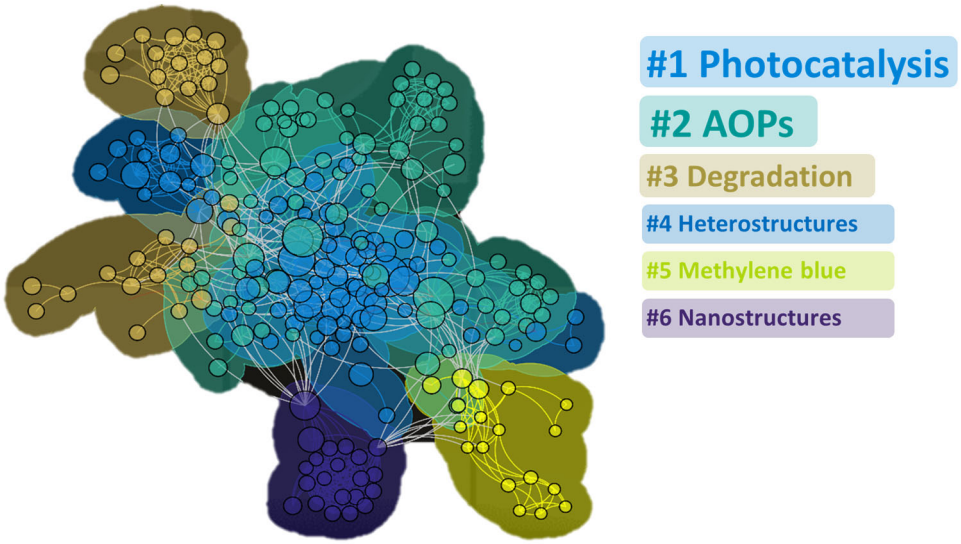

Figure 9. Keyword collaboration network for AOPs with niobium for water decontamination in WoS.

Over the last decade, research into ECs has evolved significantly, driven by advancements in analytical methods and growing awareness of the ecological and health impacts of these pollutants. Niobium-based materials, despite their underutilization relative to more established catalysts like TiO_2 and ZnO, have gained attention for their potential to address ECs in water systems. Keywords such as photocatalysis, AOPs, and degradation dominate the literature, reflecting the primary research directions in this field.

A cluster of keywords related to composite materials, including g-C_3N_4, graphene, and various metal oxides, demonstrates the emphasis on heterojunction and nanocomposite architectures that enhance light absorption and inhibit electron–hole recombination. Another set of terms, such as methylene blue, dyes, and pharmaceuticals, confirms that these model pollutants continue to serve as standard benchmarks for laboratory-scale evaluations, enabling consistent performance comparisons across different studies.

Terms associated with hybrid process integration, for example, photocatalytic ozonation, photoelectrocatalysis, and Fenton-like reactions, appear increasingly often and indicate a shift toward multifunctional treatment schemes. Researchers are combining photocatalytic methods with chemical oxidation pathways in order to achieve synergistic pollutant degradation and to address challenges posed by complex effluent matrices.

These emerging areas, mapped throughout the research, not only indicate current investigative trends but also highlight knowledge gaps that demand attention. Among these, the integration of technologies that employ renewable energy sources and the need to strengthen international cooperation stand out as key elements to accelerate the development of sustainable solutions in this field.

3. Nb_2O_5: An Overview

Niobium pentoxide has established itself as a transition metal oxide of high scientific and technological interest, driven by a unique combination of physicochemical properties. This material is distinguished by its exceptional chemical and thermal stability, remarkable corrosion resistance, non-toxicity, and relative abundance in Earth's crust [35,36]. Its relevance transcends the laboratory, serving as a crucial component in various high-technology industries, from the formulation of superalloys for the aerospace sector to the manufacturing of microelectronics. The true technological value of Nb_2O_5, however, lies not in a single superlative property but in its versatility as a "material platform". Its structural and electronic characteristics can be finely tuned to meet the demands of radically different applications, ranging from catalysis and energy storage to optical and biomedical

devices. This multifunctionality, intrinsically linked to its rich solid-state chemistry, makes Nb_2O_5 an object of continuous study and a promising candidate for future technological innovations [35–37].

The most striking structural feature of Nb_2O_5 is its complex polymorphism, with more than fifteen distinct crystalline phases identified, a central factor in understanding its functional behavior. The fundamental building block for most of these polymorphs is the distorted NbO_6 octahedra. The different crystal structures emerge from the various ways these octahedra interconnect, either by sharing vertices or edges, resulting in arrangements with different symmetries and properties [37]. The formation of a specific phase is strongly dependent on the synthesis conditions, particularly the heat treatment temperature, which allows for targeted phase engineering [35].

The sequence of thermally induced phase transformations is a well-documented and reproducible process, typically initiated from an amorphous phase. The amorphous material, obtained from uncalcined precursors or at very low temperatures, is characterized by the absence of long-range crystalline order and, frequently, by a high specific surface area, a highly desirable property for applications in heterogeneous catalysis. Upon heating, typically in the 300–500 °C range, crystallization into the pseudohexagonal phase (TT-Nb_2O_5) occurs. This phase is considered a metastable and less crystalline variant of the orthorhombic phase, often stabilized by impurities or structural defects, and its X-ray diffraction pattern is similar to that of the T phase, albeit with broader peaks [35,36]. By raising the temperature to the 550–750 °C range, the orthorhombic phase (T-Nb_2O_5) is formed. This is one of the most studied phases, possessing a unique open crystal structure described as a "room-and-pillar" arrangement, composed of NbO_6 and NbO_7 polyhedra that share vertices and edges. This particular architecture is fundamental to its remarkable high-speed ion intercalation properties. Finally, at temperatures above 900–1100 °C, the material converts to the monoclinic phase (H-Nb_2O_5), which is the most thermodynamically stable polymorph [11,37,38].

This predictable sequence of phase transitions (Amorphous → TT → T → H) represents more than a mere crystallographic observation; it constitutes a powerful "phase engineering" tool. Through precise control of the calcination temperature, it is possible to deliberately select a specific polymorph whose intrinsic properties are optimized for a given application. For example, a researcher seeking to develop a high-power battery anode would aim to obtain the T phase by performing calcination around 650 °C, while consciously avoiding temperatures above 900 °C that would lead to the less suitable H phase for this purpose. This control establishes a direct causal relationship between thermal processing, the resulting crystal structure, and, ultimately, the material's functionality, transforming heat treatment into a deterministic design step [11,39].

Nb_2O_5's chemical robustness is one of its most notable properties, exhibiting high stability in oxidizing atmospheres and corrosive acidic media, which distinguishes it from other metal oxides and broadens its field of application. A critical functional property, especially for catalysis, is its surface acidity. The material exhibits strong acidity, comprising both Brønsted acid sites (BASs), capable of donating protons and associated with surface hydroxyl groups in hydrated forms, and Lewis acid sites (LASs), which act as electron-pair acceptors and are associated with coordinatively unsaturated niobium cations (Nb^{5+}). In its hydrated form, its high acid strength ($H0 = -5.6$) classifies it as a "solid superacid", a characteristic that makes it an effective catalyst for a range of organic reactions, such as esterification, hydrolysis, and dehydration [35,36,40].

The electronic and optical properties of Nb_2O_5 are equally important. It possesses a high dielectric constant, making it valuable for the fabrication of capacitors, and a high refractive index, exploited in optical coatings. These characteristics contrast with its

intrinsically low electrical conductivity, which places it in the category of insulators or wide-bandgap semiconductors. The nature of the surface acidity is not static but can be dynamically modulated by the material's thermal history. Low-temperature and hydrated forms are rich in Brønsted sites. Heat treatment at higher temperatures promotes surface dehydroxylation, systematically removing hydroxyl groups and, consequently, the Brønsted sites. This process exposes a greater number of coordinatively unsaturated Nb^{5+} centers, which function as Lewis sites. This ability to tune not only the strength but also the type of predominant acidity offers a sophisticated mechanism for controlling selectivity in catalytic reactions, as different adsorption mechanisms and reaction pathways are favored by either Brønsted or Lewis acid sites [35,40].

The versatility of Nb_2O_5 is demonstrated by its successful application across a wide range of technological fields, consolidating its status as a material of high interest. In energy storage systems, Nb_2O_5 has emerged as an extremely promising anode material for high-power lithium-ion batteries [41]. The T and TT polymorphs exhibit a unique charge storage mechanism known as "intercalation pseudocapacitance". This process allows for the rapid insertion and extraction of lithium ions throughout the material's bulk, without the need for solid-state diffusion and without inducing a destructive phase transition. The result is an extraordinary rate performance, enabling ultrafast charging and discharging, and excellent cycling stability, in contrast to the slower, diffusion-limited mechanism observed in the H phase [41].

In the field of optics and smart devices, Nb_2O_5 is a key material for electrochromic applications, such as "smart windows", mirrors with variable reflectivity, and displays [42]. The operating principle is based on the reversible intercalation and deintercalation of ions (such as Li^+ or H^+) into its crystal structure under the application of an electrical potential. This process alters the population of electronic states in the material, modulating its optical absorption and allowing for dynamic control over its transparency. The TT phase, in particular, has demonstrated exceptional performance, with fast switching kinetics, high durability, and the unique ability to selectively modulate transmittance in the visible and near-infrared regions. Additionally, its high refractive index makes it an excellent material for anti-reflective coatings and other optical components [42,43].

Beyond these areas, Nb_2O_5 maintains its established role as a robust solid acid catalyst and a chemically stable support for other catalytically active phases in industrial processes [44]. Its high dielectric constant is exploited in microcapacitors, a fundamental application in microelectronics. More recently, growing interest has been directed toward the use of Nb_2O_5 in biomedical technologies. Its combination of excellent biocompatibility, chemical inertness, and corrosion resistance makes it an ideal candidate for drug delivery systems, biosensors, and as a coating for orthopedic and dental implants, where long-term stability in physiological environments is paramount [35].

4. Mechanisms of Action of Nb_2O_5

While TiO_2 remains the most widely utilized semiconductor in photocatalytic applications, Nb_2O_5 presents a unique combination of properties that make it a compelling material for environmental remediation. A meaningful comparison requires separating the material's physical characteristics from its intrinsic electronic structure. Properties such as surface area and porosity are fundamentally dependent on the synthesis methodology and are not inherent advantages of one material over the other; for a valid comparison, materials prepared under analogous conditions should be considered [40].

The key distinctions relevant to photocatalytic mechanisms lie in the electronic structure and chemical properties of the materials. The band gap of Nb_2O_5 is typically around 3.4 eV, slightly wider than that of anatase TiO_2 (≈3.2 eV). However, a more detailed anal-

ysis of the band edge positions reveals important trade-offs. The band edge potentials versus the Normal Hydrogen Electrode (NHE) at pH 7 are approximately −0.69 V (CB) and +2.71 V (VB) for Nb_2O_5, and approximately −0.5 V (CB) and +2.7 V (VB) for anatase TiO_2 [36,45].

These positions dictate the thermodynamic driving force for generating reactive oxygen species. For the reduction of molecular oxygen to the superoxide radical ($E_0(O_2/O_2^{\bullet-})$ = −0.33 V vs. NHE), the more negative conduction band of Nb_2O_5 provides a greater thermodynamic potential compared to TiO_2. Conversely, for the oxidation of water to hydroxyl radicals ($E_0(H_2O/^{\bullet}OH) \approx$ +2.3 V vs. NHE), the slightly more positive valence band of anatase TiO_2 offers a stronger driving force for hole-mediated oxidation [46]. Therefore, the primary advantages of Nb_2O_5 over TiO_2 lie not necessarily in its band positions, but rather in its distinct physicochemical properties. A key distinction is its superior chemical stability, as Nb_2O_5 exhibits greater robustness under the acidic and oxidative conditions common in AOPs, which reduces catalyst deactivation and leaching. Furthermore, its unique surface acidity, characterized by strong Lewis and Brønsted acid sites, allows it to interact with pollutants and oxidants like H_2O_2 in ways that TiO_2 cannot, opening up alternative catalytic pathways beyond direct ROS oxidation [47].

A comprehensive understanding of Nb_2O_5 photocatalytic mechanisms is crucial for optimizing its performance and expanding its applicability. Incomplete oxidation can produce transformation products that may be more persistent or toxic than the original contaminant. The fundamental process relies on the excitation of Nb_2O_5 under light irradiation, leading to electron–hole pair generation [11]. These charge carriers participate in redox reactions, where holes (h^+) in the VB oxidize organic pollutants, and electrons (e^-) in the CB contribute to the reduction of oxygen species, forming ROS such as hydroxyl radicals ($^{\bullet}OH$), superoxide radicals ($O_2^{\bullet-}$), and hydroperoxyl radicals ($^{\bullet}OOH$).

The oxidation mechanism in semiconductors during photocatalysis under UV irradiation has been previously discussed and reported in the literature [11,40,48]. In general, heterogeneous photocatalysis relies on exciting a semiconductor with solar or artificial light as long as the photon energy exceeds the band gap (the energy difference between the valence band and the conduction band), promoting an electron (e^-) from the VB to CB, creating a hole (h^+) in the VB (Equation (2)) [36]. These species (e^- and h^+) can trigger various oxidation and reduction reactions, producing highly oxidizing radicals such as $^{\bullet}OH$, $^{\bullet}OOH$, and $O_2^{\bullet-}$ which act on organic compounds [40,48,49].

Nb_2O_5 has a band gap ranging from 3.1 to 4.0 eV can be activated by near-UV light, much like TiO_2, which ranges from 3.0 to 3.2 eV [11,40,48,50,51]. In the VB, h^+ may directly oxidize organic molecules or react with hydroxide ions (OH^-) to form ($^{\bullet}OH$), while in the CB, e^- can reduce dissolved oxygen O_2 to form superoxide radicals ($O_2^{\bullet-}$) and, in subsequent steps, the ($^{\bullet}OOH$).

$$Nb_2O_5 + h\upsilon_{(UV)} \rightarrow Nb_2O_5(h^+_{(VB)} + e^-_{(CB)}) \quad (2)$$

After these species are formed, a series of both reduction and oxidation reactions can occur. The h^+ species in the VB can react in the presence of OH^-, usually derived from water molecules adsorbed on the material's surface, which leads to the formation of $^{\bullet}OH$ with high oxidation potential capable of degrading organic contaminants (R) (Equations (3) and (4)).

$$Nb_2O_5\ (h^+_{(VB)}) + H_2O \rightarrow Nb_2O_5 + H^+ + OH^- \quad (3)$$

$$Nb_2O_5\ (h^+_{(VB)}) + OH^- \rightarrow Nb_2O_5 + {}^{\bullet}OH \quad (4)$$

In addition, another oxidation mechanism occurs when h^+ in the VB directly oxidize organic molecules in a one-step reaction through the adsorption of the molecule on the material's surface.

$$Nb_2O_5\ (h^+_{(VB)}) + R_{(ads)} \rightarrow R^+ \text{ (oxidation byproducts)} \quad (5)$$

On the other hand, e^- in the CB can generate other oxidative species, such as superoxide anion radicals ($O_2^{\bullet -}$), by interacting with dissolved oxygen. In the presence of H^+ ions, these can also form other oxidants, like the hydroperoxyl radical (Equations (6) and (7)), which conducts the indirect oxidation of organic contaminants (Equations (8) and (9)) [36,37].

$$Nb_2O_5\ (e^-_{(CB)}) + O_{2\ (dissolved)} \rightarrow O_2^{\bullet -} \quad (6)$$

$$O_2^{\bullet -} + H^+ \rightarrow {}^{\bullet}OOH \quad (7)$$

$$O_2^{\bullet -} + R_{(ads)} \rightarrow R^+ \text{ (oxidation byproducts)} \quad (8)$$

$${}^{\bullet}OOH + R_{(ads)} \rightarrow R^+ \text{ (oxidation byproducts)} \quad (9)$$

The solution pH is a master variable that modulates the entire catalytic mechanism of Nb_2O_5, influencing both the catalyst's surface chemistry and the dominant pathways for ROS generation. Its effect can be understood through two primary lenses: its control over the catalyst's surface charge and its role in the acid/base equilibria of the reactive species.

The surface charge of a metal oxide in an aqueous solution is determined by the pH relative to its isoelectric point (IEP), the pH at which the net surface charge is zero. For Nb_2O_5, the IEP is typically in the acidic range, reported to be approximately pH 3.8 [52]. This has direct consequences for pollutant interaction. At a pH below the IEP, the surface hydroxyl groups are protonated ($S–OH + H^+ \leftrightarrow S–OH^{2+}$), resulting in a net positive surface charge that favors the electrostatic adsorption of anionic pollutants. Conversely, at a pH above the IEP, the surface hydroxyl groups are deprotonated ($S–OH + OH^- \leftrightarrow S–O^- + H_2O$), resulting in a net negative surface charge that promotes the adsorption of cationic pollutants, such as methylene blue. Since the initial adsorption of the pollutant onto the catalyst surface is often a rate-limiting step, the pH plays an important role in determining the overall degradation efficiency [53].

Beyond surface interactions, pH also directly governs the formation and equilibrium of ROS. The reduction of dissolved oxygen by conduction band electrons first forms the superoxide radical anion ($O_2^{\bullet -}$). This species is in a pH-dependent equilibrium with its protonated form, the hydroperoxyl radical ($^{\bullet}OOH$), as shown in Equation (10).

$$O_2^{\bullet -} + H^+ \leftrightarrow {}^{\bullet}OOH\ (pKa \approx 4.8) \quad (10)$$

The pKa for this equilibrium is approximately 4.8. This means that in strongly acidic media (pH < 4.8), the more reactive hydroperoxyl radical ($^{\bullet}OOH$) is the dominant species. In neutral to basic media (pH > 4.8), the superoxide anion ($O_2^{\bullet -}$) predominates. The hydroperoxyl radical can subsequently participate in reactions that lead to the formation of the highly oxidizing hydroxyl radical ($^{\bullet}OH$), for instance, through disproportionation ($2\,{}^{\bullet}OOH \rightarrow H_2O_2 + O_2$) followed by the decomposition of the generated hydrogen peroxide. Furthermore, the generation of hydroxyl radicals via the direct oxidation of water by valence band holes (h^+) is also pH-dependent. This pathway is generally more favorable in alkaline conditions, where the concentration of hydroxide ions (OH^-) is higher, as they are more easily oxidized to $^{\bullet}OH$ than neutral water molecules.

Some studies have shown that heterogeneous photocatalysis can form byproducts through the direct reduction of a few organic molecules. However, their proportion is much smaller compared to the oxidation reactions in the system (Equation (10)). In this scenario, when a photoactive organic molecule comes into direct contact with the light source, it can absorb photons and enter an excited state. Later, once adsorbed on the surface, it may activate the material by promoting its electron to the semiconductor's CB (Equations (11)–(14)).

$$Nb_2O_5\ (e^-_{(CB)}) + R_{(ads)} \rightarrow R^-\ \text{(reduction byproducts)} \quad (11)$$

$$R + h\nu_{(UV)} \rightarrow R^* \quad (12)$$

$$R^* + Nb_2O_5 \rightarrow R^{\bullet+} + Nb_2O_5\ (e^-_{(CB)}) \quad (13)$$

$$Nb_2O_5\ (e^-_{(CB)}) + \text{intermediates} + R_{(ads)} \rightarrow R^+\ \text{(oxidation byproducts)} \quad (14)$$

This mechanism is known as photosensitization, in which the molecule in question absorbs visible-range energy and, once in the excited state, can donate an excited electron to the semiconductor's CB. As reported by Lopes et al. (2014) [36], it was possible to degrade rhodamine B (RhB) under visible-light irradiation because the dye was excited and transferred an electron to the Nb_2O_5 CB, which could then reduce molecular oxygen to form superoxide radicals. In this case, the molecule needs to remain adsorbed on the semiconductor long enough to be activated and carry out the aforementioned reactions [36].

As noted earlier, the high recombination rate of electron–hole pairs limits the application of semiconductors in photocatalysis. To address this issue, strategies like coupling two semiconductors or combining a semiconductor and a metal have been adopted to create an interface that enhances charge transport and prevents recombination, known as a heterojunction [51,54].

In the case of Nb_2O_5, heterojunctions with other semiconductors offer advantages beyond improved charge separation. The implementation of porous co-catalysts with high surface area provides additional active sites, enhancing light absorption and photocatalytic activity. Moreover, combining Nb_2O_5 (with strong oxidative potential) with semiconductors possessing high reductive potential can further promote efficient redox reactions. Different types of heterojunctions, including p–n junctions, type II, Z-scheme, and S-scheme configurations, have been reported for Nb_2O_5-based catalysts [27,36,37,51].

The p–n heterojunctions are formed by integrating an n-type semiconductor (such as Nb_2O_5) in which electrons are the majority carriers and holes are the minority carriers. Thus, when the materials are immersed in an aqueous solution, n-type semiconductors conduct electricity primarily through electrons, whereas p-type ones do so through holes. This junction creates an internal electric field that drives the migration of electrons and holes in opposite directions, thereby reducing recombination and enhancing photocatalytic efficiency (Figure 10) [55,56]. Several studies have modified Nb2O5 to alter its semiconductor capacity and its photocatalytic activity. As mentioned by Silva et al. (2020) [57], impregnating a p-type semiconductor in Nb_2O_5 forms a p–n junction and increases photocatalytic performance [37,51,58].

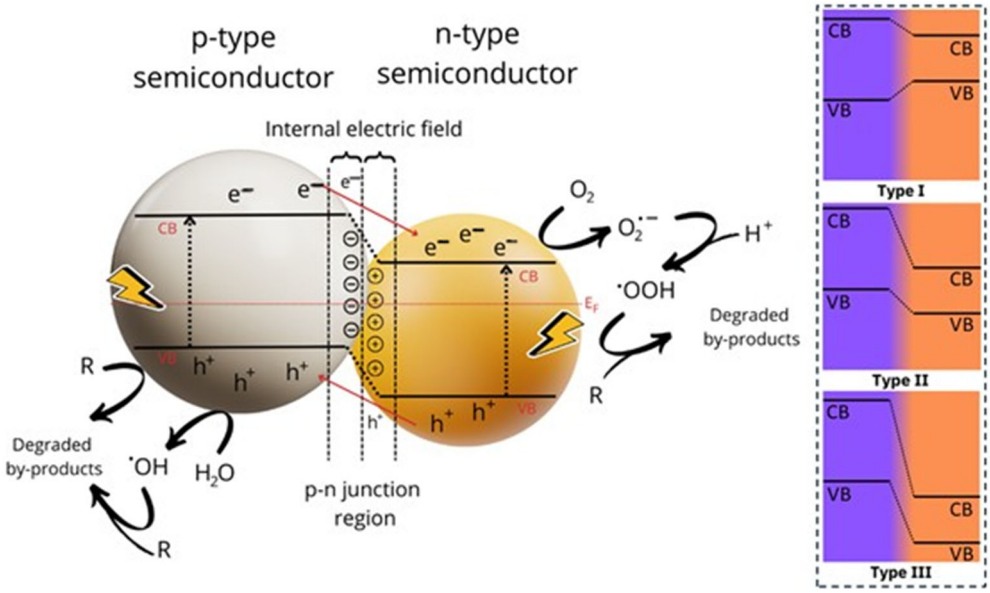

Figure 10. Scheme of charge transfer of photogenerated electrons and holes in the p-n heterojunction and types of heterostructures according to the position of VB and CB of each semiconductor (in purple and orange) (Adapted from [45]).

This property, related to charge movement at the semiconductor interface, depends on the heterojunction type and arises from differences in the chemical potential of electrons in the crystal structures, represented by the Fermi level. Heterostructures can be grouped into three distinct types based on the VB and CB energy levels (Figure 10). In a type I (straddling gap) junction, the conduction band (CB) and valence band (VB) edges of one semiconductor lie within the bandgap of the other, causing electrons and holes to accumulate in the same region and thus increasing recombination. Type III (broken gap) junctions present a large band offset, where the CB of one semiconductor is located below the VB of the other, typically hindering effective charge transfer. In contrast, type II (staggered gap) heterojunctions are the most efficient for photocatalysis, where the conduction band (CB) of one material is more positive and the valence band (VB) of the other is more negative. The photogenerated charges migrate in opposite directions due to the relationship between the semiconductors' energy bands; electrons migrate to the semiconductor with the lower CB, while holes migrate to the higher VB, facilitating spatial separation of charges, extending carrier lifetimes, preventing species recombination, and enhancing photocatalytic efficiency [37,40,51].

Beyond these traditional configurations, other systems, such as the Z-scheme, have been extensively proposed. In Z-scheme heterojunctions, electrons in the CB of one semiconductor recombine with holes in the VB of another, leaving the strongly reductive electrons and oxidative holes spatially separated, thereby preserving high redox potential. Nb_2O_5-based Z-scheme heterojunctions represent an advanced strategy to overcome the limitations of conventional type II heterojunctions. While type II systems promote separation of photogenerated charges, they often sacrifice strong redox potentials. In contrast, Z-scheme systems allow for both efficient charge separation and the preservation of strong reduction and oxidation potential, making them highly promising for photocatalysis. The principle of the Z-scheme relies on a selective recombination process, where photogenerated electrons with weaker reduction ability recombine with photogenerated holes of weaker oxidation potential. As a result, highly reducing electrons remain in the CB of one semiconductor, while strongly oxidizing holes remain in the VB of the other, enabling redox reactions [37,40,51].

Z-scheme heterojunctions can be divided into three categories: the traditional Z-scheme, which employs redox mediators in solution but have some theoretical contradic-

tions and practical limitations due to recombination and instability; the all-solid-state (ASS) Z-scheme, which uses solid conductors such as Ag, Au, reduced graphene oxide (rGO), or carbon nanotubes as mediators; and the direct Z-scheme, where two semiconductors form an interfacial contact and no external mediator is required (Figure 11A). Despite their advantages, ASS Z-schemes face challenges such as the possible formation of Schottky junctions instead of true Z-scheme interfaces, uncertainty in conductor loading, competition between the conductor and catalyst for light absorption, and reduced charge transfer efficiency due to poor dimensional control of mediators. Direct Z-schemes, however, successfully overcome many of these deficiencies by ensuring the direct contact between semiconductors and strong interfacial built-in electric fields that enhance carrier transfer [37,40,59].

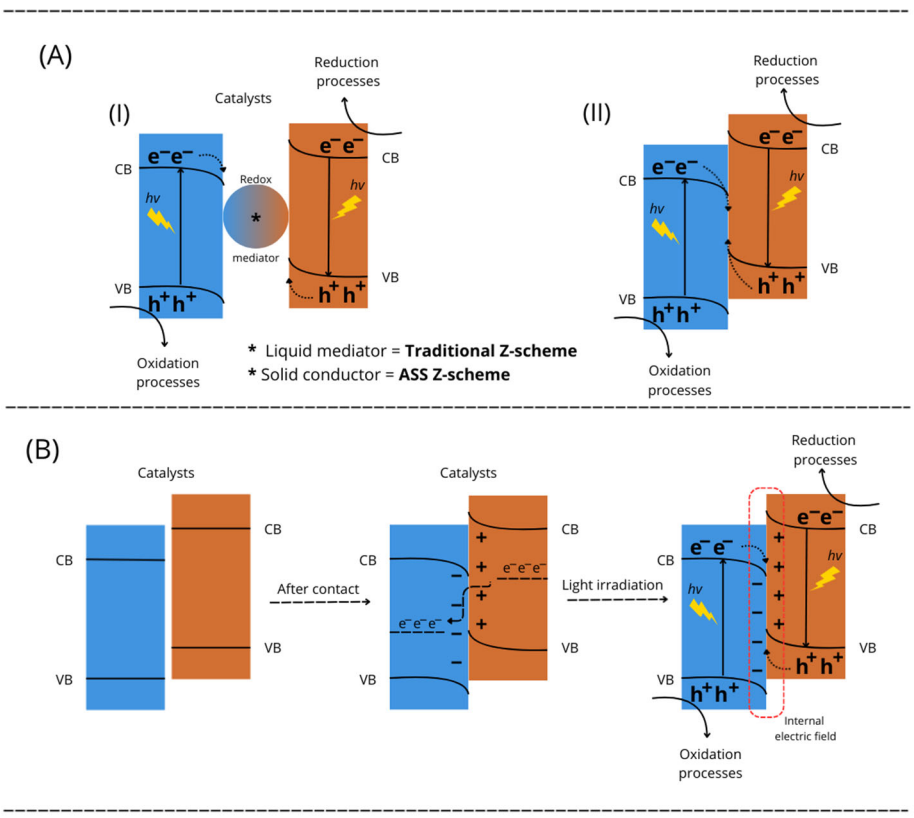

Figure 11. Schematic illustration of (**A**) Z-scheme heterojunctions ((**I**) = Traditional and (**II**) = All-Solid-State ASS system) and (**B**) Charge-transfer processes in an S-scheme heterojunction.

Another system called the S-scheme heterojunction was also explored to address some of the conceptual limitations of the Z-scheme model and to provide a clearer understanding of charge transfer mechanisms in photocatalysis. Unlike traditional Z-schemes, which rely on mediator-assisted or direct recombination routes that sometimes suffer from contradictory or unclear carrier transport explanations, the S-scheme describes a more precise mechanism of charge migration between semiconductors with staggered band structures. In this model, a reduction photocatalyst with higher Fermi levels is coupled with an oxidation photocatalyst with lower Fermi levels. Upon contact, electrons naturally transfer from the reduction to the oxidation photocatalyst, leading to the formation of an electron-rich and electron-depleted environment, respectively. This charge redistribution establishes a built-in electric field directed between the catalysts, which, with electrostatic interactions, facilitates selective recombination of low-energy charge carriers. During photoexcitation, the photogenerated electrons with weak reduction capacity in the oxidation photocatalyst recombine with the photogenerated holes with weak oxidation capacity in the reduction photocatalyst. Conversely, the electrons in the CB of the reduction photocatalyst and the

holes in the VB of the oxidation photocatalyst are preserved (which have strong redox potentials) and drive reduction and oxidation reactions, respectively. Thus, the S-scheme mechanism ensures both efficient charge separation and the retention of strong redox potentials, overcoming the classical trade-off seen in type II heterojunctions [37,51,60,61].

Recently, ternary heterostructure photocatalysts have been investigated as a strategy to further enhance photocatalytic performance beyond binary heterojunctions. In these systems, Nb_2O_5 is typically combined with two additional components that act synergistically to prevent the photoinduced electron–hole recombination, broaden light absorption, accelerate charge transfer, and preserve strong redox ability. Ternary Nb_2O_5-based heterojunctions incorporating components such as Ag, Ru, g-C_3N_4, and BiOCl have demonstrated enhanced photocatalytic activity. The integration of carbon-based materials, in particular, improves light absorption and facilitates charge transfer. Ramar et al. (2024) [62] reported that in a g-C_3N_4/Nb_2O_5/Ag ternary nanocomposite, the presence of g-C_3N_4 promoted the generation of reactive oxidative species capable of efficiently degrading pollutants such as dyes. Additionally, g-C_3N_4 contributed to bandgap tuning of Nb_2O_5, enhancing its visible light response, while Ag nanoparticles played a key role in improving electron transfer and overall system stability [63].

Guo et al. (2022) [64] developed a ternary Zr-doped g-C_3N_4/Nb_2O_5 heterojunction that exhibited enhanced photocatalytic activity for the degradation of organic pollutants under visible light. In this system, Zr doping played a key role in modifying the band structure and improving interfacial charge separation, while the formation of the heterojunction between g-C_3N_4 and Nb_2O_5 facilitated efficient electron–hole transfer. As a result, the composite showed significantly higher degradation efficiency compared to its individual components, effectively using visible light and minimizing recombination losses.

Similarly, other studies, using Nb_2O_5 and BiOCl in ternary structures with Bi_4NbO_8Cl, have also demonstrated high photocatalytic activity, along with enhanced charge separation, attributed to the presence of an internal electric potential that improves overall efficiency. These heterostructures also exhibited increased light absorption and effective suppression of photoinduced charge carrier recombination, further illustrating how the synergistic effects inherent to ternary heterojunctions can substantially enhance photocatalytic efficiency, particularly in applications related to wastewater treatment [65,66].

In photocatalysis, a type II heterojunction is the most appropriate, as photogenerated charges migrate in opposite directions due to the relationship between the semiconductors' energy bands, preventing species recombination [51].

In electrocatalytic systems, niobium-based materials are used both as electrodes and as surface modifiers to enhance charge transfer kinetics. When employed as an electrode component, niobium or Nb_2O_5 facilitates the oxidation of contaminants by promoting electron transfer at the interface. A simplified overall reaction at the electrode surface can be represented as Equation (15).

$$R \rightarrow R^+ + e^- \quad (15)$$

The presence of Nb or Nb_2O_5 enhances charge mobility and lowers overpotentials. In modified electrodes, a niobium coating creates an active surface layer that stabilizes reactive intermediates while suppressing side reactions. Although detailed mechanisms vary, improvements are observed in current densities and catalytic efficiencies [67,68].

Photocatalytic ozonation combines the principles of photocatalysis and ozonation to achieve synergistic pollutant degradation. In these systems, Nb_2O_5, often doped or composite, undergoes photoexcitation while simultaneously interacting with ozone (O_3).

Ozone molecules adsorb onto the catalyst surface and react with photogenerated electrons, reducing electron–hole recombination (Equation (16)).

$$O_3 + e^-_{(CB)} \rightarrow O_3^{\bullet -} \quad (16)$$

The ozonide radical then decomposes to produce additional hydroxyl radicals (Equation (17)).

$$O_3^{\bullet -} + H^+ \rightarrow {}^{\bullet}OH + O_2 \quad (17)$$

Through this combined effect, both photocatalytic excitation and ozone decomposition work in tandem to generate higher amounts of ROS, leading to improved degradation rates [69].

The conventional Fenton reaction is a homogeneous process that uses ferrous iron (Fe^{2+}) to catalyze the decomposition of hydrogen peroxide (H_2O_2), generating highly reactive $^{\bullet}OH$ radicals according to Equation (18).

$$Fe^{2+} + H_2O_2 \rightarrow Fe^{3+} + {}^{\bullet}OH + OH^- \quad (18)$$

The catalytic cycle is sustained by the slower reduction of Fe^{3+} back to Fe^{2+} by H_2O_2. This process is most effective under acidic conditions (pH 2.8–3.5) to keep iron in solution and prevent its precipitation as ferric hydroxide, which is a major source of iron sludge.

The photo-Fenton reaction enhances this process by introducing light irradiation (UV or visible). The primary role of the photons is to accelerate the regeneration of the catalytically active Fe^{2+} species through the photoreduction of ferric complexes (Equation (19)).

$$Fe^{3+} + H_2O_2 + h\nu \rightarrow Fe^{2+} + {}^{\bullet}OH + H^+ \quad (19)$$

This light-driven step overcomes the kinetic bottleneck of the dark Fenton reaction, leading to a higher steady-state concentration of $^{\bullet}OH$ radicals and, consequently, more efficient pollutant mineralization.

When niobium-based materials are integrated into systems with H_2O_2, they function as heterogeneous Fenton-like catalysts. Unlike the iron-based redox cycle, Nb_2O_5 is a transition-metal oxide known for its stability under acidic conditions and its ability to activate H_2O_2 through surface-mediated mechanisms. The process begins with the interaction of H_2O_2 with surface hydroxyl groups (S–OH) of Nb_2O_5, leading to the formation of hydroperoxide ions (HO_2^-) through the dissociation reaction, Equation (20).

$$H_2O_2\ (aq) + S\text{–}OH(surf) \rightarrow HO_2^-(aq) + S\text{–}OH_2^+(surf) \quad (20)$$

The HO_2^- formed in the liquid phase subsequently reacts with another H2O2 molecule via an electroprotic mechanism, generating $^{\bullet}OH$, $O_2^{\cdot -}$, and water (Equation (21)) [70].

$$H_2O_2(aq) + HO_2^-(aq) \rightarrow HO^{\bullet}(aq) + O_2^{\bullet -}(aq) + H_2O(aq) \quad (21)$$

The efficiency of ROS formation is strongly influenced by the pH. The reaction is most effective under acidic conditions (pH $\approx$ 3), where the dissociation of surface hydroxyl groups (S–OH) at pH levels above the isoelectric point (IEP) of Nb_2O_5 enhances the availability of active catalytic sites, and the generated $O_2^{\cdot -}$ radicals are stabilized by adsorption on the niobia surface. At higher pH values, surface peroxide species (O_2^{2-}) become the dominant ROS, altering the reaction pathway.

When integrated into photo-Fenton systems, niobium-based materials can play a dual role. They not only contribute to activating H2O2 but can also act as photocatalysts, where

light irradiation generates electron–hole pairs that produce additional ROS, leading to a synergistic effect (Equation (22)) [71].

$$Nb_2O_5 + H_2O_2 + h\nu \rightarrow Nb_2O_5\ (h^+ + e^-) + {}^{\bullet}OH \quad (22)$$

The efficiency of ROS formation is strongly influenced by the pH. Under acidic conditions (pH ~ 3), the reaction is most effective due to two main factors: (1) Presence of S–O^- species: At pH levels above the isoelectric point (IEP) of Nb_2O_5, the dissociation of surface hydroxyl groups (S–OH) increases, enhancing the availability of active catalytic sites. (2) Stabilization of superoxide anions: The $O_2{}^{\bullet-}$ radicals generated are stabilized by adsorption on the Nb_2O_5 surface, prolonging their reactivity [72]. At higher pH values, surface peroxide species ($O_2{}^-$) become the dominant ROS, altering the reaction pathway and potentially reducing the degradation efficiency for specific pollutants.

5. Common Synthesis Methods of Nb_2O_5-Based Materials

The performance of Nb_2O_5-based catalysts employed in AOPs is significantly influenced by the synthesis methodologies, as they define crucial physicochemical properties, including surface area, crystallinity, morphology, and defect density. The choice of method also determines the final form of the catalyst, which can be broadly categorized into suspended powders or immobilized thin films, each having distinct advantages for different reactor configurations.

The catalyst's design does not merely alter the rate of degradation but can fundamentally change the degradation pathway. This is because different catalyst formulations can favor the generation of different dominant ROS, which in turn attack different functional groups on a pollutant molecule.

A common experimental technique to identify the primary ROS responsible for degradation is the use of chemical scavengers. In these experiments, a specific chemical agent known to react selectively with a particular ROS is added to the system. A significant decrease in the degradation rate in the presence of the scavenger indicates the importance of that ROS. Common scavengers include isopropanol or tert-butyl alcohol for hydroxyl radicals, p-benzoquinone for superoxide radicals, and triethanolamine (TEOA) or ammonium oxalate for photogenerated holes (h+) [73].

For instance, in the degradation of rhodamine B using g-C_3N_4/Nb_2O_5 nanofibers, Wang et al. (2021) [73] found that the addition of p-benzoquinone and TEOA significantly inhibited the reaction, identifying $O_2{\bullet}^-$ and h+ as the major active species. In contrast, for the degradation of ciprofloxacin (CIP) with a Nb_2O_5-RGO/MoO_3 ternary composite, scavenger tests revealed that •OH radicals were the predominant active species [74]. These findings demonstrate that the catalyst architecture directly influences the dominant oxidative pathway.

For the production of powdered catalysts, which are typically used in slurry-type photoreactors, methods such as sol–gel, hydrothermal/solvothermal synthesis, and co-precipitation are the most prevalent in the literature. Among these methodologies, the sol–gel route stands out for its ability to yield highly homogeneous Nb_2O_5 structures with adjustable surface characteristics and porosity. Recent studies demonstrate that calcination conditions following sol–gel preparation play a critical role in balancing crystallinity and surface properties, directly affecting photocatalytic performance for environmental remediation [75–77].

Hydrothermal and solvothermal techniques offer alternative synthetic routes, utilizing aqueous or organic solvents under elevated temperature and pressure conditions [63,65,78]. These methods permit effective control of the crystalline phase, particle size, and shape, leading to highly crystalline Nb_2O_5 materials with distinctive morphological features such

as nanorods, nanocubes, and hierarchical microspheres. Such tailored morphologies significantly enhance active site accessibility, charge separation, and pollutant degradation efficiency. Recent works highlight the successful use of hydrothermally derived Nb_2O_5 composites integrated with materials like MXenes, achieving notable efficiency in photocatalytic degradation of persistent contaminants [8].

Microwave-assisted synthesis has recently gained attention due to its rapid reaction times and efficient heating mechanisms, enabling the production of Nb_2O_5 with unique structural properties such as increased defect sites and reduced particle sizes [79,80]. These defects and nanoscale features are directly linked to improved photocatalytic and photo-Fenton activity, enhancing the material's response to visible-light irradiation and reactive species generation. Recent reports on microwave-synthesized, iron-doped Nb_2O_5 have demonstrated substantial catalytic enhancements for organic contaminant degradation [79].

Another innovative strategy, electrospinning, facilitates the direct fabrication of Nb_2O_5 materials into continuous nanofibrous mats. These self-supporting fibrous structures exhibit a high surface-to-volume ratio, interconnected porosity, and ease of handling, making them ideal candidates for continuous-flow photocatalytic systems. Recent studies employing electrospun Nb_2O_5-based heterostructures, combined with graphitic carbon nitride (g-C_3N_4), have reported significantly enhanced photocatalytic activities towards organic pollutants, validating the effectiveness of this technique for environmental remediation applications [73].

For immobilized catalysts, which are advantageous for preventing post-treatment recovery steps and for use in continuous flow systems, thin-film fabrication techniques are employed. Methods such as sputtering, chemical vapor deposition (CVD), and dip-coating are commonly used to deposit a uniform layer of Nb_2O_5 onto various substrates, such as glass, silicon wafers, or conductive electrodes. These techniques provide precise control over the film's thickness, adhesion, and uniformity, which are crucial for applications in photo-electrocatalysis and membrane reactors where the stability and reusability of the catalyst are paramount.

Thin-film deposition techniques, such as chemical vapor deposition (CVD), are essential when immobilized catalytic materials are required, especially in photoelectrochemical applications [68,81,82]. The uniform deposition of Nb_2O_5 thin films by CVD methods results in high-quality layers that demonstrate excellent adherence, mechanical stability, and reproducibility, advantageous for electrode-based AOP setups. Recent research emphasizes the beneficial use of CVD-produced Nb_2O_5 coatings in electrodes, enhancing their durability and overall catalytic performance in photocatalytic and electrochemical oxidation systems [82].

In comparative terms, each synthesis method provides distinct advantages and limitations, making the choice highly dependent on the desired catalytic application. Solution-based methods such as sol–gel, hydrothermal, and solvothermal syntheses typically produce materials ideal for powder-based photocatalysis due to their high surface areas and controlled morphologies. Conversely, methods like CVD are indispensable for immobilized catalytic systems. Microwave-assisted synthesis and electrospinning provide modern, versatile routes that combine rapid production and structurally unique catalysts, respectively, offering new possibilities for the optimization and integration of Nb_2O_5 materials in advanced oxidation processes. Strategic selection of the synthesis method is thus crucial for achieving optimal performance in targeted environmental remediation applications.

6. Modification Strategies and Research Progress Advancement on Nb for Pollutant Degradation

Recent advances in photocatalysis have highlighted the fundamental role of structural and compositional modification strategies in enhancing the photocatalytic performance of semiconductors. For Nb_2O_5-based materials, these strategies are crucial for overcoming intrinsic limitations, such as a wide band gap and a high electron–hole pair recombination rate. As illustrated in Figure 12, the main modification approaches, which have proven to be the most effective in improving the efficiency of organic pollutant degradation, can be broadly categorized into five groups: heterostructures/composites, metallic and non-metallic doping, incorporation of carbonaceous materials, surface morphology regulation, and phase and defect control [83–86].

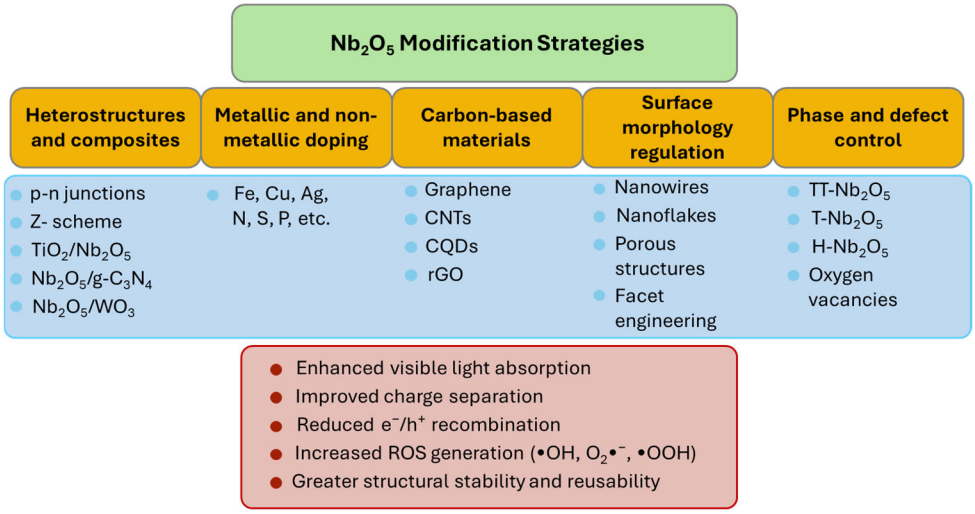

Figure 12. Schematic of the main modification strategies for Nb_2O_5-based catalysts aimed at optimizing catalytic performance in Advanced Oxidation Processes.

The formation of heterostructures and composites has been extensively investigated due to their ability to optimize charge carrier separation and minimize electron recombination effects, thereby favoring the generation of reactive species for pollutant degradation. These hybrid structures exploit the synergy between semiconductors with different band gaps, promoting broader spectral absorption and significantly increasing the photochemical stability of catalysts. Meanwhile, surface morphology regulation focuses on modifying the structural characteristics of photocatalysts, such as particle size, specific surface area, and crystal facet configuration. These modifications play a crucial role in photocatalytic efficiency, as they directly influence the catalyst–pollutant interaction, light absorption, and charge carrier dynamics.

6.1. Heterostructures and Composites

The formation of heterostructures and composites represents one of the most promising approaches to optimizing the photocatalytic efficiency of semiconductors by exploiting synergistic interactions between distinct materials. In the case of Nb_2O_5, constructing heterostructures enhances charge separation, extends light absorption, and increases the material's chemical stability, making it more efficient for the degradation of organic pollutants. Recent studies have demonstrated that combining Nb_2O_5 with other semiconductors and co-catalysts results in hybrid materials with significantly improved photocatalytic activity, thereby enhancing the efficiency of AOPs [87,88].

However, while many reports highlight enhanced activity, few provide a detailed mechanistic interpretation of how heterojunction formation alters charge carrier dynam-

ics specifically in Nb_2O_5-based systems. For example, although type II and Z-scheme heterostructures are both widely used, direct comparisons between their performance under standardized conditions are lacking. This makes it difficult to determine whether the observed improvements stem from favorable band alignment or merely from additive effects of the individual components [89,90]. Furthermore, although combinations with visible-light-active semiconductors—such as CdS, $BiVO_4$, g-C_3N_4, and WO_3—are often justified by their ability to enhance solar response [91,92], the exact nature of interfacial interactions and the degree of band bending or built-in electric fields remain poorly quantified. Few studies employ techniques such as Mott–Schottky analysis or photoluminescence lifetime measurements to validate charge separation mechanisms in these systems, leaving important questions unanswered.

Incorporation of niobium into TiO_2, whether by substitutional doping or via formation of a TiO_2/Nb_2O_5 heterojunction, introduces new electronic states within the intrinsic band gap of both oxides, enabling absorption of lower-energy (visible light) photons. When Nb^{5+} replaces Ti^{4+} in the TiO_2 lattice, charge neutrality is maintained through the formation of oxygen vacancies; these vacancies and Nb-induced defect levels lie approximately 0.3–0.8 eV below the conduction band minimum of TiO_2, effectively narrowing the optical band gap from ≈3.2 eV to as low as 2.7 eV [93]. These mid-gap states permit the promotion of electrons under visible-light irradiation ($\lambda > 400$ nm). In heterostructured TiO_2/Nb_2O_5 composites, the staggered (type II) band alignment drives photogenerated electrons into the conduction band of Nb_2O_5 and holes into the valence band of TiO_2, further extending the photoresponse into the visible range and suppressing recombination [94,95].

However, these theoretical benefits are often assumed rather than demonstrated experimentally. In many cases, the actual contribution of Nb_2O_5 within a composite remains unclear due to the lack of appropriate controls (performance of each component separately under identical conditions). Moreover, while band alignment explanations are frequently proposed, few studies corroborate them with spectroscopic or electrochemical data.

The architecture of heterostructures also directly influences charge separation efficiency, with these systems classified into type I, II, p-n, and Z-scheme heterojunctions [96]. Z-scheme systems, for instance, have been extensively studied due to their ability to preserve the high redox potential of individual semiconductors, ensuring the simultaneous retention of strong oxidative and reductive properties [90,97]. Despite this, their scalability and long-term operational stability are seldom evaluated. Additionally, the synthesis of Z-scheme systems often requires multi-step fabrication, which may limit reproducibility and industrial applicability.

Another important benefit of Nb_2O_5-based heterostructures is the improvement in the chemical and structural stability of photocatalysts. With continuous use, many semiconductors undergo photoinduced degradation, compromising their efficiency over multiple reuse cycles. Incorporating a second semiconductor or a co-catalyst into the Nb_2O_5 structure can reduce corrosion and increase the material's mechanical resistance [98]. For instance, Goswami et al. demonstrated that an $rGO/Nb_2O_5/TiO_2$ composite achieved 98.7% malachite green degradation in its first cycle and still delivered 94.7% removal after three consecutive visible-light photocatalysis runs, corresponding to only a 4% activity loss. Likewise, Ücker et al. found that Nb_2O_5/TiO_2 heterostructures retained over 92% RhB discoloration efficiency after four UV-C reuse cycles. These results confirm the excellent operational stability and reusability of TiO_2/Nb_2O_5 heterostructured catalysts [99,100].

Nonetheless, long-term durability is reported in only a minority of studies. The absence of degradation pathway analysis and structural characterizations post-cycling is a significant shortcoming, especially for catalysts intended for practical application.

Reusability is often assessed under idealized lab conditions, with little attention given to real wastewater matrices or variable pH environments.

Beyond semiconductor synergy, the presence of metal and non-metal dopants has also proven to be an effective strategy for further enhancing the efficiency of Nb_2O_5 composites. Elements such as iron (Fe), copper (Cu), silver (Ag), and gold (Au) can act as electron transfer mediators, reducing charge resistance and promoting surface interactions that favor the generation of highly reactive free radicals [100,101]. Likewise, structural modifications with non-metallic dopants like nitrogen (N), sulfur (S), and phosphorus (P) can introduce intermediate states within the Nb_2O_5 bandgap, allowing for more efficient excitation under visible light and increasing the selectivity for degrading specific compounds [102,103].

Carbonaceous Modifications

The incorporation of carbonaceous materials into photocatalytic semiconductors has emerged as an effective strategy for optimizing the degradation of organic pollutants in aqueous media. The synergy between Nb_2O_5 and carbon-based materials, such as graphene, carbon nanotubes (CNTs), carbon quantum dots (CQDs), and amorphous carbon, provides significant improvements in the optical, electronic, and structural properties of photocatalysts [104].

These carbonaceous components are frequently described as electron shuttles, facilitating charge separation and limiting recombination of photogenerated carriers. Graphene, in particular, offers high electronic mobility and excellent interfacial conductivity, which favors more efficient electron transfer between Nb_2O_5 and surrounding species [105]. However, while this enhancement is consistently cited, the actual interfacial mechanisms and kinetics of electron transfer remain insufficiently explored. Many studies assume improved performance based on enhanced pollutant removal, yet do not provide direct evidence through spectroscopic or electrochemical characterization. As a result, the interpretation of electron migration pathways often remains speculative.

Additionally, modification with carbon-based materials enables expansion of the photocatalyst's absorption into the visible region, maximizing the utilization of solar light as an energy source. Nb_2O_5, which has a relatively wide bandgap (~3.4 eV), is only activated by ultraviolet radiation, limiting its efficiency under direct sunlight. Incorporating structures such as carbon quantum dots (CQDs) and carbon nanotubes (CNTs) allows these nanostructures to act as photon-absorbing centers, promoting energy transfer to Nb_2O_5 and reducing its excitation threshold, ultimately leading to a more efficient photocatalyst under visible light [106–108].

Another relevant aspect of carbon modification is the increase in the specific surface area of photocatalysts, which enhances the adsorption of organic pollutants on the material's surface. This greater contact area allows organic compounds to be more easily degraded as they remain closer to the photocatalyst's active sites. Graphene, for instance, due to its highly porous two-dimensional structure, facilitates efficient interactions between pollutants and the catalyst surface, maximizing the photochemical conversion of contaminant compounds [108,109]. Nonetheless, the extent of this shift is highly dependent on the carbon source, synthesis method, and integration strategy. In many cases, absorption red-shifts are reported without corresponding increases in quantum efficiency, indicating that enhanced light harvesting alone is not sufficient to improve photocatalytic activity unless coupled with efficient charge separation and transport.

Another significant claim regarding carbon-based materials is their ability to stabilize photocatalysts under repeated use. The incorporation of conductive carbon frameworks is said to inhibit photocorrosion and preserve crystal integrity over multiple cycles [110,111]. While this is a desirable attribute, long-term performance evaluations remain sporadic, and

few studies investigate structural or chemical changes post-use. Deactivation mechanisms, such as fouling or surface oxidation of the carbon phase, are rarely addressed.

Thus, modifying Nb_2O_5 through heterostructure and composite formation represents a significant advancement in the quest for more efficient and stable photocatalysts for environmental applications. The combination of complementary semiconductor materials, along with the use of strategic dopants, has proven highly effective in expanding spectral absorption, optimizing charge separation, and improving the chemical stability of the material, positioning Nb_2O_5-based composites as promising candidates for water treatment and the removal of persistent organic pollutants.

6.2. Surface Morphology Regulation

Surface morphology plays a pivotal role in defining the photocatalytic behavior of semiconductors, especially in systems based on Nb_2O_5. Unlike strategies centered on electronic modifications, morphological control influences how light interacts with the catalyst, how pollutants access active sites, and how efficiently charge carriers migrate across the structure [112]. Studies have shown that increasing the specific surface area through nanostructuring, such as the formation of flakes, tubes, or porous frameworks, can promote more effective pollutant adsorption and accelerate degradation kinetics [113,114]. However, the relationship between surface area and activity is not always straightforward, since factors such as pore connectivity and diffusional resistance are rarely considered in these analyses.

Particle size and shape also impact photocatalytic performance. Hierarchical and hollow morphologies, for instance, often enable more efficient light harvesting and reduced charge recombination due to shortened migration distances [47]. While these features are frequently cited as beneficial, comparisons across studies are complicated by inconsistencies in reporting and by the coexistence of other modifications, such as doping or heterojunction formation, which may also contribute to the observed activity. In many cases, the performance gains attributed to morphology could partially result from these overlapping factors.

Recent advances have combined morphological engineering with semiconductor coupling strategies, leading to materials with enhanced activity under visible light and improved resistance to deactivation [103]. In particular, Z-scheme heterostructures supported on nanostructured scaffolds have shown promising results in degrading complex pollutants [115,116]. However, questions remain regarding their long-term mechanical and structural stability, especially under realistic water matrices and extended operating periods. Most studies still rely on ideal laboratory conditions to evaluate these systems, limiting the understanding of their robustness in real scenarios.

Surface morphology modification has a strong impact on the configuration of the material's crystal facets, which directly influences charge transfer processes and the ability to generate reactive species. Recent studies have demonstrated that the selective exposure of certain Nb_2O_5 crystal facets can induce the formation of more favorable electronic states for the migration of photogenerated charges, reducing recombination and increasing efficiency in hydroxyl radical and superoxide anion production. The formation of rough, highly textured surfaces also promotes the homogeneous dispersion of incident light, improving absorption efficiency and reducing energy losses due to reflection [117–119].

Crystallinity and phase purity are equally critical. Nb_2O_5 can be synthesized in various polymorphs, including pseudohexagonal (TT), orthorhombic (T), and monoclinic (H), each offering distinct band-edge positions and defect profiles. Ücker et al. (2019) [120] reported that the TT phase, less ordered and richer in surface defects, provided superior RhB degradation compared to more crystalline forms. This finding aligns with others showing

that moderate disorder can enhance light absorption and ROS generation by introducing mid-gap states [121,122]. Additionally, defects and oxygen vacancies introduced during phase transitions alter the electronic band structure and create mid-gap states that facilitate the generation of reactive species. This interplay between phase composition, surface area, and defect density ultimately governs the catalyst's performance in AOPs [123].

Furthermore, as mentioned by Ücker et al. (2021) [124], a less organized, defect-rich structure of as-prepared Nb_2O_5 without treatment (wt) is more favorable for photocatalysis. As heat treatment temperature increases, the material becomes more crystalline, and particle size grows. This change not only reduces the surface area available for adsorption but also increases the recombination rate of electron–hole pairs, ultimately decreasing photocatalytic performance [36,125,126]. Samples of Nb_2O_5 prepared without heat treatment (Nb_2O_5_wt) achieved complete RhB degradation in 90 min, whereas those treated at 500 °C (Nb_2O_5_TT) and 800 °C (Nb_2O_5_T) exhibited lower degradation efficiencies. The reduction in activity is attributed, in part, to the decrease in defect density, which facilitates ROS formation. Thus, a less ordered crystalline structure appears to be beneficial for dye degradation.

7. Contaminant Removal

Of the 381 articles selected through a rigorous evaluation using the Methodi Ordinatio method, approximately 77% focus on contaminant degradation with Nb_2O_5, primarily for dye removal. This is followed by 9% addressing the removal of pharmaceuticals, 3% targeting heavy metals, 2% concerning personal care products, 7% dedicated to pesticides, and only 1% focusing on hormones.

The contamination of water resources with a diverse array of pollutants poses profound risks to environmental ecosystems and public health. Dyes, commonly discharged from textile and manufacturing industries, can disrupt aquatic life and reduce light penetration in water bodies. Pesticides and hormones, extensively used in agriculture and healthcare, contaminate water sources, leading to endocrine disruption and adverse health effects in humans and ecosystems. Pharmaceuticals, often detected at trace levels, contribute to the development of antibiotic-resistant bacteria and other unintended consequences. Heavy metals, such as lead and mercury, are highly toxic even at low concentrations, posing severe neurological and physiological hazards. Personal care products, including surfactants and preservatives, degrade water quality and harm aquatic organisms. Addressing the removal of these contaminants is imperative to safeguard water quality, protect biodiversity, and ensure the availability of safe drinking water [127,128].

7.1. Dyes

Although dyes constitute the majority of model pollutants in AOP studies, they are not representative of the most pressing classes of emerging contaminants. Pharmaceuticals, hormones, and fluorinated compounds, often found in surface waters at comparable or higher concentrations, present different structural complexities, persistence profiles, and toxicological concerns [129–131]. Still, dyes remain widely adopted as benchmark substrates, largely due to their intense coloration, easy detection, and recalcitrant nature.

However, these characteristics can be misleading. Many dyes, particularly methylene blue and rhodamine B, are known to act as photosensitizers, artificially enhancing apparent photocatalytic activity. Their degradation may also result in significant chromophore removal without full mineralization. Thus, while dyes remain operationally convenient, their use as model contaminants may not accurately reflect the performance of photocatalytic systems against more environmentally relevant targets [129,132,133].

Despite these limitations, the treatment of dye effluents remains an urgent task. The textile, paper, leather, and dyeing industries discharge significant volumes of wastewater

containing persistent and often toxic compounds [134]. Synthetic dyes are engineered for colorfastness, with complex aromatic structures, including chromophores and auxochromes, that confer exceptional stability [135–137]. Azo dyes, which represent over 70% of global production, are particularly challenging due to their carcinogenic potential and resistance to biodegradation [138]).

In this context, Nb_2O_5-based photocatalysts have demonstrated considerable efficiency in dye removal, often outperforming benchmark materials due to their chemical stability and ability to generate reactive species under both UV and visible light [123,139–141]. However, many studies emphasize removal efficiency without addressing byproduct formation or long-term activity. For real applications, greater emphasis should be placed on mineralization rates, reusability, and toxicity assessments.

In this context, Table 3 compiles the 58 highest-ranked articles according to the InOrdinatio method that employ niobium-based materials for dye degradation and indicates the specific niobium compound used, the AOP utilized, the type of dye pollutant targeted, the reported removal efficiency, and the corresponding references.

Table 3. Applications of Nb in the removal of dyes.

Material	AOP	Pollutant	Dye Removal	Reference
Ti/SnO_2-Nb_2O_5 electrodes	Electrochemical	232 Pt-Co	83% (30 min)	[142]
Bi_3NbO_7	Photocatalysis (Visible light (vis))	Acid red G	88% (120 min)	[91]
Nb_2O_5/glass foams	Photocatalysis (UV-C)	Acid yellow 23 BY	91.1% (300 min)	[143]
Bentonite clay/Nb_2O_5	Photocatalysis (UV)	Blue 19	98% (120 min)	[144]
ZnO-Nb_2O_5	Photocatalysis (UV)	Bromophenol blue	81% (120 min)	[145]
NbO-BRGO	Photocatalysis (UV–Vis)	Crystal Violet (CV)	97% (90 min)	[146]
TiO_2/Nb_2O_5/SnO_2/RGO	Photocatalysis (Visible light)	CV and MO	100% and 95% (120 min)	[147]
$SrNbO_2N$	Photocatalysis (Visible light)	DCIP	46% (180 min)	[148]
Nb_2O_5	Photocatalysis (UV)	Indigo Carmine	85% (90 min)	[149]
Nb_2O_5 and $ZnNb_2O_6$	H_2O_2	MB	100% (60 min)/91% (240 min)	[88]
Nb_2O_5-OX catalyst	Photocatalysis (UV)/Fenton		86% (300 min)	[78]
Nb-substituted goethite	Fenton		85% (120 min)	[150]
CdS@Nb_2O_5	Photocatalysis (UV–Vis)		70% (120 min)	[151]
Ti–Nb alloy	Photocatalysis (Visible light)		82% (120 min)	[152]
NbCeOx	H_2O_2		92% (120 min)	[153]
Hexagonal prism-shaped niobium oxide	Photocatalysis (UV)		100% (120 min)	[154]
Nb_2O_5 (1000 °C)	Photocatalysis (UV–Vis)		58% (250 min)	[155]
2.0 CeO_2–Nb_2O_5	Photocatalysis (UV–Vis)/Photocatalysis (Vis + H_2O_2)		82% (150 min)/100% (150 min)	[156]
Nb-N-TiO_2	Photocatalysis (Solar light)		97% (45 min)	[157]
Phosphate-doped Nb_2O_5	H_2O_2		78% (120 min)	[71]
NbC/C (800 °C)	Photocatalysis (Visible light)		100% (8 h)	[158]
TiO_2:Nb	Photocatalysis (UV–Vis)		93% (120 min)	[159]
g-C_3N_4/Nb_2O_5	Photocatalysis (UV–Vis)		70% (210 min)/44% (210 min)	[160]
$Fe_3-xNbxO_4$	Fenton		90% (120 min)	[161]
Nb_2O_5-doped TiO_2 (600 °C)	Photocatalysis (UV)		85% (90 min)	[162]
Nb_2O_5-doped TiO_2	Photocatalysis (UV–Vis)		100% (2.5 h)/87% (7 h)	[163]
NbC/C—cigarette litter	Photocatalysis (Visible light)		54.38% (8 h)	[164]
KSrNb-6	Photocatalysis (UV)		40% (300 min)	[165]
XC-wNb	Photocatalysis (Visible light)		60% (300 min)	[166]
Nb-doped hematite	Fenton		75% (120 min)	[167]
$Fe_2-xNbxO_3$	Photocatalysis (UV–Vis)		70% (60 min)	[168]

Table 3. *Cont.*

Material	AOP	Pollutant	Dye Removal	Reference
$Fe_{73}.5Si_{13}.5B_9Cu_1Nb_3$—alloy ribbon	Fenton	MB and Methyl Orange (MO)	85% (20 min)	[169]
TiO_2/Nb_2O_5/PANI and TiO_2/Nb_2O_5/RGO	Photocatalysis (Visible light)		97% and 94% (240 min)/95% and 92% (240 min)	[170]
p-NiO/n-Nb_2O_5 nanocomposites	Photocatalysis (Visible light)	MO	94% (180 min)	[116]
NbO_2OH	Photocatalysis (Solar light)		100% (10 min)	[171]
Nb_2O_5	Photocatalysis (Solar light) + H_2O_2		98% (40 min)	[172]
Nb_2O_5 with CAC	Photocatalysis (UV–Vis)	Ponceau-S	100% (120 min)	[173]
Ta_2O_5-Nb_2O_5-N	Photocatalysis (Solar light)	P-Rosaniline Hydrochloride	50 min (100%)	[103]
Nb_2O_5 (500 °C)	Photocatalysis (UV)	Real textile effluent	80% (300 min)	[174]
Nb_2O_5:CB	Photocatalysis (UV–Vis)		93% (5 h)	[175]
Nb_2O_5 nanoparticles—oxidant-peroxo method (OPM)	Photocatalysis (UV–Vis)	RhB	70% (250 min)/37% (250 min)	[36]
H+/nanoscrolls, H+/nanosheets, K_4Nb_6O17, $HxK_4-xNb_6O_{17}$, Nb_2O_5	Photocatalysis (Visible light)		99% (20 min), 99% (20 min), 8% (40 min), 16% (40 min), 24% (40 min)	[176]
Nb—S-scheme OCN-[N-NBO/C] nanocomposites	Photocatalysis (Visible light)		99% (30 min)	[177]
Graphene aerogel composite Nb_2O_5-g-C3N4/rGA	Photocatalysis (Visible light)		95% (100 min)	[105]
Nb_2O_5/Nb_2CTx composites	Photocatalysis (Visible light)		98.5 (120 min)	[108]
Nb_2O_5/BiOCl composite	Photocatalysis (Visible light)		96.7% (120 min)	[89]
Microwave-assisted hydrothermal Nb_2O_5	Photocatalysis (UV)		98.9% (60 min)	[178]
$KNbO_3$ perovskite nanostructures	Photocatalysis (UV)		40% (180 min)	[80]
1% Fe-Nb_2O_5	Photocatalysis (UV)		100% (60 min)	[79]
Pseudohexagonal Nb_2O_5/Orthorhombic Nb_2O_5	Photocatalysis (UV)		97% and 57% (150 min)	[124]
$Bi_4NbO_8Cl/BiOCl/Nb_2O_5$	Photocatalysis (UV–Vis)		98% (90 min)	[65]
g-C_3N_4/Nb_2O_5 nanofibers	Photocatalysis (Visible light)		100% (120 min)	[73]
Nb_2O_5 nanospheres	Photocatalysis (Visible light)		99.9% (15 min)	[112]
Nb doped TiO_2/RGO	Photocatalysis (Visible light)		98% (90 min)	[179]
N-doped $HTiNbO_5$	Photocatalysis (Visible light)		95% (100 min)	[180]
Zn-doped Nb_2O_5	Photocatalysis (UV–Vis)		85% (180 min)/78% (180 min)	[181]
Nb/TiO_2 NPs	Photocatalysis (Solar light/UV)		65% (120 min)/70% (120 min)	[96]
F–C/Nb_2O_5	Photocatalysis (Visible light)		73% (60 min)	[182]
$NaNbO_3/Na_2Nb_4O_{11}$	Photocatalysis (UV)		95% (250 min)	[183]
Nitrogen-doped $KNbO_3$ nanocubes	Photocatalysis (Visible light)	RhB and Orange G	90% (18 h)/84% (24 h)	[184]
NbC/C nano-composites	Photocatalysis (Visible light)	RhB, MB, and MO	78.6%, 67.8%, and 57.1% (120 min)	[185]
Nb_2O_5/g-C_3N_4	Photocatalysis (Visible light)		94%, 87%, and 15% (60 min)	[109]
Nb_2O_5NC	Photocatalysis (UV)	RR120	98% (120 min)	[114]

Based on the studies presented in Table 3, the vast majority have centered on heterogeneous photocatalysis under UV or visible irradiation, although other strategies such as photo-Fenton and electrochemical processes are also explored [88,142,145,160,163,173]. In many cases, Nb_2O_5 is not employed in its pure form but rather as a dopant or a structural component within composites involving TiO_2, BiOCl, ZnO, g-C_3N_4, or carbonaceous materials. These combinations aim to enhance charge separation, extend light absorption into the visible range, and increase ROS generation, ultimately improving degradation efficiency [144,146,147,149,170,172].

Among the model compounds evaluated, methylene blue (MB) is the most frequently used dye. Catalysts such as Nb_2O_5 combined with $ZnNb_2O_6$ and H_2O_2 achieved complete removal in 60 min, while cerium-doped systems also showed efficiencies above 90% within short reaction times [78,153,154]. Heterojunctions involving TiO_2/Nb_2O_5,

$TiO_2/Nb_2O_5/SnO_2$/RGO, or Nb_2O_5/g-C_3N_4 have consistently reached removal rates close to 100% within 60–150 min, reflecting the role of niobium in enhancing light absorption and facilitating charge transfer [91,109,160].

Notably, several authors have specifically designed their systems for visible-light activation, reinforcing the capacity of Nb to reduce the band gap and activate catalysts under solar or simulated sunlight. This is evident in studies with Nb-N-TiO_2 [157], phosphate-doped Nb_2O_5, and NbC/C composites [152,158,164], which achieved high degradation efficiencies under visible light, albeit often requiring longer irradiation times.

A similar pattern has been observed in the removal of RhB, where multiple studies note degradation above 95%, and in one case 99.9% within 15 min, using Nb_2O_5 structured as "urchin-like" morphologies [79,108,112]. These findings emphasize the crucial role of niobium in designing more efficient photocatalytic architectures, such as Nb_2O_5 coupled with BiOCl or ZnO, which promote better electron transfer and stronger interactions at the catalyst surface [89,144,162].

Interestingly, hybrid approaches that combine Nb_2O_5 with electrochemical configurations have also been effective. Photoelectrocatalytic or electro-Fenton systems using TiO_2/Nb_2O_5 electrodes or Fe–Nb composites showed removal rates above 90% within short reaction windows [88,114]. These systems not only improve charge separation but also accelerate ROS formation via external bias or in situ generation of reactive species like H_2O_2.

Beyond MB and RhB, several reports show that integrating niobium either as a dopant or supporting element in established semiconductors yields significant gains in the degradation of other dyes, including Blue 19, bromophenol blue, and indigo carmine [142,144,145,149]. In many of these cases, the catalysts function effectively under visible light conditions. Although Nb_2O_5 in its pure state appears in fewer studies, the consensus points to niobium's pivotal role in modifying band structures, boosting light harvest, and improving reactive species generation. Consequently, niobium-based materials have emerged as strong candidates for addressing recalcitrant dyes through AOPs [146,147,173].

7.2. Pharmaceuticals

The removal of pharmaceutical contaminants from aquatic environments has become a major focus in recent years due to their persistence, toxicity, and potential to disrupt aquatic ecosystems and human health. Given the diverse range of pharmaceutical compounds available on the market, there has been substantial scientific output dedicated to understanding their degradation mechanisms and removal efficiency. Table 4 compiles relevant studies selected via the InOrdinatio method, listing the specific niobium-based materials employed, target pollutants, reported removal efficiencies, and corresponding references.

Table 4. Applications of Nb in the removal of pharmaceuticals.

Material	AOP	Pollutant	Pollutant Removal	Reference
Nb/BDD electrode	Electrochemical oxidation	Ibuprofen	80% (300 min)	[67]
Structured Sol–Gel Nb_2O_5	Photocatalysis (UV)		92% (300 min)	[69]
Structured Sol–Gel Nb_2O_5	Catalytic ozonation		100% (30min)	
Nb-TNFs	Photocatalytic ozonation (UV)		100% (12 min)	
Non-calcined Nb_2O_5	Photocatalysis (UV)		100% (300 min)	[75]
Ag/Nb_2O_5 Immobilized in Biopolymer	Photocatalysis Continuous (UV)		36% (40 min)	
Nb_2O_5/RGO wrapped on MoO_3 nanorods	Photocatalysis (vis)		95% (240 min)	[186]

Table 4. *Cont.*

Material	AOP	Pollutant	Pollutant Removal	Reference
Ti/IrO_2–Nb_2O_5 electrode Nb_2O_5/C_3N_4 (NOCN) p–n g-C_3N_4-mNb_2O_5 ZnS_{1-x} layers coated Nb_2O_{5-x}	Photocatalysis (UV)	Ibuprofen	44.5% (120 min)	[11]
		Acetylsalicylic acid	46% (120 min)	
		Paracetamol	55% (120 min)	
		17α-etinylestradiol	88.7% (120 min)	
Nb_2O_5/g-C_3N_4	Photocatalysis (UV)	17α-etinylestradiol	77.7% (120 min)	[187]
Nb_2O_5/Nb_2CT_X	Photocatalysis (UV)		69.2% (120 min)	
V/$NaNbO_3$	Photocatalysis Continuous (UV)		37.3% (120 min)	
Nb/BDD electrode	Photocatalysis (VIS)	Sulfasalazine	88.2% (60 min)	[74]
Nb/BDD electrode		Ciprofloxacin	85.4% (60 min)	
$Cd_{0.5}Zn_{0.5}S$/Nb_2O_5	Photoelectrochemical (UV–Vis)	Levofloxacin	100% (90 min)	[188]
ZOMO–NbO_x	Photolysis		100% (90 min)	
Nb_2O_5/H_2O_2	Electrochemical		<10% (90 min)	
Nb_2O_5/C	Photocatalytic-assisted activation of persulfate (UV)	Tetracycline	95% (160 min)	[189]
C_3N_4/Nb_2O_5	Photocatalysis (vis)		97.5% (180 min)	[190]
Fe_2O_3/Nb_2O_5	Photocatalysis (vis)		70% (80 min)	[191]
Nb/BDD electrode	Photocatalysis (UV–Vis)		90% (60 min)	[192]
Nb/BDD electrode	Photocatalysis (vis)		91.2% (180 min)	[108]
Nb_2O_5 nanofibers	Photocatalysis (vis)	Tetracycline	60% (90 min)	[193]
Fe/Nb_2O_5		Ciprofloxacin	71% (150 min)	
Cu/Nb_2O_5 + B51AA50:D52		Enrofloxacin	64.6% (150 min)	
Fe/Nb_2O_5	Electrochemical oxidation	Atenelol	100% (240 min)	[194]
Cu–Fe/Nb_2O_5	Electrochemical oxidation	Atenelol	100% (240 min)	[68]
Zr-doped g-C_3N_4/Nb_2O_5	Photocatalysis (vis)	Cephalexin	78% (60 min)	[61]
$CoFe_2O_4$@Nb_2O_5		Ciprofloxacin	83% (60 min)	
CeO_2–Nb_2O_5	Photocatalysis (vis)	Ciprofloxacin	98% (60 min)	[195]
Pt–TiO_2– Nb_2O_5	H_2O_2		95% (30 min)	[71]
Nb/BDD electrode	Electrochemical generation of H_2O_2	Levofloxacin	96% (270 min)	[196]
Nb/BDD electrode	Photocatalysis (vis)		91% (120 min)	[197]
Nb_2O_5/Ti electrodes	*hv* + H_2O_2 + Fe/Nb	Caffeine	100% (50 min)	[70]
Nb/BDD electrode	Heterogeneous Fenton		<10% (120 min)	
Structured Sol–Gel Nb_2O_5	*hv* + H_2O_2 + Fe/Nb	Catechol	94% (240 min)	
	Heterogeneous Fenton		95% (240 min)	
Structured Sol–Gel Nb_2O_5	Electrochemical oxidation	Sulfamethoxazole	88.8% (150 min)	[10]
Nb-TNFs		Propranolol	96% (150 min)	
Non-calcined Nb_2O_5		Carbamazepine	82.5% (150 min)	
Ag/Nb_2O_5 immobilized in biopolymer	Electro-Fenton process	Pentachlorophenol	100% (75 min)	[9]
Nb_2O_5/RGO wrapped on MoO_3 nanorods		Terbutryn	84.1% (75 min)	
Ti/IrO_2–Nb_2O_5 electrode		Chlorofenvinphos	46.2% (75 min)	
Nb_2O_5/C_3N_5 (NOCN) p–n		Diclofenac	100% (75 min)	
g-C_3N_4-mNb_2O_5	Photocatalysis (UV)	Fluoxetine	78% (90 min)	[198]
ZnS_{1-x} layers coated Nb_2O_{5-x}	Photocatalysis (vis)	Triclosan	90% (200 min)	[50]
Nb_2O_5/g-C_3N_4	Photocatalysis (UV)	Salicylic acid	23% (120 min)	[199]
Nb_2O_5/Nb_2CT_X			<10% (120 min)	
V/$NaNbO_3$			22% (120 min)	
Nb/BDD electrode	Photocatalysis (vis)	Levofloxacin	80.15% (240 min)	[64]
Nb/BDD electrode	Photocatalysis (UV)	Paracetamol	97.5% (60 min)	[27]
$Cd_{0.5}ZnS_{0.5}$/Nb_2O_5	Photocatalysis (UV)	Metformin	67% (210 min)	[200]
ZOMO–NbO_x	Photocatalysis (UV)	Diclofenac	100% (30 min)	[90]
Nb_2O_5/H_2O_2		Ketoprofen	100% (60 min)	

Table 4. *Cont.*

Material	AOP	Pollutant	Pollutant Removal	Reference
Nb_2O_5/C	Electrochemical oxidation	Prednisone	78% (240 min)	[201]
C_3N_4/Nb_2O_5	Electro-Fenton process	Cefoperazone	96.5% (60 min)	[202]
Fe_2O_3/Nb_2O_5	Electrochemical oxidation	Defluorination	82.5% (120 min)	[203]
Nb/BDD electrode	Photocatalysis (vis)	Carbamazepine	92 (120%)	[87]

Recent studies demonstrate that niobium-based materials hold significant promise in AOPs for the degradation of pharmaceuticals such as ibuprofen. Nb_2O_5 sol–gel catalysts, for instance, have proven effective in both photocatalysis and photocatalytic ozonation, with the latter achieving enhanced degradation rates and total organic carbon (TOC) removal due to synergistic effects. The implementation of structured Nb_2O_5 catalysts in continuous-flow systems has further optimized reaction efficiency by improving mass transfer and accessibility to active sites, achieving removal rates of 92% within 300 min and complete degradation after 12 min [69]. Moreover, incorporating Nb within titanate nanoflakes has been shown to reduce the band gap to 2.85 eV (compared to 3.4 eV in pristine titanate nanotubes), significantly enhancing visible-light-driven activity and leading to 95% degradation of ibuprofen in 240 min. Such morphological and structural modifications not only improve photocatalytic efficiency but also provide opportunities for light harvesting under milder irradiation conditions [186].

The formation of other heterojunctions has been a key strategy to improve the photocatalytic efficiency of Nb_2O_5 in antibiotics. Jones et al. (2022) [74] studied the use of Honeycomb Nb_2O_5/RGO wrapped on molybdenum trioxide (MoO_3) nanorods for visible-light-driven degradation of sulfasalazine and ciprofloxacin in water, reporting removal efficiencies of 88.3% and 85.4%, respectively, within 60 min. The incorporation of reduced graphene oxide creates a charge transfer bridge between Nb_2O_5 and MoO_3, which facilitates charge carrier separation and transfer. Similarly, Fernandes et. al., 2024 [188], explored the photolysis, electrochemical, and photoelectrochemical degradation of levofloxacin using Ti/IrO_2-Nb_2O_5 electrodes, with a 100%, <10%, and 100% removal in 90 min. The authors confirmed a synergistic effect between UV–Vis irradiation and the applied current, evidenced by higher TOC removal in the combined process.

Tetracycline is another antibiotic that has been extensively studied, with numerous investigations showcasing high degradation efficiencies achieved using niobium-based photocatalysts under optimized conditions. For instance, Nb_2O_5/C_3N_5 Z-scheme photocatalysts achieved over 95% degradation within 60 min under visible-light-assisted persulfate activation, emphasizing the synergistic effects of the Z-scheme structure and persulfate activation [189]. Nb_2O_5 modified g-C_3N_4 photocatalysts have similarly demonstrated efficient and stable antibiotic removal, reaching 90% degradation in 60 min under visible-light irradiation [192]. Vanadium-doped $NaNbO_3$ photocatalysts enhanced antibiotic degradation, achieving over 60% efficiency within 90 min, attributed to improved charge separation and increased generation of ROS [193]. Furthermore, Nb_2O_5/Nb_2CTx composites demonstrated exceptional performance in visible-light-driven photocatalysis, achieving up to 91% degradation of organic pollutants in 180 min [108].

The degradation of beta-blockers has also been explored using niobium-based materials. Heberle et al. (2019) [194] investigated the electrochemical oxidation of atenolol using Nb/BDD (boron-doped diamond) electrodes, demonstrating that Nb/BDD electrodes effectively generate hydroxyl radicals with high oxidative potential, leading to 75% mineralization of atenolol within 120 min. Comparable findings were reported by da Silva et al. (2019) [68], who applied Nb/BDD electrodes to degrade atenolol, focusing on the operational parameters influencing the efficiency of the process.

The comparison of these studies demonstrates the reproducibility and reliability of Nb/BDD electrodes for pharmaceutical degradation. Ibuprofen has also been degraded with Nb/BDD electrodes. The use of Nb as a substrate was shown to impact the conductivity of the material. Zanin et al. (2013) [67] reported that the density current for Si/BDD is lower than for Nb/BDD due to the better conductivity of niobium. The voltammograms show that the diamond has enough quality to be applied to electro-degradation, and also does not have the different characteristics of voltammograms obtained on plates or wafers.

Endocrine disruptors have also been a target for Nb_2O_5-based AOPs. Lenzi et al., 2022 [187], employed Ag/Nb_2O_5 immobilized in a biopolymer matrix to degrade 17α-ethinylestradiol in a continuous process. The integration of silver nanoparticles enhanced the photocatalytic activity of Nb_2O_5 by improving light absorption and facilitating charge transfer. This system's performance was particularly notable for its stability and reusability, factors that are critical for practical applications. Comparatively, Hong et al. (2016) [192] used a Nb_2O_5-modified g-C_3N_4 photocatalyst for the removal of antibiotic pollutants, emphasizing the enhanced visible light activity achieved through heterojunction formation. The contrast between these studies highlights the diverse strategies for functionalizing Nb-based materials to target specific pharmaceutical contaminants.

7.3. Heavy Metals

Heavy metals such as lead (Pb), mercury (Hg), cadmium (Cd), chromium (Cr), arsenic (As), nickel (Ni), and iron (Fe) are introduced into aquatic systems through industrial discharge, mining, agriculture, and improper waste disposal. While these metals are essential in industries such as textiles, paper production, and steel fabrication, their release into the environment poses serious risks. They accumulate in soil, water, and air, leading to long-term environmental and health issues. Their toxicity and persistence allow them to bioaccumulate, affecting biodiversity, food chains, and human health. Prolonged exposure can cause neurological damage, kidney failure, respiratory problems, and cancer, making effective detection, removal, and remediation crucial to reducing their harmful effects [204,205].

In this context, Table 5 presents key studies that explore niobium-based materials in the photodegradation, reduction, and oxidation of heavy metals.

The studies summarized in Table 5 indicate the application of niobium-based materials in the removal of heavy metals from wastewater through various photocatalytic and oxidation methods. One significant portion of the research focuses on photoreduction methods, particularly in the context of wastewater treatment involving dyes. A key aspect of these studies is the removal of Cr(VI), which plays an essential role in improving the efficiency of dye degradation. This highlights the relevance of Cr(VI) removal in enhancing overall treatment performance.

Table 5. Articles found with niobium with the ability to enhance the absorption and oxidation capacity of heavy metals.

Material	AOP	Pollutant	Heavy Metal Removal	Reference
Nb_2O_5 nanospheres	Photocatalysis (Visible light)	Pb	100% (80 min)	[206]
Nb_2O_5/microalgae C. reinhardtii	Photocatalysis (UV)	Cr(VI)	71% (120 min)	[207]
$Cu_{0.5}/Nb_2O_5$	Photocatalysis (UV)	Hg	95% (200 min; 150 °C)	[208]
Nb-Co-Ce/Al_2O_3 (electrode)	Oxidation		75% (60 min)	[209]
Nb-doped TiO_2	Oxidação	Id	70% (90 min)	[102]
	Photoreduction (UV)	Cd	100% (120 min)	

Table 5. *Cont.*

Material	AOP	Pollutant	Heavy Metal Removal	Reference
$Ti_{57}Nb_26Cu_{17}$	Photoreduction (Solar light)	Cr	97% (50 min)	[210]
$Nb_3O_7(OH)$	Photoreduction (UV)		90% (50 min)	[211]
$K_3NbO_2F_4$	Photoreduction (Solar light)		30% (3 h)	[212]
Nb_2O_5 nanorods/graphene	Photoreduction (UV)		95% (4 h)	[213]
Nb_2O_5/RGO	Photoreduction (UV)		87.7% (240 min)	[214]
Nb_2O_5/CuO	Photoreduction (Solar light)		84% (240 min)	[97]
Nb_2O_5 (anodizing)	Photoreduction (UV)		92% (120 min)	[215]
p-NiO/n- Nb_2O_5	Photoreduction (UV)		97% (180 min)	[116]
Nb_2O_5/red phosphorus	Photoreduction (UV)		97% (30 min)	[51]
Nb_2O_5 nanowires/carbon fibers	Photoreduction (UV)		99.9% (60 min)	[110]
Nb_2O_5 (anodic nanoporous)	Photoreduction (UV)		100% (45 min)	[14]
Nb_2O_5	Photoreduction (UV)		90% (120 min)	[216]

Studies on Cr(VI) removal highlight the effectiveness of Nb_2O_5-based photocatalysts, with multiple reports demonstrating significant reductions. Nb_2O_5/microalgae C. reinhardtii achieved 71% Cr(VI) removal within 120 min under UV light, while another study found that Nb_2O_5 exhibited 20% greater Cr(VI) reduction than TiO_2 under similar conditions [216]. Advanced anodic nanoporous Nb_2O_5 structures have further optimized photoreduction performance, offering a highly ordered porous structure that facilitates Cr(VI) adsorption and diffusion [14,215]. Heterojunctions, such as Nb_2O_5/red phosphorus, have also been developed to enhance electron transfer and electrochemical performance [51].

Beyond Cr(VI), Nb_2O_5-based materials show strong photocatalytic activity for other heavy metals. Nb_2O_5 nanospheres achieved 100% Pb removal within 80 min under visible light [212], while $Cu_{0.5}/Nb_2O_5$ demonstrated 95% Hg removal in 200 min at 150 °C. Nb_2O_5/graphene and Nb_2O_5/CuO have further improved pollutant removal rates, reaching 95% and 84% efficiencies under UV light, respectively [97,217]. Mesoporous heterostructures, as in Nb_2O_5/CuO, increase electron transfer, extending charge carrier lifetime. Additionally, anodic nanoporous Nb_2O_5 structures have demonstrated 100% pollutant removal within 45 min, emphasizing their potential for rapid and effective heavy metal remediation [14].

Oxidation-based methods, while somewhat less efficient than photocatalysis, still show promising results. Nb-Co-Ce/Al_2O_3 electrodes achieved 75% pollutant removal in 60 min, while Nb-doped TiO_2 reached 70% removal in 90 min [102]. Additionally, $Nb_3O_7(OH)$ nanoaggregates modified with carbonyl groups have shown high performance in visible-light-driven Cr(VI) reduction [190]. These studies suggest that Nb-based catalysts can be tailored for both photocatalytic and electrochemical oxidation pathways, offering versatility in environmental remediation strategies.

7.4. Personal Care Products

Personal care products (PCPs), including soaps, shampoos, deodorants, toothpaste, and lotions, contribute significantly to environmental pollution due to the presence of persistent organic pollutants such as microplastics, phthalates, parabens, sulfates, and chemical UV filters. These products have emerged as key pollutants because the chemicals in them can negatively affect the environment when washed off or improperly disposed

of. Growing concerns about their persistence in the ecosystem, bioaccumulation, and potential endocrine-disrupting effects have led to increased calls for more sustainable formulations, the use of biodegradable ingredients, and the adoption of eco-friendly packaging. Addressing these issues requires improvements in waste management practices, stricter regulations, and advancements in both product reformulation and wastewater treatment technologies [218–220].

Table 6 outlines various materials and their applications in pollutant removal using different processes such as Fenton, sonoelectrochemical methods, electrooxidation, and photocatalysis. Each entry provides detailed information on the target pollutants, removal efficiency under specific conditions, and references for further studies.

Table 6. Articles found with niobium with the ability to enhance the removal capacity of Personal Hygiene.

Material	AOP	Pollutant	PCP Removal	Reference
Nb-C/Fe(III)	Fenton	Dimethyl phthalate (DMP)	100% (60 min, pH 3.2)	[8]
Diamond-coated Nb (electrode)	Sonoelectrochemical	Triclosan	92% (15 min)	[221]
Nb_2O_5/Ti 3D printed electrode	Electrooxidation	Florfenicol	97.0% (120 min)	[203]
Nb_2O_5/RGO Sr doped	Photocatalysis (UV)	Benzophenone-3	94.6% (120 min)	[214]
Fe/Nb2O5-immobilized	Photocatalysis (UV)	Triclosan 2.8-dichlorodibenzene-p-dioxin	95% (15 min) 99% (15 min)	[50]
Cu/Nb_2O_5 Fe/Nb_2O_5 $Cu-Fe/Nb_2O_5$	Photocatalysis (UV)	Salicylic Acid	29% (400 °C, 120 min, pH 3.3) 27% (400 °C, 120 min, pH 7.0) 22% (400 °C, 120 min, pH 7.0)	[199]
Niobium BDD/anode	Electrooxidation	Methy paraben	99% (120 min)	[222]
TiO_2-Nb_2O_5	Photocatalysis (UV)	Salicylic Acid	72.9% (pH 5.0, 30 min)	[223]
Amorphous Nb_2O_5	Photocatalysis (UV)	Triclosan	99.9% (10 min)	[224]

Among the studies presented in Table 6, Zhang et al., 2024 [8], employed Nb-C/Fe(III) in the Fenton process and effectively removed DMP, achieving 100% degradation within 60 min at pH 3.2. In contrast, the Fe(III)/H_2O_2 system degrades only 28% of DMP in the same period. This enhanced performance was attributed to the material, as Fe(III) was almost completely reduced to Fe(II) within 10 min in the Nb_2C-6/Fe(III) system, demonstrating that Nb_2C-6 can directly and rapidly reduce Fe(III).

Photocatalysis has also demonstrated strong potential in the degradation of PCP pollutants using Nb_2O_5-based materials. Fe/Nb_2O_5-immobilized photocatalysts achieved 95% and 99% removal of triclosan and 2,8-dichlorodibenzodioxin, respectively, in just 15 min under UV irradiation [50]. For example, composites of Cu/Nb_2O_5 and Fe/Nb_2O_5 were calcined at 400 °C and tested for salicylic acid degradation at various pH values; after 120 min, removal efficiencies ranged from 22% to 29% [199]. TiO_2-Nb_2O_5 [223] is another photocatalytic material that removes salicylic acid with 72.9% efficiency in just 30 min under UV light at pH 5.0. Lastly, amorphous Nb_2O_5 [224] shows outstanding photocatalytic activity, achieving nearly complete removal (99.9%) of triclosan in just 10 min.

The incorporation of graphene-based materials and metal doping strategies has further enhanced the photocatalytic efficiency of Nb_2O_5. Nb_2O_5/RGO Sr-doped photocatalysts exhibited 94.6% degradation of benzophenone-3 under UV irradiation within 120 min [214].

In electrochemical oxidation processes, niobium has demonstrated promising applications as an electrode material. Diamond-coated Nb electrodes employed in sonoelectrochemical degradation achieved 92% removal of triclosan in 15 min [221]. Additionally, electrooxidation using an Nb/BDD anode led to 99% removal of methyl paraben within 120 min [222]. Studies have also shown that niobium-based electrodes offer advantages over silicon-based substrates for electrochemical advanced oxidation processes (EAOPs), providing scalability for industrial applications [68].

7.5. Pesticides

The use of Nb_2O_5 in the degradation of pesticides has gained attention in recent years due to its photocatalytic properties and its effectiveness in AOPs. These niobium catalysts are synthesized through different methods, typically involving the sol–gel, Pechini, or hydrothermal processes, sometimes with the addition of nanoparticles to enhance photocatalyst efficiency. During synthesis, parameters such as calcination temperature and stirring speed are evaluated. These materials are commonly characterized by techniques such as X-ray diffraction, thermogravimetric analysis, scanning and transmission electron microscopy, infrared spectroscopy, energy-dispersive spectroscopy, and diffuse reflectance spectroscopy, among others [36].

The sol–gel method has been used in several studies to synthesize Nb_2O_5 nanoparticles for the photocatalytic degradation of herbicides such as methyl viologen. It has proven to be a promising approach for degrading contaminants, although its efficiency is strongly influenced by calcination temperature. As crystallinity rises with increasing temperature, the catalyst's capacity to adsorb compounds on its surface decreases, leading to lower degradation rates [225].

Likewise, other herbicides like atrazine and 2,4-dichlorophenoxyacetic acid (2,4-D), widely used to control weeds in crops such as corn, rice, soybeans, and sugarcane, have been studied as target molecules using niobium-based photocatalysts produced by the Pechini method. Both synthesis and doping with different materials can significantly improve the photocatalytic activity of niobium oxides. In comparative experiments, direct photolysis of these contaminants versus photocatalysis with synthesized Nb-based materials revealed a substantial improvement in herbicide removal, reaching 40% and 81%, respectively, which marks an important step toward large-scale water treatment [76]. Atrazine degradation has also been assessed using niobium-based catalysts decorated with cobalt ($CoFe_2O_4$) and magnesium ($MgFe_2O_4$) ferrite nanoparticles. These systems showed higher efficiencies than photolysis, although comparisons with pure Nb_2O_5 did not indicate a significant difference in herbicide removal [226].

Heterostructures based on niobates and nickel oxide have been employed to degrade compounds like phenol, yielding significant removals and advancing knowledge of effluent treatment with niobium-based materials [227]. Another material used to form heterojunctions with Nb_2O_5 is fibrous silica-titania (FST), which showed high efficacy in phenol degradation. The Si–O–Nb and Ti–O–Nb interactions act as electron traps, reducing charge carrier recombination [228]. Graphitic carbon nitride nanosheets have demonstrated a similar effect by preventing recombination and facilitating charge transfer, thereby boosting photocatalytic activity under visible-light irradiation [73].

Due to their high surface area, porous-structured anodes have also proven efficient in degrading certain organic contaminants. Niobium carbide (NbC) has been used in these processes because of its high melting point and resistance to chemical attack and thermal shock, although few studies have examined its electrocatalytic applications. In one case, promising electrocatalytic activity led to phenol removal of about 83%, which increased to

complete contaminant removal when the material was modified with metal oxides such as RuO_2 [229].

Other combinations of metal oxides, such as tin oxide (SnO_2), antimony oxide Sb_2O_3, and lead oxide (PbO_2), have been employed to synthesize a niobium-based anode for phenol degradation by electrochemical processes [217]. Zirconium dioxide (ZrO_2) has also been tested with Nb_2O_5 for phenol photodegradation [230]. In addition, ZnO nanorods with Nb_2O_5 were synthesized to evaluate photocatalytic activity for the same contaminant under solar, fluorescent, and UV irradiation. These nanocomposites provided more efficient degradation and demonstrated higher photocatalytic activity than pure materials, likely due to a lower electron–hole recombination rate [231]. Nb_2O_5 nanorods can also be coated with TiO_2 nanoparticles to form photocatalytic nanocomposites. However, employing reduced graphene oxide to immobilize these compounds has been reported to further enhance photocatalytic performance, given its high adsorption capacity, increased sensitivity to visible light, reduced charge recombination, improved electron transfer, and a larger number of catalytic sites [99].

Although niobium-based electrodes are primarily used in heterogeneous photocatalysis, other AOPs have also employed these catalysts. For instance, Nb_2O_5/CeO_2 materials have been implemented in photo-Fenton-type processes under visible-light irradiation [156]. Further methods, such as electrooxidation, electro-Fenton, and photo-electro-Fenton, have been tested to remove various organochlorines and organophosphorus compounds like pentachlorophenol and chlorfenvinphos, an insecticide and acaricide used against multiple pests in fruit and vegetable crops. A boron-doped diamond film on a niobium mesh also proved effective in degrading several micropollutants, achieving removal rates of up to 80% across all processes [9]. To parallel the approach seen in other removal investigations, these pesticide-related studies confirm that niobium-based catalysts exhibit considerable versatility in AOPs, and other studies have also been developed (Table 7).

Table 7. Applications of Nb in the removal of pesticides.

Material	AOP	Pollutant	Pollutant Removal	Reference
$Zr_6Nb_2O_{17}/Nb_2O_5$ heterojunction	Photocatalysis (UV-B and Visible light)	Phenol	90% (150 min)/91% (360 min)	[232]
Nb_2O_5/ZnO nanocomposites	Photocatalysis (UV-A)		100% (60 min)	[233]
PtRu/NbC membrane anode	Electrochemical oxidation		99.7% (6 min)	[234]
Nb/PbO_2 anode	Electrochemical oxidation	Dimethoate	90% COD removal (8 h)	[235]
NbPd-zeolite nanocomposites	Photocatalysis (Visible light)	2-chloro phenol and 4-chloro phenol	97% (270 min)/87% (180 min)	[236]
Nb/Ti binary oxides	Photocatalysis (UV-B)	Phenol, tetrahydrofuran and Cyclohexanol	94.6%/56.8%/51.4% (100 min)	[237]
$CdNb_2O_6/Cd_2Nb_2O_7$ heterojunction	Photocatalysis (UV-A and Visible light)	Phenol	100% (70 min)/97% (120 min)	[238]

7.6. Hormones

Endocrine-disrupting chemicals (EDCs), including synthetic and natural hormones, have been identified as major environmental pollutants due to their widespread presence in pharmaceuticals, personal care products, agricultural runoff, and industrial effluents. These compounds interfere with hormonal regulation in living organisms, leading to reproductive and developmental disruptions, particularly in aquatic ecosystems [239]. The persistence of EDCs in water bodies necessitates advanced treatment strategies to effectively mitigate their impact.

Recent studies have explored the potential of niobium-based materials to enhance the removal of hormone pollutants via AOPs. Table 8 summarizes key studies on the use of niobium-based photocatalysts and electrochemical materials for hormone degradation.

Table 8. Studies using niobium-type catalyst to enhance hormone degradation.

Material	AOP	Pollutant	Hormones Removal	Reference
Nb/BDD anode	Electrooxidation	Estrone	98% (30 min, filter-press reactor)	[240]
$NiCu/Nb_2O_5$	Photocatalysis (UV-A)	17β-estradiol	82% (180 min)	[241]
Nb_2O_5	Photocatalysis (UV)	17α-ethinylestradiol	88.7% (120 min)	[11]
Ag/Nb_2O_5	Photocatalysis (UV)	17α-ethinylestradiol	77.7% (120 min)	[187]
$KNbO_3$	Photocatalysis (UV)	Bisphenol A (BPA)	78.7% (1200 min)	[184]
$Bi_4NbO_8Cl/BiOCl/Nb_2O_5$	Photocatalysis (UV–Vis)	Bisphenol A	67% (240 min)	[66]

Table 8 presents various materials and their effectiveness in removing hormone pollutants, specifically targeting different types of estrogen hormones. The materials used include Nb/BDD anodes, $NiCu/Nb_2O_5$, Nb_2O_5, and Ag/Nb_2O_5, each applying different processes like electrooxidation and photocatalysis, with varying degrees of removal efficiency under specific conditions.

Electrochemical oxidation using niobium-based electrodes has demonstrated remarkable efficiency in hormone removal. For instance, Nb/BDD anodes exhibited 98% removal of estrone within 30 min using a filter-press reactor [240]. This high efficiency is attributed to the strong oxidative power of hydroxyl radicals generated at the Nb/BDD surface, facilitating the breakdown of estrogenic compounds. Photocatalytic degradation using Nb_2O_5-based materials has also shown promising results. $NiCu/Nb_2O_5$ heterojunctions achieved 82% degradation of 17β-estradiol under UV-A irradiation in 180 min [241]. Similarly, pristine Nb_2O_5 photocatalysts demonstrated 88.7% removal of 17α-ethinylestradiol within 120 min under UV exposure. In this work, various calcination temperatures (373–873 K) were evaluated. It was observed that the band gap of the structure decreased as the temperature of calcination increased. The authors indicate that this behavior corroborates theories of interatomic spacing, which grows as atomic vibrations intensify, leading to a decrease in the potential observed by electrons in the material and, consequently, reducing the size of the band gap [11].

The incorporation of silver into Nb_2O_5 has been investigated as a strategy to enhance photocatalytic efficiency. Ag/Nb_2O_5 composites exhibited 77.7% degradation of 17α-ethinylestradiol after 120 min of UV irradiation [187]. However, immobilization of this material in alginate spheres resulted in a lower degradation rate, reducing efficiency to 69.2% in batch systems and 37.3% in continuous-flow systems (10 L h^{-1}), indicating the influence of mass transfer limitations on catalyst performance.

Structural modifications and phase control have also been explored to optimize the photocatalytic activity of niobium-based materials. Potassium niobite ($KNbO_3$) perovskites were synthesized via hydrothermal methods. When doped with nitrogen by heating with urea at 425 °C, the material maintained its nanocubic morphology. Nitrogen doping further enhanced the photocatalytic performance of $KNbO_3$ by reducing its band gap from 3.13 to 2.76 eV, leading to improved visible-light absorption and charge carrier separation [184].

Heterostructured $Bi_4NbO_8Cl/BiOCl/Nb_2O_5$ composites exhibited enhanced BPA degradation under UV–Vis irradiation, achieving 67% removal within 240 min. The photocatalytic performance of these materials was found to be highly dependent on synthesis conditions, particularly acid concentration, which influenced the formation of distinct heterojunctions [66].

8. Environmental Implications

The utilization of Nb_2O_5-based catalysts in AOPs presents significant environmental benefits, primarily through the effective removal of recalcitrant pollutants from aquatic ecosystems. Their ability to degrade a wide range of contaminants, such as pharmaceuticals, pesticides, dyes, and personal care products, addresses critical environmental concerns, reducing bioaccumulation, ecological toxicity, and risks to human health [100]. Furthermore, the chemical stability and reusability of niobium-based materials may minimize secondary waste generation, enhancing the sustainability of wastewater treatment processes [242].

Despite these benefits, careful consideration of potential toxicological risks is necessary. While Nb_2O_5 itself is relatively inert and non-toxic, modifications involving metal doping or coupling with other materials may introduce components that could pose environmental risks. For instance, certain transition metals utilized as dopants might leach into treated water, potentially affecting aquatic life and human health at elevated concentrations. Additionally, incomplete degradation of pollutants might lead to intermediate products with unknown or enhanced toxicity compared to the original contaminants, necessitating comprehensive toxicity assessments of treated effluents [75,223].

Therefore, future research should systematically evaluate the ecotoxicity and environmental compatibility of Nb_2O_5-based catalytic systems. Integrated studies combining catalytic efficiency with ecotoxicological analyses, such as bioassays and chronic toxicity tests, will be crucial to ensure that the application of these advanced catalysts effectively mitigates environmental harm without inadvertently generating new ecological hazards.

9. Current Limitations and Future Directions

Despite promising performance in lab-scale studies, Nb_2O_5-based catalysts face several challenges that hinder their broader implementation in advanced oxidation processes. One persistent issue is long-term stability. Although niobium displays intrinsic chemical robustness, including resistance to corrosion and leaching, systematic assessments of activity retention over extended reuse cycles remain limited. Some encouraging examples exist—such as anodized Nb_2O_5 monoliths maintaining ~98% dye removal over 10 consecutive runs—but these tests are typically conducted under idealized conditions that fail to capture the variability and complexity of real wastewater systems.

Another key barrier is scalability. While Nb_2O_5 materials can be engineered into highly active forms, the synthetic routes often rely on techniques like atomic layer deposition or hydrothermal growth, which are energy-intensive, equipment-dependent, and poorly suited to large-scale production [40]. The relatively low abundance and higher cost of niobium, compared to oxides like TiO_2 or Fe_2O_3, further complicate commercialization. Although Nb-doped TiO_2 anodes have shown cost–performance advantages over Magnéli phases and BDD electrodes [243], producing these materials in industrial quantities with consistent quality remains an unsolved issue [244].

In addition to material and process scalability, a central conceptual limitation persists. Many studies emphasize pollutant removal efficiency as the primary performance metric, while aspects such as mineralization, transformation product identification, and residual toxicity are often overlooked. This gap compromises the environmental relevance of the findings, especially considering that partially oxidized pharmaceutical or hormone derivatives may retain bioactivity or even form more persistent intermediates. Without comprehensive analysis of degradation pathways, total organic carbon removal, and toxicological impacts, the real benefits and risks of applying Nb_2O_5-based systems remain difficult to evaluate.

Bridging these gaps will require the transition from model systems to real-world validation. While initial studies have explored dye degradation in synthetic solutions, future

efforts must prioritize testing Nb_2O_5 catalysts under authentic effluent conditions, such as industrial discharges, hospital wastewater, or surface water impacted by agricultural runoff. These environments introduce interfering species, fluctuating pH, and complex contaminant mixtures that could impact catalyst performance, stability, and reusability. Initial demonstrations in textile wastewater models are promising, but broader studies under these realistic scenarios are urgently needed to evaluate issues such as catalyst fouling, oxidant depletion, and light attenuation.

Scaling from batch systems to continuous-flow configurations is another critical frontier. Reactor engineering must consider photon distribution, oxidant diffusion, hydraulic retention time, and catalyst immobilization strategies. Designing systems like fixed-bed photocatalytic reactors, photoelectrochemical cells, or membrane-supported Nb_2O_5 layers could offer scalable, reusable formats suitable for field application. Pilot-scale implementations would also allow for cost–benefit analyses and durability tests under operational loads, providing insight into the techno-economic viability of Nb-based AOPs.

Equally important is the need for deeper mechanistic understanding. Although Nb_2O_5 exhibits unique Lewis acid sites and can form surface-bound peroxo and superoxo species upon contact with oxidants like H_2O_2 [71], the detailed pathways of ROS generation, radical selectivity, and catalyst–pollutant interactions are not yet fully elucidated. Key structural motifs, such as the roles of NbO_4 versus NbO_6 coordination sites, or the effect of Nb–O–metal bonding in doped systems, require further clarification. Progress in this area will likely depend on in situ and operando techniques, such as DRIFTS, EPR, synchrotron XAS, or time-resolved photoluminescence, to directly observe reaction intermediates and surface dynamics. Understanding how charge carriers migrate, how surface acidity modulates adsorption and activation, and how various ROS interact with complex organic molecules will enable more purposeful catalyst design. Strategies such as band gap engineering, co-catalyst integration, and surface modification can then be optimized not only for activity, but also for selectivity, stability, and environmental compatibility.

10. Conclusions

Niobium-based materials have emerged as promising catalysts in AOPs, demonstrating high efficiency in the degradation of emerging contaminants. The findings presented in this review underscore the impact of structural modifications, dopant incorporation, and heterojunction engineering in enhancing the photocatalytic, electrocatalytic, and ozonation-assisted degradation mechanisms. Notably, the ability of Nb_2O_5 to extend light absorption, improve charge separation, and facilitate ROS generation reinforces its potential as an alternative to conventional photocatalysts.

Despite significant progress in the development of niobium-based materials for water treatment technologies, several challenges remain that hinder their large-scale application. Issues related to long-term stability, recyclability, and scalability continue to limit their feasibility for environmental remediation. While extensive research has focused on the degradation of synthetic dyes, a more pressing concern is the removal of pollutants with higher ecological risks, such as pharmaceuticals, endocrine-disrupting compounds, and industrial contaminants. These substances are frequently detected in natural water bodies and wastewater streams, necessitating the development of more efficient treatment solutions.

One promising approach to enhancing the applicability of niobium-based catalysts is their integration into hybrid AOPs and solar-driven treatment systems. The combination of niobium catalysts with other photocatalysts or co-catalysts enables synergistic interactions, facilitating charge separation and improving catalytic performance. Furthermore, the utilization of solar energy for photocatalytic activation aligns with global sustainability objectives by reducing energy consumption and operational costs. These advancements

contribute to the development of energy-efficient and environmentally friendly water treatment technologies.

Based on the reviewed literature, no single AOP emerges as universally superior; rather, the most effective process is highly dependent on the target pollutant class. Heterogeneous photocatalysis, particularly with visible-light-active heterostructures, demonstrates exceptional efficiency for the decolorization of dyes due to the direct attack on chromophoric structures. Electrochemical oxidation on high-overpotential anodes like Nb/BDD shows particular promise for recalcitrant compounds that are resistant to other methods, though at a higher energy cost. Fenton-like processes using Nb_2O_5 offer a sludge-free alternative to traditional Fenton but are highly sensitive to pH, limiting their operational window.

For complex pharmaceuticals like antibiotics, hybrid processes such as photocatalytic ozonation and photo-electrocatalysis appear more effective, achieving higher rates of mineralization by generating a greater flux and variety of ROS. This is because the combination of methods can overcome the intrinsic limitations of a single process. This synergy often leads to significantly improved kinetics and a greater potential for complete mineralization, addressing the shortcomings of the individual techniques. It must be noted, however, that a direct comparison of efficiencies across studies remains challenging due to significant variations in experimental conditions, highlighting a need for standardized testing protocols in the field.

The selection of optimal material features is directly dictated by the target pollutant class. For large cationic dyes, properties that enhance adsorption and rapid decolorization are paramount, such as high surface area, favorable surface charge (negative at pH > 3.8), and abundant defects found in amorphous or TT-Nb_2O_5 phases. Conversely, the complete mineralization of complex pharmaceuticals and hormones requires advanced heterostructures that preserve strong redox potentials for potent ROS generation, supplemented by Nb_2O_5's intrinsic Lewis acidity for alternative surface activation pathways. In other AOPs, different features become critical. For heavy metal photoreduction, a highly negative conduction band potential is the key feature for electron donation. Finally, for the most recalcitrant pollutants, the focus shifts to robust systems where high-overpotential Nb/BDD anodes enable near-complete electrochemical mineralization, and the chemical stability of Nb_2O_5 in acidic media makes it an effective catalyst for sludge-free, Fenton-like reactions.

Future research should focus on the rational design of niobium-based heterostructures to maximize catalytic efficiency and stability. The incorporation of co-catalysts, such as noble metals, carbon-based materials, or metal oxides, may further enhance the reactivity and selectivity of these catalysts. Additionally, the application of machine learning methodologies represents a promising strategy for optimizing reaction conditions, predicting catalyst performance, and accelerating the discovery of new niobium-based materials.

To transition from laboratory-scale studies to large-scale implementation, standardized evaluation criteria for niobium-based catalysts must be established. Strengthening collaborative research networks among academic institutions, industry partners, and regulatory agencies will be essential to overcoming existing limitations and promoting the practical deployment of these materials in water treatment systems. By addressing these challenges through interdisciplinary research and technological innovation, niobium-based materials can significantly contribute to environmental remediation and sustainable water management.

Supplementary Materials: The following supporting information can be downloaded at: https://www.mdpi.com/article/10.3390/environments12090311/s1, Table S1: PRISMA 2020 Checklist.

Author Contributions: M.Z.F.: Conceptualization, Methodology, Formal analysis, Writing—Original Draft, Visualization. J.F.: Conceptualization, Data curation, Methodology, Formal analysis, Writing—Original Draft. W.S.: Conceptualization, Data curation, Methodology, Formal analysis, Writing—Original Draft. T.S.L.: Data curation, Methodology, Writing—Original Draft. G.G.L.: Supervision, Writing—Original Draft, Writing—Review and Editing. A.J.M.: Supervision, Writing—Original Draft, Writing—Review and Editing. All authors have read and agreed to the published version of the manuscript.

Funding: This study was financed by the São Paulo Research Foundation (FAPESP), Brazil—Process numbers: 2022/12895-1, 2024/12716-5, 2024/13723-5, 2022/15337-0, and 2022/04561-6.

Data Availability Statement: No new data were created or analyzed in this study. Data sharing is not applicable to this article.

Conflicts of Interest: The authors declare no conflict of interest.

References

1. Amebelu, A.; Ban, R.; Bhagwan, J.; Brown, J.; Chilengi, R.; Chandler, C.; Colford, J.M.; Cumming, O.; Curtis, V.; Evans, B.E.; et al. The Lancet Commission on Water, Sanitation and Hygiene, and Health. *Lancet* **2021**, *398*, 1469–1470. [CrossRef]
2. Wolf, J.; Hubbard, S.; Brauer, M.; Ambelu, A.; Arnold, B.F.; Bain, R.; Bauza, V.; Brown, J.; Caruso, B.A.; Clasen, T.; et al. Effectiveness of Interventions to Improve Drinking Water, Sanitation, and Handwashing with Soap on Risk of Diarrhoeal Disease in Children in Low-Income and Middle-Income Settings: A Systematic Review and Meta-Analysis. *Lancet* **2022**, *400*, 48–59. [CrossRef]
3. Yuan, H.; Wang, X.; Gao, L.; Wang, T.; Liu, B.; Fang, D.; Gao, Y. Progress towards the Sustainable Development Goals Has Been Slowed by Indirect Effects of the COVID-19 Pandemic. *Commun. Earth Environ.* **2023**, *4*, 184. [CrossRef]
4. Licci, S.; Marmonier, P.; Wharton, G.; Delolme, C.; Mermillod-Blondin, F.; Simon, L.; Vallier, F.; Bouma, T.J.; Puijalon, S. Scale-Dependent Effects of Vegetation on Flow Velocity and Biogeochemical Conditions in Aquatic Systems. *Sci. Total Environ.* **2022**, *833*, 155123. [CrossRef]
5. Shevgan, M. *Advanced Oxidation Technologies Market Analysis & Forecast: 2025–2032*; Coherent Market Insights: Burlingame, CA, USA, 2025.
6. Miklos, D.B.; Remy, C.; Jekel, M.; Linden, K.G.; Drewes, J.E.; Hübner, U. Evaluation of Advanced Oxidation Processes for Water and Wastewater Treatment–A Critical Review. *Water Res.* **2018**, *139*, 118–131. [CrossRef]
7. Mazivila, S.J.; Ricardo, I.A.; Leitão, J.M.M.; Esteves da Silva, J.C.G. A Review on Advanced Oxidation Processes: From Classical to New Perspectives Coupled to Two- and Multi-Way Calibration Strategies to Monitor Degradation of Contaminants in Environmental Samples. *Trends Environ. Anal. Chem.* **2019**, *24*, e00072. [CrossRef]
8. Zhang, Z.X.; Zhou, C.Y.; Zhou, P.; Liu, Y.; Zhang, H.; Du, Y.; He, C.S.; Xiong, Z.K.; Lai, B. Exceptionally Accelerated Fe(III)/Fe(II) Redox Couple by Niobium Carbide MXene: A Green and Long-Lasting Enhanced Fenton Oxidation. *Appl. Catal. B Environ.* **2024**, *342*, 123385. [CrossRef]
9. Roccamante, M.; Salmerón, I.; Ruiz, A.; Oller, I.; Malato, S. New Approaches to Solar Advanced Oxidation Processes for Elimination of Priority Substances Based on Electrooxidation and Ozonation at Pilot Plant Scale. *Catal. Today* **2020**, *355*, 844–850. [CrossRef]
10. García-Espinoza, J.D.; Nacheva, P.M. Effect of Electrolytes on the Simultaneous Electrochemical Oxidation of Sulfamethoxazole, Propranolol and Carbamazepine: Behaviors, by-Products and Acute Toxicity. *Environ. Sci. Pollut. Res.* **2019**, *26*, 6855–6867. [CrossRef]
11. Abreu, E.; Fidelis, M.Z.; Fuziki, M.E.; Malikoski, R.M.; Mastsubara, M.C.; Imada, R.E.; Diaz de Tuesta, J.L.; Gomes, H.T.; Anziliero, M.D.; Baldykowski, B.; et al. Degradation of Emerging Contaminants: Effect of Thermal Treatment on Nb2o5 as Photocatalyst. *J. Photochem. Photobiol. A Chem.* **2021**, *419*, 113484. [CrossRef]
12. Hodges, B.C.; Cates, E.L.; Kim, J.-H. Challenges and Prospects of Advanced Oxidation Water Treatment Processes Using Catalytic Nanomaterials. *Nat. Nanotechnol.* **2018**, *13*, 642–650. [CrossRef]
13. Mahdi, M.M.; Salim, E.T.; Obaid, A.S. A Comparison Study of Au@Nb_2O_5 Core–Shell Nanoparticle Using Two Different Laser Flounces. *Plasmonics* **2025**, *20*, 6313–6326. [CrossRef]
14. Alias, N.; Hussain, Z.; Tan, W.K.; Kawamura, G.; Muto, H.; Matsuda, A.; Lockman, Z. Nanoporous Anodic Nb_2O_5 with Pore-in-Pore Structure Formation and Its Application for the Photoreduction of Cr(VI). *Chemosphere* **2021**, *283*, 131231. [CrossRef] [PubMed]
15. Pagani, R.N.; Pedroso, B.; dos Santos, C.B.; Picinin, C.T.; Kovaleski, J.L. Methodi Ordinatio 2.0: Revisited under Statistical Estimation, and Presenting FInder and RankIn. *Qual. Quant.* **2023**, *57*, 4563–4602. [CrossRef]

16. Sundarapandi Edward, I.E.; Ponpandi, R. Challenges, Strategies and Opportunities for Wind Farm Incorporated Power Systems: A Review with Bibliographic Coupling Analysis. *Environ. Sci. Pollut. Res.* **2022**, *30*, 11332–11356. [CrossRef] [PubMed]
17. Zanata, A.C.; Bertan, F.A.B.; Bernardi, C.; dos Santos, C.S.; Ferreira, G.A.; De Oliveira, J.A.; Fernandes, M.D.C.C.; Anschau, A. Obtention of Microalgal Biomass Tolerant to Herbicides for Production of Bio-Fertilizers: A Review Based on Methodi Ordinatio Methodology. *Orbital Electron. J. Chem.* **2019**, *11*, 399–401. [CrossRef]
18. da Silva, V.L.; Kovaleski, J.L.; Pagani, R.N.; Gomes, M.A.S. Industry 4.0 Implementations: A Systematic Review of Approaches and Main Applicabilities in the Broiler Meat Production Chain. *Worlds Poult. Sci. J.* **2023**, *79*, 563–579. [CrossRef]
19. Batista, D.M.; Goulart, E.V.; de Oliveira, A.R.P.; Santos, P.F.; Valois, R.C.; Ferreira, M.G.S. ASSISTIVE AND EDUCATIONAL TECHNOLOGIES FOR CHILDREN WITH AUTISM SPECTRUM DISORDER: A BIBLIOMETRIC STUDY. *Cogitare Enferm.* **2024**, *29*, e95019. [CrossRef]
20. Da Silva, V.L.; Kovaleski, J.L.; Pagani, R.N.; Gomes, M.A.S. Technology Transfer Model Oriented to Industry 4.0. *Braz. J. Oper. Prod. Manag.* **2024**, *21*, 1777. [CrossRef]
21. Hernández-Contreras, M.; Cruz, J.C.; Gurrola, M.P.; Pamplona Solis, B.; Vega-Azamar, R.E. Application of Nanosilica in the Construction Industry: A Bibliometric Analysis Using Methodi Ordinatio. *MethodsX* **2024**, *12*, 102642. [CrossRef]
22. Yoshino, R.T.; Pinto, M.M.A.; Pontes, J.; Treinta, F.T.; Justo, J.F.; Santos, M.M.D. Educational Test Bed 4.0: A Teaching Tool for Industry 4.0. *Eur. J. Eng. Educ.* **2020**, *45*, 1002–1023. [CrossRef]
23. Zarhri, Z.; Rosado Martinez, W.; Dominguez Lepe, J.A.; Vega Azamar, R.E.; Chan Juarez, M.; Pamplona Solis, B.B. 30 Years of Rubberized Concrete Investigations (1990–2020). A Bibliometric Analysis. *Rev. ALCONPAT* **2022**, *12*, 1. [CrossRef]
24. de Carvalho, G.D.G.; Sokulski, C.C.; da Silva, W.V.; de Carvalho, H.G.; de Moura, R.V.; de Francisco, A.C.; da Veiga, C.P. Bibliometrics and Systematic Reviews: A Comparison between the Proknow-C and the Methodi Ordinatio. *J. Informetr.* **2020**, *14*, 101043. [CrossRef]
25. Barros, M.V.; Ferreira, M.B.; do Prado, G.F.; Piekarski, C.M.; Picinin, C.T. The Interaction between Knowledge Management and Technology Transfer: A Current Literature Review between 2013 and 2018. *J. Technol. Transf.* **2020**, *45*, 1585–1606. [CrossRef]
26. Sierdovski, M.; Pilatti, L.A.; Rubbo, P. Organizational Competencies in the Development of Environmental, Social, and Governance (ESG) Criteria in the Industrial Sector. *Sustainability* **2022**, *14*, 13463. [CrossRef]
27. Oliveira, J.R.P.; Ribas, L.S.; Napoli, J.S.; Abreu, E.; Diaz de Tuesta, J.L.; Gomes, H.T.; Tusset, A.M.; Lenzi, G.G. Green Magnetic Nanoparticles $CoFe_2O_4$@Nb_5O_2 Applied in Paracetamol Removal. *Magnetochemistry* **2023**, *9*, 200. [CrossRef]
28. Regatieri, H.R.; Ando Junior, O.H.; Salgado, J.R.C. Systematic Review of Lithium-Ion Battery Recycling Literature Using ProKnow-C and Methodi Ordinatio. *Energies* **2022**, *15*, 1485. [CrossRef]
29. Sarmento, A.L.C.; Sá, B.S.; Vasconcelos, A.G.; Arcanjo, D.D.R.; Durazzo, A.; Lucarini, M.; de Souza de Almeida Leite, J.R.; Sousa, H.A.; Kückelhaus, S.A.S. Perspectives on the Therapeutic Effects of Pelvic Floor Electrical Stimulation: A Systematic Review. *Int. J. Environ. Res. Public Health* **2022**, *19*, 14035. [CrossRef]
30. Lizot, M.; Júnior, P.P.A.; Trojan, F.; Magacho, C.S.; Thesari, S.S.; Goffi, A.S. Analysis of Evaluation Methods of Sustainable Supply Chain Management in Production Engineering Journals with High Impact. *Sustainability* **2019**, *12*, 270. [CrossRef]
31. De Bail, R.F.; Kovaleski, J.L.; da Silva, V.L.; Pagani, R.N.; de Chiroli, D.M.G. Internet of Things in Disaster Management: Technologies and Uses. *Environ. Hazards* **2021**, *20*, 493–513. [CrossRef]
32. Rosa, F.M.; Mota, T.F.M.; Busso, C.; de Arruda, P.V.; Brito, P.E.M.; Miranda, J.P.M.; Trentin, A.B.; Dekker, R.F.H.; Cunha, M.A.A. da Filamentous Fungi as Bioremediation Agents of Industrial Effluents: A Systematic Review. *Fermentation* **2024**, *10*, 143. [CrossRef]
33. Wang, B.; Zhou, X.; Xie, Y.; Han, X.; Zhang, S.; Zhu, Z.; Park, S.; Han, J. The Application of MnO_x/TiO_2 Catalyst in SCR-NH3 Reaction. *Preprint* **2023**. [CrossRef]
34. Page, M.J.; McKenzie, J.E.; Bossuyt, P.M.; Boutron, I.; Hoffmann, T.C.; Mulrow, C.D.; Shamseer, L.; Tetzlaff, J.M.; Akl, E.A.; Brennan, S.E.; et al. The PRISMA 2020 Statement: An Updated Guideline for Reporting Systematic Reviews. *BMJ* **2021**, *372*, n71. [CrossRef]
35. Khalid, M.U.; Rudokaite, A.; da Silva, A.M.H.; Kirsnyte-Snioke, M.; Stirke, A.; Melo, W.C.M.A. A Comprehensive Review of Niobium Nanoparticles: Synthesis, Characterization, Applications in Health Sciences, and Future Challenges. *Nanomaterials* **2025**, *15*, 106. [CrossRef]
36. Lopes, O.F.; de Mendonça, V.R.; Silva, F.B.F.; Paris, E.C.; Ribeiro, C. NIOBIUM OXIDES: AN OVERVIEW OF THE SYNTHESIS OF Nb_2O_5AND ITS APPLICATION IN HETEROGENEOUS PHOTOCATALYSIS. *Quim. Nova* **2014**, *38*. [CrossRef]
37. Ahmad, I.; Al-Qattan, A.; Iqbal, M.Z.; Anas, A.; Khasawneh, M.A.; Obaidullah, A.J.; Mahal, A.; Duan, M.; Al Zoubi, W.; Ghadi, Y.Y.; et al. A Systematic Review on Nb2O5-Based Photocatalysts: Crystallography, Synthetic Methods, Design Strategies, and Photocatalytic Mechanisms. *Adv. Colloid Interface Sci.* **2024**, *324*, 103093. [CrossRef] [PubMed]
38. Lin, J.; Zhao, S.; Jervis, R.; Shearing, P. Probing the Electrochemical Processes of Niobium Pentoxides (Nb_2O_5) for High-Rate Lithium-ion Batteries: A Review. *ChemElectroChem* **2024**, *11*, e202300581. [CrossRef]
39. Raba, A.M.; Bautista-Ruíz, J.; Joya, M.R. Synthesis and Structural Properties of Niobium Pentoxide Powders: A Comparative Study of the Growth Process. *Mater. Res.* **2016**, *19*, 1381–1387. [CrossRef]

40. Su, K.; Liu, H.; Gao, Z.; Fornasiero, P.; Wang, F. Nb_2O_5-Based Photocatalysts. *Adv. Sci.* **2021**, *8*, 2003156. [CrossRef]
41. Moin, M.; Moin, M.; Zhao, H.; Ahsan, Z.; Dong, L.; Penki, T.R.; Harika, V.K.; Thumu, U. Unveiling the Potential of Hetero-Atom Substitution in Niobium Oxide Hydride Materials: A Computational Insights to next-Generation Li-Ion Batteries. *J. Energy Storage* **2025**, *131*, 115883. [CrossRef]
42. Amate, R.U.; Morankar, P.J.; Teli, A.M.; Beknalkar, S.A.; Chavan, G.T.; Ahir, N.A.; Dalavi, D.S.; Jeon, C.-W. Versatile Electrochromic Energy Storage Smart Window Utilizing Surfactant-Assisted Niobium Oxide Thin Films. *Chem. Eng. J.* **2024**, *484*, 149556. [CrossRef]
43. Pehlivan, E.; Tepehan, F.Z.; Tepehan, G.G. Electrochromic Properties of Pure and Doped Nb_2O_5 Thin Films. *Key Eng. Mater.* **2004**, *264–268*, 375–378. [CrossRef]
44. Sena, M.P.; de Lima, S.P.; Carvalho, L.S.; Ruiz, D.; Ballarini, A.; Martins, A.R. Synthesis, Characterization and Catalytic Evaluation of Cobalt and Niobium Oxide Solids Modified with Alkaline Earth Metals. *Matéria* **2020**, *25*. [CrossRef]
45. Bledowski, M.; Wang, L.; Ramakrishnan, A.; Khavryuchenko, O.V.; Khavryuchenko, V.D.; Ricci, P.C.; Strunk, J.; Cremer, T.; Kolbeck, C.; Beranek, R. Visible-Light Photocurrent Response of TiO_2–Polyheptazine Hybrids: Evidence for Interfacial Charge-Transfer Absorption. *Phys. Chem. Chem. Phys.* **2011**, *13*, 21511. [CrossRef]
46. Genco, A.; García-López, E.I.; Megna, B.; Ania, C.; Marcì, G. Nb_2O_5 Based Photocatalysts for Efficient Generation of H_2 by Photoreforming of Aqueous Solutions of Ethanol. *Catal. Today* **2025**, *447*, 115147. [CrossRef]
47. Pang, R.; Wang, Z.; Li, J.; Chen, K. Polymorphs of Nb2O5 Compound and Their Electrical Energy Storage Applications. *Materials* **2023**, *16*, 6956. [CrossRef]
48. Gopinath, K.P.; Madhav, N.V.; Krishnan, A.; Malolan, R.; Rangarajan, G. Present Applications of Titanium Dioxide for the Photocatalytic Removal of Pollutants from Water: A Review. *J. Environ. Manag.* **2020**, *270*, 110906. [CrossRef]
49. Lopes, O.F.; De Mendonça, V.R.; Silva, F.B.F.; Paris, E.C.; Ribeiro, C. Óxidos de Nióbio: Uma Visão Sobre a Síntese Do Nb_2O_{5e} Sua Aplicação Em Fotocatálise Heterogênea. *Quim. Nova* **2015**, *38*, 106–117.
50. Fidelis, M.Z.; Abreu, E.; Josué, T.G.; de Almeida, L.N.B.; Lenzi, G.G.; Dos Santos, O.A.A. Continuous Process Applied to Degradation of Triclosan and 2.8-Dichlorodibenzene-p-Dioxin. *Environ. Sci. Pollut. Res.* **2021**, *28*, 23675–23683. [CrossRef] [PubMed]
51. Aimaiti, G.; Ma, Y.H.; Shi, Y.J.; Wang, X.; Wang, S.Y.; Wang, Z.H.; Li, Y.C.; Li, J.W.; Qi, X.H.; Chen, X. Nb_2O_5/Red Phosphorus S-Scheme Heterojunction Photocatalyst for Removal of Organic Contaminant and Cr(VI): Electrochemical Performance and Mechanism. *Mater. Sci. Semicond. Process* **2023**, *160*, 107421. [CrossRef]
52. Crisóstomo, C.; Damaceno, F.; Barbosa, L.; Almeida, J.; Batista, W.V.; Malagutti, A.R.; de Mesquita, J.P.; Torres, J.; Iga, G.; de Oliveira, C.; et al. FACILE HYDROTHERMAL SYNTHESIS OF NIOBIUM PENTOXIDE SEMICONDUCTOR AND THEIR APPLICATION IN THE PHOTODEGRADATION OF DYES AND REDUCTION OF FREE FAT ACIDS IN WASTE OIL. *Quim. Nova* **2025**, *48*, e-20250015. [CrossRef]
53. Maarisetty, D.; Komandur, J.; Sharma, S.; Baral, S.S.; Mohapatra, P. Unravelling the Rate Controlling Step in Degradation of Phenol on a Higher Potential Photocatalyst. *J. Environ. Chem. Eng.* **2020**, *8*, 103938. [CrossRef]
54. Ruiyi, L.; Xiaoyue, L.; Zaijun, L. Nb_2O_5-Graphene Heterojunction Composite with Ultrahigh Photocatalytic Activity for Solar Light Driven Photodegradation of Ciprofloxacin. *J. Photochem. Photobiol. A Chem.* **2024**, *446*, 115188. [CrossRef]
55. Chen, X.H.; Ren, J.Y.; Li, N.B.; Luo, H.Q. Constructing of CoP-Nb2O5 p-n Heterojunction with Built-in Electric Field to Accelerate the Charge Migration in Electrocatalytic Hydrogen Evolution. *J. Colloid Interface Sci.* **2023**, *651*, 760–768. [CrossRef]
56. Osman, N.S.; Sulaiman, S.N.; Muhamad, E.N.; Mukhair, H.; Tan, S.T.; Abdullah, A.H. Synthesis of an Ag_3PO_4/Nb_2O_5 Photocatalyst for the Degradation of Dye. *Catalysts* **2021**, *11*, 458. [CrossRef]
57. Silva, I.F.B.; Martins, A.R.; Krambrock, K.; Rosmaninho, M.G.; Binatti, I.; Moura, F.C.C. Understanding Photocatalytic Activity and Mechanism of Nickel-Modified Niobium Mesoporous Nanomaterials. *J. Photochem. Photobiol. A Chem.* **2020**, *388*, 112168. [CrossRef]
58. Moradi, Z.; Jahromi, S.Z.; Ghaedi, M. Design of Active Photocatalysts and Visible Light Photocatalysis. *Interface Sci. Technol.* **2021**, *32*, 557–623.
59. Li, H.; Tu, W.; Zhou, Y.; Zou, Z. Z-Scheme Photocatalytic Systems for Promoting Photocatalytic Performance: Recent Progress and Future Challenges. *Adv. Sci.* **2016**, *3*, 1500389. [CrossRef] [PubMed]
60. Zhang, L.; Zhang, J.; Yu, H.; Yu, J. Emerging S-Scheme Photocatalyst. *Adv. Mater.* **2022**, *34*, 2107668. [CrossRef]
61. Shao, X.; Wang, K.; Peng, L.; Li, K.; Wen, H.; Le, X.; Wu, X.; Wang, G. In-Situ Irradiated XPS Investigation on 2D/1D $Cd_{0.5}Zn_{0.5}S$/Nb_2O_5 S-Scheme Heterojunction Photocatalysts for Simultaneous Promotion of Antibiotics Removal and Hydrogen Evolution. *Colloids Surf. A Physicochem. Eng. Asp.* **2022**, *652*, 129846. [CrossRef]
62. Ramar, S.; Elango, P.; Velusamy, A.; Athinarayanan, B.; Jothi, V.K.; Hsu-Wei; Pattappan, D.; Gurusamy, A.; Lai, Y.-T. An Eco-Safety g-C_3N_4/Nb_2O_5/Ag Ternary Nanocomposite for Photocatalytic Degradation of Pharmaceutical Wastes and Dyes in Wastewater and Zebrafish Embryonic Assessment. *J. Mol. Struct.* **2024**, *1317*, 139127. [CrossRef]

63. Xu, W.; Li, X.; Peng, C.; Yang, G.; Cao, Y.; Wang, H.; Peng, F.; Yu, H. One-Pot Synthesis of Ru/Nb_2O_5@Nb_2C Ternary Photocatalysts for Water Splitting by Harnessing Hydrothermal Redox Reactions. *Appl. Catal. B* **2022**, *303*, 120910. [CrossRef]
64. Guo, X.; Duan, J.; Li, C.; Zhang, Z.; Wang, W. Fabrication of Highly Stabilized Zr Doped G-C_3N_4/Nb_2O_5 Heterojunction and Its Enhanced Photocatalytic Performance for Pollutants Degradation under Visible Light Irradiation. *Colloids Surf. A Physicochem. Eng. Asp.* **2022**, *649*, 129474. [CrossRef]
65. Qu, X.; Liu, M.; Gao, Z.; Zhai, H.; Ren, W.; Shi, L.; Du, F. A Novel Ternary Bi_4NbO_8Cl/BiOCl/Nb_2O_5 Architecture via in-Situ Solvothermal-Induced Electron-Trap with Enhanced Photocatalytic Activities. *Appl. Surf. Sci.* **2020**, *506*, 144688. [CrossRef]
66. Sun, Z.; Sun, X.; Gou, X.T.; Zhao, X.H.; Shi, L.; Qu, X.F. In Situ Formation of a Ternary Bi_4NbO_8Cl/BiOCl/Nb_2O_5 Photocatalyst and Its Enhanced Photocatalytic Performance. *J. Mater. Sci.* **2023**, *58*, 2539–2551. [CrossRef]
67. Zanin, H.; Teófilo, R.F.; Peterlevitz, A.C.; Oliveira, U.; de Paiva, J.C.; Ceragioli, H.J.; Reis, E.L.; Baranauskas, V. Diamond Cylindrical Anodes for Electrochemical Treatment of Persistent Compounds in Aqueous Solution. *J. Appl. Electrochem.* **2013**, *43*, 323–330. [CrossRef]
68. da Silva, S.W.; do Prado, J.M.; Heberle, A.N.A.; Schneider, D.E.; Rodrigues, M.A.S.; Bernardes, A.M. Electrochemical Advanced Oxidation of Atenolol at Nb/BDD Thin Film Anode. *J. Electroanal. Chem.* **2019**, *844*, 27–33. [CrossRef]
69. Fidelis, M.Z.; Favaro, Y.B.; Santos, A.; Pereira, M.F.R.; Brackmann, R.; Lenzi, G.G.; Soares, O.; Andreo, O.A.B. Enhancing Ibuprofen and 4-Isobutylacetophenone Degradation: Exploiting the Potential of Nb_2O_5 Sol-Gel Catalysts in Photocatalysis, Catalytic Ozonation, and Photocatalytic Ozonation. *J. Environ. Chem. Eng.* **2023**, *11*, 110690. [CrossRef]
70. Gonçalves, M.; Guerreiro, M.C.; Oliveira, L.C.A.; da Rocha, C.L. Materiais à base de óxido de ferro para oxidação de compostos presentes no efluente da despolpa do café. *Quim. Nova* **2008**, *31*, 1636–1640. [CrossRef]
71. Wolski, L.; Sobanska, K.; Munko, M.; Czerniak, A.; Pietrzyk, P. Unraveling the Origin of Enhanced Activity of the Nb_2O_5/H_2O_2 System in the Elimination of Ciprofloxacin: Insights into the Role of Reactive Oxygen Species in Interface Processes. *ACS Appl. Mater. Interfaces* **2022**, *14*, 31824–31837. [CrossRef]
72. Ziolek, M.; Sobczak, I.; Decyk, P.; Sobańska, K.; Pietrzyk, P.; Sojka, Z. Search for Reactive Intermediates in Catalytic Oxidation with Hydrogen Peroxide over Amorphous Niobium(V) and Tantalum(V) Oxides. *Appl. Catal. B* **2015**, *164*, 288–296. [CrossRef]
73. Wang, L.; Li, Y.; Han, P. Electrospinning Preparation of G-C_3N_4/Nb_2O_5 Nanofibers Heterojunction for Enhanced Photocatalytic Degradation of Organic Pollutants in Water. *Sci. Rep.* **2021**, *11*, 22950. [CrossRef]
74. Jones, B.M.F.; Mamba, G.; Maruthamani, D.; Muthuraj, V. Honeycomb Nb_2O_5/RGO Wrapped on MoO_3 Nanorods for Visible Light-Driven Degradation of Sulfasalazine and Ciprofloxacin in Water. *Colloids Surf. A Physicochem. Eng. Asp.* **2022**, *653*, 129836. [CrossRef]
75. Fidelis, M.Z.; Abreu, E.; Andreo, O.A.B.; Soares, O.S.G.P.; Janzen, F.C.; Lenzi, G.G. Application of Structured Sol-Gel Nb_2O_5 Catalyst in Photocatalytic Continuous Process Prototype for Ibuprofen Degradation. *Top. Catal.* **2024**, *67*, 828–842. [CrossRef]
76. Fávaro, Y.B.; Fuziki, M.E.K.; Fidelis, M.Z.; Abreu, E.; Tusset, A.M.; Brackmann, R.; Lenzi, G.G. Sol-Gel and Pechini Niobium Modified: Synthesis, Characterization and Application in the 2,4-D Herbicide Degradation. *J. Environ. Sci. Health Part B* **2024**, *59*, 50–61. [CrossRef]
77. Dias, D.T.; Rodrigues, A.O.; Pires, P.B.; Semianko, B.C.; Fuziki, M.E.K.; Lenzi, G.G.; Sabino, S.R.F. Photoacoustic Spectroscopy of Titanium Dioxide, Niobium Pentoxide, Titanium:Niobium, and Ruthenium-Modified Oxides Synthesized Using Sol-Gel Methodology. *Appl. Spectrosc.* **2024**, *78*, 1028–1042. [CrossRef]
78. do Prado, N.T.; Oliveira, L.C.A. Nanostructured Niobium Oxide Synthetized by a New Route Using Hydrothermal Treatment: High Efficiency in Oxidation Reactions. *Appl. Catal. B* **2017**, *205*, 481–488. [CrossRef]
79. Ücker, C.L.; Goetzke, V.; Riemke, F.C.; Oliveira, M.E.; Carreno, N.L.V.; Morisso, F.D.P.; Teodoro, M.D.; Mastelaro, V.R.; Moreira, M.L.; Raubach, C.W.; et al. The Photocatalytic Performance of Fe Inserted in Nb_2O_5 Obtained by Microwave-Assisted Hydrothermal Synthesis: Factorial Design of Experiments. *J. Photochem. Photobiol. A Chem.* **2023**, *435*, 114294. [CrossRef]
80. Wermuth, T.B.; Arcaro, S.; Venturini, J.; Hubert Ribeiro, T.M.; de Assis Lawisch Rodriguez, A.; Machado, E.L.; Franco de Oliveira, T.; Franco de Oliveira, S.E.; Baibich, M.N.; Bergmann, C.P. Microwave-Synthesized $KNbO_3$ Perovskites: Photocatalytic Pathway on the Degradation of Rhodamine B. *Ceram. Int.* **2019**, *45*, 24137–24145. [CrossRef]
81. Sultana, R.; Islam, K.; Chakraborty, S. Tuning Optical and Electrochemical Properties of Nb_2O_5 Thin Films via WO_3 Doping. *Trans. Electr. Electron. Mater.* **2024**, *26*, 48–59. [CrossRef]
82. Sathasivam, S.; Williamson, B.A.D.; Althabaiti, S.A.; Obaid, A.Y.; Basahel, S.N.; Mokhtar, M.; Scanlon, D.O.; Carmalt, C.J.; Parkin, I.P. Chemical Vapor Deposition Synthesis and Optical Properties of Nb_2O_5Thin Films with Hybrid Functional Theoretical Insight into the Band Structure and Band Gaps. *ACS Appl. Mater. Interfaces* **2017**, *9*, 18031–18038. [CrossRef]
83. Singh, K.; Abhimanyu; Sonu, S.; Chaudhary, V.; Raizada, P.; Rustagi, S.; Singh, P.; Thakur, P.; Kumar, V.; Kaushik, A. Defect and Heterostructure Engineering Assisted S-Scheme Nb_2O_5 Nanosystems-Based Solutions for Environmental Pollution and Energy Conversion. *Adv. Colloid. Interface Sci.* **2024**, *332*, 103273. [CrossRef]
84. Wang, X.; Jiang, J.; Wang, L.; Guo, H. Efficient Nb_2O_5@g-C_3N_4 Heterostructures for Enhanced Photocatalytic CO_2 Reduction with Highly Selective Conversion to CH_4. *Inorg. Chem. Front.* **2024**, *11*, 123–132. [CrossRef]

85. Liu, J.; Zuo, S.; Lin, S.; Shan, B.; Zhou, X.; Zhao, J.; Qi, C.; Yang, P. Promoting the Performance of Nb2O5 by Doping Transition Metal Oxide for Catalytic Degradation of Monochlorobenzene and Toluene. *J. Mater. Res. Technol.* **2023**, *25*, 3642–3653. [CrossRef]
86. Ücker, C.L.; Rodrigues, F.S.M.; Riemke, F.C.; Morisso, F.D.P.; Teodoro, M.D.; Mastelaro, V.R.; Ferrer, M.M.; Raubach, C.W.; da Cava, S.S. Surface Modification of T-Nb_2O_5 with Low-Crystallinity Nb_2O_5 to Enhance Photocatalytic Degradation of Rhodamine B. *Ceram. Int.* **2023**, *49*, 34333–34338. [CrossRef]
87. Zu, D.Y.; Song, H.R.; Wang, Y.W.; Chao, Z.; Li, Z.; Wang, G.; Shen, Y.M.; Li, C.P.; Ma, J. One-Pot in-Situ Hydrothermal Synthesis of CdS/Nb_2O_5/Nb_2C Heterojunction for Enhanced Visible-Light-Driven Photodegradation. *Appl. Catal. B Environ.* **2020**, *277*, 119140. [CrossRef]
88. Wolski, L.; Ziolek, M. Insight into Pathways of Methylene Blue Degradation with H_2O_2 over Mono and Bimetallic Nb, Zn Oxides. *Appl. Catal. B* **2018**, *224*, 634–647. [CrossRef]
89. Zulkiflee, A.; Mansoob Khan, M.; Yusuf Khan, M.; Khan, A.; Hilni Harunsani, M. Nb_2O_5/BiOCl Composite as a Visible-Light-Active Photocatalyst for the Removal of RhB Dye and Photoelectrochemical Studies. *J. Photochem. Photobiol. A Chem.* **2024**, *446*, 115177. [CrossRef]
90. Sacco, O.; Murcia, J.J.; Lara, A.E.; Hernández-Laverde, M.; Rojas, H.; Navío, J.A.; Hidalgo, M.C.; Vaiano, V. Pt-TiO_2-Nb_2O_5 Heterojunction as Effective Photocatalyst for the Degradation of Diclofenac and Ketoprofen. *Mater. Sci. Semicond. Process* **2020**, *107*, 104839. [CrossRef]
91. Zhang, G.; Yang, J.; Zhang, S.; Xiong, Q.; Huang, B.; Wang, J.; Gong, W. Preparation of Nanosized Bi_3NbO_7 and Its Visible-Light Photocatalytic Property. *J. Hazard. Mater.* **2009**, *172*, 986–992. [CrossRef]
92. Xiao, J.; Xie, Y.; Rabeah, J.; Brückner, A.; Cao, H. Visible-Light Photocatalytic Ozonation Using Graphitic C_3N_4Catalysts: A Hydroxyl Radical Manufacturer for Wastewater Treatment. *Acc. Chem. Res.* **2020**, *53*, 1024–1033. [CrossRef]
93. Nogueira, M.V.; Lustosa, G.M.M.M.; Kobayakawa, Y.; Kogler, W.; Ruiz, M.; Monteiro Filho, E.S.; Zaghete, M.A.; Perazolli, L.A. Nb-Doped TiO_2 Photocatalysts Used to Reduction of CO_2 to Methanol. *Adv. Mater. Sci. Eng.* **2018**, *2018*. [CrossRef]
94. Tee, S.Y.; Kong, J.; Koh, J.J.; Teng, C.P.; Wang, X.; Wang, X.; Teo, S.L.; Thitsartarn, W.; Han, M.-Y.; Seh, Z.W. Structurally and Surficially Activated TiO_2 Nanomaterials for Photochemical Reactions. *Nanoscale* **2024**, *16*, 18165–18212. [CrossRef]
95. Wang, S.; Yun, J.-H.; Luo, B.; Butburee, T.; Peerakiatkhajohn, P.; Thaweesak, S.; Xiao, M.; Wang, L. Recent Progress on Visible Light Responsive Heterojunctions for Photocatalytic Applications. *J. Mater. Sci. Technol.* **2017**, *33*, 1–22. [CrossRef]
96. Ravishankar, T.N.; de O, M.; Ramakrishnappa, T.; Teixeira, S.R.; Dupont, J. Ionic Liquid–Assisted Hydrothermal Synthesis of Nb/TiO_2 Nanocomposites for Efficient Photocatalytic Hydrogen Production and Photodecolorization of Rhodamine B under UV-Visible and Visible Light Illuminations. *Mater. Today Chem.* **2019**, *12*, 373–385. [CrossRef]
97. Nogueira, A.E.; Lopes, O.F.; Neto, A.B.S.; Ribeiro, C. Enhanced Cr(VI) Photoreduction in Aqueous Solution Using Nb_2O_5/CuO Heterostructures under UV and Visible Irradiation. *Chem. Eng. J.* **2017**, *312*, 220–227. [CrossRef]
98. Serenario, M.E.D.; Santos, B.A.F.; Petrucelli, A.C.F.; Souza, R.C.; Moreira, G.P.C.; Miranda, L.R.M.; Bueno, A.H.S. Anti-Corrosion Coatings Based on Nb_2O_5—A Comparison Between Two Coatings Technology: Thermal Spray Coating and Epoxy Paint. *Mater. Res.* **2022**, *25*, e20210515. [CrossRef]
99. Goswami, T.; Kumar, S.; Bheemaraju, A.; Reddy, K.M.; Sharma, A.K.; Kataria, A.; Shrivastav, A. TiO_2 Nanoparticles and Nb_2O_5 Nanorods Immobilized RGO for Efficient Visible-Light Photocatalysis and Catalytic Reduction. *Catal. Lett.* **2023**, *153*, 605–621. [CrossRef]
100. Ücker, C.L.; Riemke, F.; Goetzke, V.; Moreira, M.L.; Raubach, C.W.; Longo, E.; Cava, S. Facile Preparation of Nb_2O_5/TiO_2 Heterostructures for Photocatalytic Application. *Chem. Phys. Impact* **2022**, *4*, 100079. [CrossRef]
101. Jin, F.; Ma, X.; Guo, S.-Q. F-Doped Hierarchical Nb2O5: Structural, Optical and Photocatalytic Performance. *Mater. Lett.* **2023**, *347*, 134664. [CrossRef]
102. Lim, J.; Murugan, P.; Lakshminarasimhan, N.; Kim, J.Y.; Lee, J.S.; Lee, S.H.; Choi, W. Synergic Photocatalytic Effects of Nitrogen and Niobium Co-Doping in TiO_2 for the Redox Conversion of Aquatic Pollutants under Visible Light. *J. Catal.* **2014**, *310*, 91–99. [CrossRef]
103. Rajan, S.T.; Senthilnathan, J.; Arockiarajan, A. Sputter-Coated N-Enriched Mixed Metal Oxides (Ta_2O_5-Nb_2O_5-N) Composite: A Resilient Solar Driven Photocatalyst for Water Purification. *J. Hazard. Mater.* **2023**, *452*, 131283. [CrossRef]
104. Fogaça, L.Z.; Vicentini, J.C.M.; de Freitas, C.F.; Braga, T.L.; da Silva, F.A.; de Souza, M.; Baesso, M.L.; Caetano, W.; Batistela, V.R.; Scaliante, M.H.N.O. Nanocomposites of Nb2O5 and ZnO with Reduced Graphene Oxide for Heterogeneous Photocatalysis of Dyes. *Catal Commun* **2023**, *185*, 106799. [CrossRef]
105. Xu, Z.; Jiang, J.; Zhang, Q.; Chen, G.; Zhou, L.; Li, L. 3D Graphene Aerogel Composite of 1D-2D Nb_2O_5-g-C3N4 Heterojunction with Excellent Adsorption and Visible-Light Photocatalytic Performance. *J. Colloid. Interface Sci.* **2020**, *563*, 131–138. [CrossRef]
106. Sethuraman, S.; Marimuthu, A.; Kattamuthu, R.; Karuppasamy, G. Highly Surface Active Niobium Doped G-C_3N_4/g-C_3N_4 Heterojunction Interface towards Superior Photocatalytic and Selective Ammonia Response. *Appl. Surf. Sci.* **2021**, *561*, 150077. [CrossRef]

107. Wang, Y.; Su, N.; Liu, J.; Lin, Y.; Wang, J.; Guo, X.; Zhang, Y.; Qin, Z.; Liu, J.; Zhang, C.; et al. Enhanced Visible-Light Photocatalytic Properties of SnO_2 Quantum Dots by Niobium Modification. *Results Phys.* **2022**, *37*, 105515. [CrossRef]
108. Cui, C.; Guo, R.; Ren, E.; Xiao, H.; Lai, X.; Qin, Q.; Jiang, S.; Shen, H.; Zhou, M.; Qin, W. Facile Hydrothermal Synthesis of Rod-like Nb_2O_5/Nb_2CT_x Composites for Visible-Light Driven Photocatalytic Degradation of Organic Pollutants. *Environ. Res.* **2021**, *193*, 110587. [CrossRef] [PubMed]
109. Yang, X.; Duan, J.; Zhang, X.; Zhang, H.; Liu, X.; Feng, Y.; Zheng, M. Heterojunction Architecture of Nb_2O_5/g-C_3N_4 for Enhancing Photocatalytic Activity to Degrade Organic Pollutants and Deactivate Bacteria in Water. *Chin. Chem. Lett.* **2022**, *33*, 3792–3796. [CrossRef]
110. Du, Y.C.; Zhang, S.H.; Wang, J.S.; Wu, J.S.; Dai, H.X. Nb_2O_5 Nanowires in-Situ Grown on Carbon Fiber: A High-Efficiency Material for the Photocatalytic Reduction of Cr(VI). *J. Environ. Sci.* **2018**, *66*, 358–367. [CrossRef] [PubMed]
111. Gomis-Berenguer, A.; Velasco, L.F.; Velo-Gala, I.; Ania, C.O. Photochemistry of Nanoporous Carbons: Perspectives in Energy Conversion and Environmental Remediation. *J. Colloid. Interface Sci.* **2017**, *490*, 879–901. [CrossRef] [PubMed]
112. Chen, J.; Wang, H.; Huang, G.; Zhang, Z.; Han, L.; Song, W.; Li, M.; Zhang, Y. Facile Synthesis of Urchin-like Hierarchical Nb_2O_5 Nanospheres with Enhanced Visible Light Photocatalytic Activity. *J. Alloys Compd.* **2017**, *728*, 19–28. [CrossRef]
113. Qi, S.; Zuo, R.; Liu, Y.; Wang, Y. Synthesis and Photocatalytic Activity of Electrospun Niobium Oxide Nanofibers. *Mater. Res. Bull.* **2013**, *48*, 1213–1217. [CrossRef]
114. Khan, S.U.; Perini, J.A.L.; Hussain, S.; Khan, H.; Khan, S.; Boldrin Zanoni, M.V. Electrochemical Preparation of Nb_2O_5 Nanochannel Photoelectrodes for Enhanced Photoelectrocatalytic Performance in Removal of RR120 Dye. *Chemosphere* **2020**, *257*, 127164. [CrossRef]
115. Breault, T.M.; Bartlett, B.M. Composition Dependence of TiO_2:(Nb,N)-*x* Compounds on the Rate of Photocatalytic Methylene Blue Dye Degradation. *J. Phys. Chem. C* **2013**, *117*, 8611–8618. [CrossRef]
116. Hashemzadeh, F.; Gaffarinejad, A.; Rahimi, R. Porous P-NiO/n-Nb_2O_5 Nanocomposites Prepared by an EISA Route with Enhanced Photocatalytic Activity in Simultaneous Cr(VI) Reduction and Methyl Orange Decolorization under Visible Light Irradiation. *J. Hazard. Mater.* **2015**, *286*, 64–74. [CrossRef]
117. Valerio, T.L.; Maia, G.A.R.; Gonçalves, L.F.; Viomar, A.; Banczek, E.d.P.; Rodrigues, P.R.P. Study of the Nb_2O_5 Insertion in ZnO to Dye-Sensitized Solar Cells. *Materials Research* **2019**, *22*, e20180864. [CrossRef]
118. Peng, C.; Xie, X.; Xu, W.; Zhou, T.; Wei, P.; Jia, J.; Zhang, K.; Cao, Y.; Wang, H.; Peng, F.; et al. Engineering Highly Active Ag/Nb_2O_5@Nb_2CT (MXene) Photocatalysts via Steering Charge Kinetics Strategy. *Chem. Eng. J.* **2021**, *421*, 128766. [CrossRef]
119. Xie, T.; Zhang, Z.; Yang, J.; Wang, J.; Xu, L. Bird's Nest-like Nb_2O_5: Preparation, Characterization and Multifunctional Photocatalytic Application. *Mater. Technol.* **2024**, *39*, 2364552. [CrossRef]
120. Ücker, C.L.; Gularte, L.T.; Fernandes, C.D.; Goetzke, V.; Moreira, E.C.; Raubach, C.W.; Moreira, M.L.; Cava, S.S. Investigation of the Properties of Niobium Pentoxide for Use in Dye-sensitized Solar Cells. *J. Am. Ceram. Soc.* **2019**, *102*, 1884–1892. [CrossRef]
121. Fidelis, M.Z.; de Paula, E.; Abreu, E.; Fuziki, M.E.K.; Santos, O.A.A.D.; Brackmann, R.; Lenzi, G.G. Nb_2O_5: Percentage Effect of T/H Phase and Evaluation of Catalytic Activity, a Preliminary Study. *Catal. Res.* **2023**, *3*, 023. [CrossRef]
122. Nico, C.; Monteiro, T.; Graça, M.P.F. Niobium Oxides and Niobates Physical Properties: Review and Prospects. *Prog. Mater. Sci.* **2016**, *80*, 1–37. [CrossRef]
123. Gomes, G.H.M.; Olusegun, S.J.; Gabriel, J.B.; Costa, R.C.V.; Mohallem, N.D.S. The Role of Crystalline Nb_2O_5 Nanoparticles for Enhanced Dye Adsorption and Photodegradation. *Ceram. Int.* **2023**, *49*, 6164–6176. [CrossRef]
124. Ücker, C.L.; Riemke, F.C.; de Andrade Neto, N.F.; de Santiago, A.A.G.; Siebeneichler, T.J.; Carreño, N.L.V.; Moreira, M.L.; Raubach, C.W.; Cava, S. Influence of Nb_2O_5 Crystal Structure on Photocatalytic Efficiency. *Chem. Phys. Lett.* **2021**, *764*, 138271. [CrossRef]
125. Suzuki, N.; Athar, T.; Huang, Y.-T.; Shimasaki, K.; Miyamoto, N.; Yamauchi, Y. Synthesis of Mesoporous Nb_2O_5 with Crystalline Walls and Investigation of Their Photocatalytic Activity. *J. Ceram. Soc. Jpn.* **2011**, *119*, 405–411. [CrossRef]
126. Zhao, Y.; Zhou, X.; Ye, L.; Chi Edman Tsang, S. Nanostructured Nb_2O_5 Catalysts. *Nano Rev.* **2012**, *3*, 17631. [CrossRef]
127. Li, X.; Shen, X.; Jiang, W.; Xi, Y.; Li, S. Comprehensive Review of Emerging Contaminants: Detection Technologies, Environmental Impact, and Management Strategies. *Ecotoxicol. Environ. Saf.* **2024**, *278*, 116420. [CrossRef]
128. Ejiohuo, O.; Onyeaka, H.; Akinsemolu, A.; Nwabor, O.F.; Siyanbola, K.F.; Tamasiga, P.; Al-Sharify, Z.T. Ensuring Water Purity: Mitigating Environmental Risks and Safeguarding Human Health. *Water Biol. Secur.* **2025**, *4*, 100341. [CrossRef]
129. Das, S.; Parida, V.K.; Tiwary, C.S.; Gupta, A.K.; Chowdhury, S. Emerging Contaminants in the Aquatic Environment: Fate, Occurrence, Impacts, and Toxicity. In *Bioremediation of Emerging Contaminants in Water*; ACS: Washington, DC, USA, 2024; pp. 1–32.
130. Lei, M.; Zhang, L.; Lei, J.; Zong, L.; Li, J.; Wu, Z.; Wang, Z. Overview of Emerging Contaminants and Associated Human Health Effects. *Biomed. Res. Int.* **2015**, *2015*, 404796. [CrossRef] [PubMed]
131. Mitoraj, D.; Lamdab, U.; Kangwansupamonkon, W.; Pacia, M.; Macyk, W.; Wetchakun, N.; Beranek, R. Revisiting the Problem of Using Methylene Blue as a Model Pollutant in Photocatalysis: The Case of $InVO_4/BiVO_4$ Composites. *J. Photochem. Photobiol. A Chem.* **2018**, *366*, 103–110. [CrossRef]

132. Barbero, N.; Vione, D. Why Dyes Should Not Be Used to Test the Photocatalytic Activity of Semiconductor Oxides. *Environ. Sci. Technol.* **2016**, *50*, 2130–2131. [CrossRef]
133. Rochkind, M.; Pasternak, S.; Paz, Y. Using Dyes for Evaluating Photocatalytic Properties: A Critical Review. *Molecules* **2014**, *20*, 88–110. [CrossRef] [PubMed]
134. De Gisi, S.; Lofrano, G.; Grassi, M.; Notarnicola, M. Characteristics and Adsorption Capacities of Low-Cost Sorbents for Wastewater Treatment: A Review. *Sustain. Mater. Technol.* **2016**, *9*, 10–40. [CrossRef]
135. Yagub, M.T.; Sen, T.K.; Afroze, S.; Ang, H.M. Dye and Its Removal from Aqueous Solution by Adsorption: A Review. *Adv. Colloid. Interface Sci.* **2014**, *209*, 172–184. [CrossRef] [PubMed]
136. Alegbe, E.O.; Uthman, T.O. A Review of History, Properties, Classification, Applications and Challenges of Natural and Synthetic Dyes. *Heliyon* **2024**, *10*, e33646. [CrossRef]
137. Ardila-Leal, L.D.; Poutou-Piñales, R.A.; Pedroza-Rodríguez, A.M.; Quevedo-Hidalgo, B.E. A Brief History of Colour, the Environmental Impact of Synthetic Dyes and Removal by Using Laccases. *Molecules* **2021**, *26*, 3813. [CrossRef]
138. Al-Tohamy, R.; Ali, S.S.; Li, F.; Okasha, K.M.; Mahmoud, Y.A.-G.; Elsamahy, T.; Jiao, H.; Fu, Y.; Sun, J. A Critical Review on the Treatment of Dye-Containing Wastewater: Ecotoxicological and Health Concerns of Textile Dyes and Possible Remediation Approaches for Environmental Safety. *Ecotoxicol. Environ. Saf.* **2022**, *231*, 113160. [CrossRef]
139. Alzain, H.; Kalimugogo, V.; Hussein, K. A Review of Environmental Impact of Azo Dyes. *Int. J. Res. Rev.* **2023**, *10*, 64–689. [CrossRef]
140. Anwer, H.; Mahmood, A.; Lee, J.; Kim, K.-H.; Park, J.-W.; Yip, A.C.K. Photocatalysts for Degradation of Dyes in Industrial Effluents: Opportunities and Challenges. *Nano Res.* **2019**, *12*, 955–972. [CrossRef]
141. de Carvalho, G.S.G.; de Siqueira, M.M.; do Nascimento, M.P.; de Oliveira, M.A.L.; Amarante, G.W. Nb_2O_5 Supported in Mixed Oxides Catalyzed Mineralization Process of Methylene Blue. *Heliyon* **2020**, *6*, e04128. [CrossRef]
142. Le Luu, T.; Ngan, P.T.K. Fabrication of High Performance Ti/SnO_2-Nb_2O_5 Electrodes for Electrochemical Textile Wastewater Treatment. *Sci. Total Environ.* **2023**, *860*, 160366. [CrossRef]
143. Rangel, E.M.; Riemke, F.C.; Ücker, C.L.; Raubach, C.W.; Adebayo, M.A.; Machado Machado, F. Photodegradation of Acid Yellow 23 BY Nb_2O_5 Supported on Eco-Friendly Glass Foams. *J. Clean. Prod.* **2022**, *371*, 133231. [CrossRef]
144. Hass Caetano Lacerda, E.; Monteiro, F.C.; Kloss, J.R.; Fujiwara, S.T. Bentonite Clay Modified with Nb_2O_5: An Efficient and Reused Photocatalyst for the Degradation of Reactive Textile Dye. *J. Photochem. Photobiol. A Chem.* **2020**, *388*, 112084. [CrossRef]
145. Pereira da Costa, G.; Rafael, R.A.; Soares, J.C.S.; Gaspar, A.B. Synthesis and Characterization of ZnO-Nb_2O_5 Catalysts for Photodegradation of Bromophenol Blue. *Catal. Today* **2020**, *344*, 240–246. [CrossRef]
146. Hamzad, S.; Kumar, K.Y.; Prashanth, M.K.; Radhika, D.; Parashuram, L.; Alharti, F.A.; Jeon, B.H.; Raghu, M.S. Boron Doped RGO from Discharged Dry Cells Decorated Niobium Pentoxide for Enhanced Visible Light-Induced Hydrogen Evolution and Water Decontamination. *Surf. Interfaces* **2023**, *36*, 102544. [CrossRef]
147. Zarrin, S.; Heshmatpour, F. Facile Preparation of New Nanohybrids for Enhancing Photocatalytic Activity toward Removal of Organic Dyes under Visible Light Irradiation. *J. Phys. Chem. Solids* **2020**, *140*, 109271. [CrossRef]
148. Iborra-Torres, A.; Kulak, A.N.; Palgrave, R.G.; Hyett, G. Demonstration of Visible Light-Activated Photocatalytic Self-Cleaning by Thin Films of Perovskite Tantalum and Niobium Oxynitrides. *ACS Appl. Mater. Interfaces* **2020**, *12*, 33603–33612. [CrossRef] [PubMed]
149. Prado, A.G.S.; Bolzon, L.B.; Pedroso, C.P.; Moura, A.O.; Costa, L.L. Nb_2O_5 as Efficient and Recyclable Photocatalyst for Indigo Carmine Degradation. *Appl. Catal. B* **2008**, *82*, 219–224. [CrossRef]
150. Oliveira, L.C.A.; Ramalho, T.C.; Souza, E.F.; Gonçalves, M.; Oliveira, D.Q.L.; Pereira, M.C.; Fabris, J.D. Catalytic Properties of Goethite Prepared in the Presence of Nb on Oxidation Reactions in Water: Computational and Experimental Studies. *Appl. Catal. B* **2008**, *83*, 169–176. [CrossRef]
151. Oliveira, L.C.A.; Oliveira, H.S.; Mayrink, G.; Mansur, H.S.; Mansur, A.A.P.; Moreira, R.L. One-Pot Synthesis of CdS@Nb_2O_5 Core-Shell Nanostructures with Enhanced Photocatalytic Activity. *Appl. Catal. B* **2014**, *152–153*, 403–412. [CrossRef]
152. Xu, Z.; Yang, W.; Li, Q.; Gao, S.; Shang, J.K. Passivated N-p Co-Doping of Niobium and Nitrogen into Self-Organized TiO_2 Nanotube Arrays for Enhanced Visible Light Photocatalytic Performance. *Appl. Catal. B* **2014**, *144*, 343–352. [CrossRef]
153. Wolski, L.; Sobańska, K.; Walkowiak, A.; Akhmetova, K.; Gryboś, J.; Frankowski, M.; Ziolek, M.; Pietrzyk, P. Enhanced Adsorption and Degradation of Methylene Blue over Mixed Niobium-Cerium Oxide—Unraveling the Synergy between Nb and Ce in Advanced Oxidation Processes. *J. Hazard. Mater.* **2021**, *415*, 125665. [CrossRef]
154. de Moraes, N.P.; Silva, F.N.; da Silva, M.L.C.P.; Campos, T.M.B.; Thim, G.P.; Rodrigues, L.A. Methylene Blue Photodegradation Employing Hexagonal Prism-Shaped Niobium Oxide as Heterogeneous Catalyst: Effect of Catalyst Dosage, Dye Concentration, and Radiation Source. *Mater. Chem. Phys.* **2018**, *214*, 95–106. [CrossRef]
155. Kumari, N.; Gaurav, K.; Samdarshi, S.K.; Bhattacharyya, A.S.; Paul, S.; Rajbongshi, B.M.; Mohanty, K. Dependence of Photoactivity of Niobium Pentoxide (Nb_2O_5) on Crystalline Phase and Electrokinetic Potential of the Hydrocolloid. *Sol. Energy Mater. Sol. Cells* **2020**, *208*, 110408. [CrossRef]

156. Ferraz, N.P.; Nogueira, A.E.; Marcos, F.C.F.; Machado, V.A.; Rocca, R.R.; Assaf, E.M.; Asencios, Y.J.O. CeO2–Nb_2O_5 Photocatalysts for Degradation of Organic Pollutants in Water. *Rare Met.* **2020**, *39*, 230–240. [CrossRef]
157. Awais, M.; Khursheed, S.; Tehreem, R.; Sirajuddin; Mok, Y.S.; Siddiqui, G.U. PH Regulated Rapid Photocatalytic Degradation of Methylene Blue Dye via Niobium-Nitrogen Co-Doped Titanium Dioxide Nanostructures under Sunlight. *Appl. Catal. A Gen.* **2022**, *643*, 118764. [CrossRef]
158. Gupta, A.; Pandey, O.P. NbC/C Heterojunction for Efficient Photodegradation of Methylene Blue under Visible Irradiation. *Sol. Energy* **2019**, *183*, 398–409. [CrossRef]
159. Breault, T.M.; Bartlett, B.M. Lowering the Band Gap of Anatase-Structured TiO_2 by Coalloying with Nb and N: Electronic Structure and Photocatalytic Degradation of Methylene Blue Dye. *J. Phys. Chem. C* **2012**, *116*, 5986–5994. [CrossRef]
160. Carvalho, K.T.G.; Nogueira, A.E.; Lopes, O.F.; Byzynski, G.; Ribeiro, C. Synthesis of G-C_3N_4/Nb_2O_5 Heterostructures and Their Application in the Removal of Organic Pollutants under Visible and Ultraviolet Irradiation. *Ceram. Int.* **2017**, *43*, 3521–3530. [CrossRef]
161. Rahim Pouran, S.; Abdul Aziz, A.R.; Wan Daud, W.M.A.; Embong, Z. Niobium Substituted Magnetite as a Strong Heterogeneous Fenton Catalyst for Wastewater Treatment. *Appl. Surf. Sci.* **2015**, *351*, 175–187. [CrossRef]
162. da Silva, A.L.; Dondi, M.; Hotza, D. Self-Cleaning Ceramic Tiles Coated with Nb_2O_5-Doped-TiO_2 Nanoparticles. *Ceram. Int.* **2017**, *43*, 11986–11991. [CrossRef]
163. Da Silva, A.L.; Muche, D.N.F.; Dey, S.; Hotza, D.; Castro, R.H.R. Photocatalytic Nb_2O_5-Doped TiO_2 Nanoparticles for Glazed Ceramic Tiles. *Ceram. Int.* **2016**, *42*, 5113–5122. [CrossRef]
164. Gupta, A.; Pandey, O.P. Visible Irradiation Induced Photodegradation by NbC/C Nanocomposite Derived from Smoked Cigarette Litter (Filters). *Sol. Energy* **2018**, *163*, 167–176. [CrossRef]
165. Matos, J.; Lanfredi, S.; Montaña, R.; Nobre, M.A.L.; de Córdoba, M.C.F.; Ania, C.O. Photochemical Reactivity of Apical Oxygen in $KSr_2Nb_5O_{15}$ Materials for Environmental Remediation under UV Irradiation. *J. Colloid. Interface Sci.* **2017**, *496*, 211–221. [CrossRef]
166. de Moraes, N.P.; Bacani, R.; da Silva, M.L.C.P.; Campos, T.M.B.; Thim, G.P.; Rodrigues, L.A. Effect of Nb/C Ratio in the Morphological, Structural, Optical and Photocatalytic Properties of Novel and Inexpensive Nb_2O_5/Carbon Xerogel Composites. *Ceram. Int.* **2018**, *44*, 6645–6652. [CrossRef]
167. Oliveira, H.S.; Almeida, L.D.; De Freitas, V.A.A.; Moura, F.C.C.; Souza, P.P.; Oliveira, L.C.A. Nb-Doped Hematite: Highly Active Catalyst for the Oxidation of Organic Dyes in Water. *Catal. Today* **2015**, *240*, 176–181. [CrossRef]
168. Silva, A.C.; Oliveira, D.Q.L.; Oliveira, L.C.A.; Anastácio, A.S.; Ramalho, T.C.; Lopes, J.H.; Carvalho, H.W.P.; Torres, C.E.R. Nb-Containing Hematites Fe_2-XNbxO_3: The Role of Nb^{5+} on the Reactivity in Presence of the H_2O_2 or Ultraviolet Light. *Appl. Catal. A Gen.* **2009**, *357*, 79–84. [CrossRef]
169. Jia, Z.; Kang, J.; Zhang, W.C.; Wang, W.M.; Yang, C.; Sun, H.; Habibi, D.; Zhang, L.C. Surface Aging Behaviour of Fe-Based Amorphous Alloys as Catalysts during Heterogeneous Photo Fenton-like Process for Water Treatment. *Appl. Catal. B* **2017**, *204*, 537–547. [CrossRef]
170. Zarrin, S.; Heshmatpour, F. Photocatalytic Activity of TiO_2/Nb_2O_5/PANI and TiO_2/Nb_2O_5/RGO as New Nanocomposites for Degradation of Organic Pollutants. *J. Hazard. Mater.* **2018**, *351*, 147–159. [CrossRef]
171. Batista, L.M.B.; dos Santos, A.J.; da Silva, D.R.; de Alves, A.P.M.; Garcia-Segura, S.; Martínez-Huitle, C.A. Solar Photocatalytic Application of NbO_2OH as Alternative Photocatalyst for Water Treatment. *Sci. Total Environ.* **2017**, *596–597*, 79–86. [CrossRef]
172. Dos Santos, A.J.; Batista, L.M.B.; Martínez-Huitle, C.A.; de Alves, A.P.M.; Garcia-Segura, S. Niobium Oxide Catalysts as Emerging Material for Textile Wastewater Reuse: Photocatalytic Decolorization of Azo Dyes. *Catalysts* **2019**, *9*, 1070. [CrossRef]
173. Patil, B.N.; Naik, D.B.; Shrivastava, V.S. Photocatalytic Degradation of Hazardous Ponceau-S Dye from Industrial Wastewater Using Nanosized Niobium Pentoxide with Carbon. *Desalination* **2011**, *269*, 276–283. [CrossRef]
174. Souza, R.P.; Freitas, T.K.F.S.; Domingues, F.S.; Pezoti, O.; Ambrosio, E.; Ferrari-Lima, A.M.; Garcia, J.C. Photocatalytic Activity of TiO_2, ZnO and Nb_2O_5 Applied to Degradation of Textile Wastewater. *J. Photochem. Photobiol. A Chem.* **2016**, *329*, 9–17. [CrossRef]
175. Domingues, F.S.; Geraldino, H.C.L.; de Freitas, T.K.F.S.; de Almeida, C.A.; de Figueiredo, F.F.; Garcia, J.C. Photocatalytic Degradation of Real Textile Wastewater Using Carbon Black-Nb $_2$ O $_5$ Composite Catalyst under UV/Vis Irradiation. *Environ. Technol.* **2021**, *42*, 2335–2349. [CrossRef]
176. Hu, C.; Zhang, L.; Cheng, L.; Chen, J.; Hou, W.; Ding, W. A Comparison of H+-Restacked Nanosheets and Nanoscrolls Derived from $K_4Nb_6O_{17}$ for Visible-Light Degradation of Dyes. *J. Energy Chem.* **2014**, *23*, 136–144. [CrossRef]
177. Qaraah, F.A.; Mahyoub, S.A.; Hezam, A.; Qaraah, A.; Drmosh, Q.A.; Xiu, G. Construction of 3D Flowers-like O-Doped g-C_3N_4-[N-Doped Nb_2O_5/C] Heterostructure with Direct S-Scheme Charge Transport and Highly Improved Visible-Light-Driven Photocatalytic Efficiency. *Chin. J. Catal.* **2022**, *43*, 2637–2651. [CrossRef]
178. Ücker, C.L.; Goetzke, V.; Almeida, S.R.; Moreira, E.C.; Ferrer, M.M.; Jardim, P.L.G.; Moreira, M.L.; Raubach, C.W.; Cava, S. Photocatalytic Degradation of Rhodamine B Using Nb2O5 Synthesized with Different Niobium Precursors: Factorial Design of Experiments. *Ceram. Int.* **2021**, *47*, 20570–20578. [CrossRef]

179. Prabhakarrao, N.; Rao, T.S.; Lakshmi, K.V.D.; Divya, G.; Jaishree, G.; Raju, I.M.; Alim, S.A. Enhanced Photocatalytic Performance of Nb Doped TiO_2/Reduced Graphene Oxide Nanocomposites over Rhodamine B Dye under Visible Light Illumination. *Sustain. Environ. Res.* **2021**, *31*, 37. [CrossRef]
180. Zhai, Z.; Huang, Y.; Xu, L.; Yang, X.; Hu, C.; Zhang, L.; Fan, Y.; Hou, W. Thermostable Nitrogen-Doped $HTiNbO_5$ Nanosheets with a High Visible-Light Photocatalytic Activity. *Nano Res.* **2011**, *4*, 635–647. [CrossRef]
181. Oliveira, J.A.; Reis, M.O.; Pires, M.S.; Ruotolo, L.A.M.; Ramalho, T.C.; Oliveira, C.R.; Lacerda, L.C.T.; Nogueira, F.G.E. Zn-Doped Nb_2O_5 Photocatalysts Driven by Visible-Light: An Experimental and Theoretical Study. *Mater. Chem. Phys.* **2019**, *228*, 160–167. [CrossRef]
182. Dai, Q.; Yuan, B.; Guo, M.; Zhang, K.; Chen, X.; Song, Z.; Nguyen, T.T.; Wang, X.; Lin, S.; Fan, J.; et al. A Novel Nano-Fibriform C-Modified Niobium Pentoxide by Using Cellulose Templates with Highly Visible-Light Photocatalytic Performance. *Ceram. Int.* **2020**, *46*, 13210–13218. [CrossRef]
183. Asencios, Y.J.O.; Quijo, M.V.; Marcos, F.C.F.; Nogueira, A.E.; Rocca, R.R.; Assaf, E.M. Photocatalytic Activity of Nb Heterostructure ($NaNbO_3$/$Na_2Nb_4O_{11}$) and Nb/Clay Materials in the Degradation of Organic Compounds. *Sol. Energy* **2019**, *194*, 37–46. [CrossRef]
184. Wang, R.; Zhu, Y.; Qiu, Y.; Leung, C.F.; He, J.; Liu, G.; Lau, T.C. Synthesis of Nitrogen-Doped $KNbO_3$ Nanocubes with High Photocatalytic Activity for Water Splitting and Degradation of Organic Pollutants under Visible Light. *Chem. Eng. J.* **2013**, *226*, 123–130. [CrossRef]
185. Gupta, A.; Mittal, M.; Singh, M.K.; Suib, S.L.; Pandey, O.P. Low Temperature Synthesis of NbC/C Nano-Composites as Visible Light Photoactive Catalyst. *Sci. Rep.* **2018**, *8*, 13597. [CrossRef]
186. Liu, W.; Zhang, W.; Liu, M.S.; Du, P.H.; Dang, C.Y.; Liang, J.L.; Li, Y.Y. Fabrication of Niobium Doped Titanate Nanoflakes with Enhanced Visible-Light-Driven Photocatalytic Activity for Efficient Ibuprofen Degradation. *Chin. Chem. Lett.* **2019**, *30*, 2177–2180. [CrossRef]
187. Lenzi, G.G.; Abreu, E.; Fuziki, M.E.K.; Fidelis, M.Z.; Brackmann, R.; de Tuesta, J.L.D.; Gomes, H.T.; dos Santos, O.A.A. 17 α-Ethinylestradiol Degradation in Continuous Process by Photocatalysis Using Ag/Nb_2O_5 Immobilized in Biopolymer as Catalyst. *Top. Catal.* **2022**, *65*, 1225–1234. [CrossRef]
188. Fernandes, C.H.M.; Goulart, L.A.; Gonçalves, R.; Santos, G.O.S.; Zanoni, M.V.B.; Mascaro, L.H.; Lanza, M.R.V. Effective Photoelectrocatalysis of Levofloxacin Antibiotic with Ti/IrO_2-Nb_2O_5 in Environmental Samples. *Electrochim. Acta* **2024**, *475*, 143586. [CrossRef]
189. Liao, W.N.; Yang, Z.Q.; Wang, Y.; Li, S.; Wang, C.Y.; Zhou, Z.L. Novel Z-Scheme Nb_2O_5/C_3N_5 Photocatalyst for Boosted Degradation of Tetracycline Antibiotics by Visible Light-Assisted Activation of Persulfate System. *Chem. Eng. J.* **2023**, *478*, 147346. [CrossRef]
190. Wang, M.Y.; Wang, H.; Ren, Y.H.; Wang, C.; Weng, Z.W.; Yue, B.; He, H.Y. Construction of G-C_3N_4-MNb_2O_5 Composites with Enhanced Visible Light Photocatalytic Activity. *Nanomaterials* **2018**, *8*, 427. [CrossRef] [PubMed]
191. Xin, C.H.; Wang, B.; Yang, J.N.; Zhao, J.W.; Yu, X.; Tian, Y.J. Construction of ZnS_{1-x} Layers Coated Nb_2O_{5-x} Mesocrystals for Boosted Removal of Organic Contaminant. *Ceram. Int.* **2023**, *49*, 37861–37871. [CrossRef]
192. Hong, Y.Z.; Li, C.S.; Zhang, G.Y.; Meng, Y.D.; Yin, B.X.; Zhao, Y.; Shi, W.D. Efficient and Stable Nb_2O_5 Modified g-C_3N_4 Photocatalyst for Removal of Antibiotic Pollutant. *Chem. Eng. J.* **2016**, *299*, 74–84. [CrossRef]
193. Wu, J.Z.; Li, W.; Guan, S.Y.; Chen, X.H.; Gao, H.Y.; Liu, X.L. Study on the Performance of Vanadium Doped $NaNbO_3$ Photocatalyst Degradation Antibiotics. *Inorg. Chem. Commun.* **2021**, *131*, 108669. [CrossRef]
194. Heberle, A.N.A.; García-Gabaldón, M.; Ortega, E.M.; Bernardes, A.M.; Pérez-Herranz, V. Study of the Atenolol Degradation Using a Nb/BDD Electrode in a Filter-Press Reactor. *Chemosphere* **2019**, *236*, 124318. [CrossRef]
195. Tong, Q.Q.; Qiu, C.T.; Zheng, G.J.; Zhu, Q.Q.; Zhou, S.M.; Wang, Y.K.; Shi, L.; Wang, H.F.; He, D.B.; Sadakane, M.; et al. Higher Acidity Promoted Photodegradation of Fluoroquinolone Antibiotics under Visible Light by Strong Interaction with a Niobium Oxide Based Zeolitic Octahedral Metal Oxide. *Appl. Catal. A Gen.* **2023**, *662*, 119284. [CrossRef]
196. Valim, R.B.; Carneiro, J.F.; Lourenço, J.C.; Hammer, P.; dos Santos, M.C.; Rodrigues, L.A.; Bertazzoli, R.; Lanza, M.; Rocha, R.D. Synthesis of Nb_2O_5/C for H_2O_2 Electrogeneration and Its Application for the Degradation of Levofloxacin. *J. Appl. Electrochem.* **2024**, *54*, 581–595. [CrossRef]
197. Rameel, M.I.; Wali, M.; Al-Humaidi, J.Y.; Liaqat, F.; Khan, M.A. Enhanced Photocatalytic Degradation of Levofloxacin over Heterostructured C_3N_4/Nb_2O_5 System under Visible Light. *Heliyon* **2023**, *9*, e20479. [CrossRef] [PubMed]
198. de Jesus, E.T.; Moreira, A.J.; Sa, M.C.; Freschi, G.P.G.; Joya, M.R.; Li, M.S.; Paris, E.C. Potential of Nb_2O_5 Nanofibers in Photocatalytic Degradation of Organic Pollutants. *Environ. Sci. Pollut. Res.* **2021**, *28*, 69401–69415. [CrossRef] [PubMed]
199. Fuziki, M.E.K.; Abreu, E.; Napoli, J.S.; Nunes, S.C.; Brackmann, R.; Machado, T.C.S.; Semianko, B.C.; Lenzi, G.G. Cu/Nb_2O_5, Fe/Nb_2O_5 and Cu-Fe/Nb_2O_5 Applied in Salicylic Acid Degradation: Parameters Studies and Photocatalytic Activity. *J. Environ. Sci. HEALTH PART A-TOXIC/Hazard. Subst. Environ. Eng.* **2022**, *57*, 797–812. [CrossRef]

200. Orsetti, F.R.; Bukman, L.; Santos, J.S.; Nagay, B.E.; Rangel, E.C.; Cruz, N.C. Methylene Blue and Metformin Photocatalytic Activity of CeO_2-Nb_2O_5 Coatings Is Dependent on the Treatment Time of Plasma Electrolytic Oxidation on Titanium. *Appl. Surf. Sci. Adv.* **2021**, *6*, 100143. [CrossRef]
201. Welter, J.B.; da Silva, S.W.; Schneider, D.E.; Rodrigues, M.A.S.; Ferreira, J.Z. Performance of Nb/BDD Material for the Electrochemical Advanced Oxidation of Prednisone in Different Water Matrix. *Chemosphere* **2020**, *248*, 126062. [CrossRef]
202. Wen, Z.J.; Ren, S.Y.; Zhang, Y.Y.; Li, J.Y.; Zhang, Z.G.; Wang, A.M. Performance of Anode Materials in Electro-Fenton Oxidation of Cefoperazone in Chloride Medium: New Insight into Simultaneous Mineralization and Toxic Byproducts Formation. *J. Clean. Prod.* **2022**, *377*, 134225. [CrossRef]
203. Zhang, Y.F.; Gao, J.L.; Chen, S.G.; Li, L.; Xu, J.H.; Li, D.; Liu, Y.F.; Quan, X.; Fu, X.; Xie, Y.Z.; et al. Advanced Electrooxidation of Florfenicol Using 3D Printed Nb_2O_5/Ti Electrodes: Degradation Efficiency, Dehalogenation Performance, and Toxicity Reduction. *Chem. Eng. J.* **2023**, *474*, 145561. [CrossRef]
204. Ali, H.; Khan, E.; Ilahi, I. Environmental Chemistry and Ecotoxicology of Hazardous Heavy Metals: Environmental Persistence, Toxicity, and Bioaccumulation. *J. Chem.* **2019**, *2019*, 6730305. [CrossRef]
205. Velarde, L.; Nabavi, M.S.; Escalera, E.; Antti, M.-L.; Akhtar, F. Adsorption of Heavy Metals on Natural Zeolites: A Review. *Chemosphere* **2023**, *328*, 138508. [CrossRef] [PubMed]
206. Selvi, M.; Balasubramaniyan, S.; Jagatheesan, R. Sphere-like Nb_2O_5 Nanoparticles by Waste Brassica Oleracea Leaf Extract for Lead Removal and Photocatalytic Degradation of Methylene Blue Dye. *J. Indian. Chem. Soc.* **2024**, *101*, 101377. [CrossRef]
207. de Sousa, C.M.; Cardoso, V.L.; Batista, F.R.X. A Coupled Photocatalytic System Using Niobium Oxide and Microalga: Cr (VI)-Contaminated Wastewater Treatment. *J. Photochem. Photobiol. A Chem.* **2023**, *439*, 114602. [CrossRef]
208. Li, Z.; Sun, D.; Yang, F.; Zhao, J.; Wu, X.; Zhao, S. Efficient Removal of Hg0 by Regulating the Bonding Degree between Cuo and Carrier Nb_2O_5. *SSRN Electron. J.* **2022**, *332*, 125796. [CrossRef]
209. Honghu, L.; Jiangjun, H.; He, W. Catalytic Oxidation Removal of Gaseous Elemental Mercury in Flue Gas over Niobium-loaded Catalyst. *Can. J. Chem. Eng.* **2016**, *94*, 1486–1494. [CrossRef]
210. Agrafioti, K.A.; Panagiotopoulos, N.T.; Moularas, C.; Deligiannakis, Y.; Prouskas, C.; Soukouli, P.P.; Evangelakis, G.A. Development of Ti-Based Nanocomposite Oxide Thin Films with CuO and Nb_2O_5 Additions Suitable for Catalytic Applications. *Thin Solid. Film.* **2023**, *775*, 139864. [CrossRef]
211. Wang, T.N.; Wang, J.S.; Wu, J.S.; Du, Y.C.; Li, Y.L.; Li, H.Y.; Yang, Y.L.; Jia, X.J. Visible-Light Responsive Cr(VI) Reduction by Carbonyl Modification $Nb_3O_7(OH)$ Nanoaggregates. *J. Mater. Sci.* **2018**, *53*, 12065–12078. [CrossRef]
212. de Moraes, N.P.; de Siervo, A.; Campos, T.M.; Thim, G.P.; Rodrigues, L.A. Structure-Directing Ability of the Kraft-Lignin/Cellulose Carbon Xerogel for the Development of C-Nb_2O_5 Sunlight-Active Photocatalysts. *J. Photochem. Photobiol. A Chem.* **2023**, *441*, 114697. [CrossRef]
213. Yang, J.; Hao, J.Y.; Xu, S.Y.; Dai, J.; Wang, Y.; Pang, X.C. Visible-Light-Driven Photocatalytic Degradation of 4-CP and the Synergistic Reduction of Cr(VI) on One-Pot Synthesized Amorphous Nb_2O_5 Nanorods/Graphene Heterostructured Composites. *Chem. Eng. J.* **2018**, *353*, 100–114. [CrossRef]
214. Kumar, K.Y.; Prashanth, M.K.; Shanavaz, H.; Parashuram, L.; Alharti, F.A.; Jeon, B.H.; Raghu, M.S. Green and Facile Synthesis of Strontium Doped Nb_2O_5/RGO Photocatalyst: Efficacy towards H_2 Evolution, Benzophenone-3 Degradation and Cr (VI) Reduction. *Catal. Commun.* **2023**, *173*, 106560. [CrossRef]
215. Alias, N.; Hussain, Z.; Tan, W.K.; Kawamura, G.; Muto, H.; Matsuda, A.; Lockman, Z. Photoreduction of Cr(VI) in Wastewater by Anodic Nanoporous Nb_2O_5 Formed at High Anodizing Voltage and Electrolyte Temperature. *Environ. Sci. Pollut. Res.* **2022**, *29*, 60600–60615. [CrossRef]
216. Josué, T.G.; Almeida, L.N.B.; Lopes, M.F.; Santos, O.A.A.; Lenzi, G.G. Cr (VI) Reduction by Photocatalyic Process: Nb_2O_5 an Alternative Catalyst. *J. Environ. Manag.* **2020**, *268*, 110711. [CrossRef]
217. Yang, X.P.; Zou, R.Y.; Huo, F.; Cai, D.C.; Xiao, D. Preparation and Characterization of Ti/SnO_2-Sb_2O_3-Nb_2O_5/PbO_2 Thin Film as Electrode Material for the Degradation of Phenol. *J. Hazard. Mater.* **2009**, *164*, 367–373. [CrossRef]
218. Bolujoko, N.B.; Unuabonah, E.I.; Alfred, M.O.; Ogunlaja, A.; Ogunlaja, O.O.; Omorogie, M.O.; Olukanni, O.D. Toxicity and Removal of Parabens from Water: A Critical Review. *Sci. Total Environ.* **2021**, *792*, 148092. [CrossRef]
219. Mukherjee, S.; Das, A.; Chowdhury, A.; Biswas, A.; Roy, S.; Majumdar, S.; Paul, S. Harmful Effect of Personal Care Products on Ecosystem and the Possible Alternative Approach. *Biocatal. Agric. Biotechnol.* **2024**, *57*, 103065. [CrossRef]
220. Osuoha, J.O.; Anyanwu, B.O.; Ejileugha, C. Pharmaceuticals and Personal Care Products as Emerging Contaminants: Need for Combined Treatment Strategy. *J. Hazard. Mater. Adv.* **2023**, *9*, 100206. [CrossRef]
221. Ren, Y.Z.; Franke, M.; Anschuetz, F.; Ondruschka, B.; Ignaszak, A.; Braeutigam, P. Sonoelectrochemical Degradation of Triclosan in Water. *Ultrason. Sonochem* **2014**, *21*, 2020–2025. [CrossRef]
222. Silva, L.M.; Silva, L.R.; Motheo, A.J. Using Niobium/BDD Anode-Based Multi-Cell Flow Reactor for the Electrochemical Oxidation of Methyl Paraben in the Presence of Surfactants. *J. Water Process Eng.* **2021**, *44*, 102439. [CrossRef]

223. Fuziki, M.E.K.; Ribas, L.S.; Abreu, E.; Fernandes, L.; dos Santos, O.A.A.; Brackmann, R.; de Tuesta, J.L.D.; Tusset, A.M.; Lenzi, G.G. N-Doped TiO_2-Nb_2O_5 Sol–Gel Catalysts: Synthesis, Characterization, Adsorption Capacity, Photocatalytic and Antioxidant Activity. *Catalysts* **2023**, *13*, 1233. [CrossRef]
224. Zhang, J.; Li, D.D.; Qiu, J.P.; Wen, Z.R.; Luo, X.H.; Bian, C.Q.; Chen, J.; Luo, M.F. Insights into the Photocatalytic Degradation of Triclosan over Amorphous Nb_2O_5 Catalysts. *Mater. Res. Express* **2020**, *7*, 112502. [CrossRef]
225. Castro, D.C.; Cavalcante, R.P.; Jorge, J.; Martines, M.A.U.; Oliveira, L.C.S.; Casagrande, G.A.; Machulek, A. Synthesis and Characterization of Mesoporous Nb_2O_5 and Its Application for Photocatalytic Degradation of the Herbicide Methylviologen. *J. Braz. Chem. Soc.* **2016**, *27*, 303–313. [CrossRef]
226. Paris, E.C.; Malafatti, J.O.D.; Sciena, C.R.; Neves Junior, L.F.; Zenatti, A.; Escote, M.T.; Moreira, A.J.; Freschi, G.P.G. Nb_2O_5 Nanoparticles Decorated with Magnetic Ferrites for Wastewater Photocatalytic Remediation. *Environ. Sci. Pollut. Res.* **2021**, *28*, 23731–23741. [CrossRef] [PubMed]
227. Costa, K.G.; Asencios, Y.J.O. Development of a Solid Catalyst Based on Pt Supported on Heterostructure ($NaNbO_3$/$NaNb_3O_8$/NiO) Applied to the Photodegradation of Phenol in Seawater. *Catalysts* **2022**, *12*, 1565. [CrossRef]
228. Zakaria, W.F.W.; Jalil, A.A.; Hassan, N.S.; Ibrahim, M.; Azami, M.S. Visible-Light Driven Photodegradation of Phenol over Niobium Oxide-Loaded Fibrous Silica Titania Composite Catalyst. *J. Chem. Technol. Biotechnol.* **2020**, *95*, 2638–2647. [CrossRef]
229. Ma, J.; Qin, G.T.; Wei, W.; Xiao, T.L.; Liu, S.M.; Jiang, L. Anti-Corrosion Porous RuO_2/NbC Anodes for the Electrochemical Oxidation of Phenol. *RSC Adv.* **2019**, *9*, 17373–17381. [CrossRef]
230. Karunakaran, C.; Dhanalakshmi, R.; Gomathisankar, P. Phenol-Photodegradation on ZrO_2. Enhancement by Semiconductors. *Spectrochim. ACTA PART A Mol. Biomol. Spectrosc.* **2012**, *92*, 201–206. [CrossRef]
231. Lam, S.M.; Sin, J.C.; Satoshi, I.; Abdullah, A.Z.; Mohamed, A.R. Enhanced Sunlight Photocatalytic Performance over Nb_2O_5/ZnO Nanorod Composites and the Mechanism Study. *Appl. Catal. A Gen.* **2014**, *471*, 126–135. [CrossRef]
232. Bai, J.; Huang, Y.L.; Wei, D.; Fan, Z.; Seo, H.J. Synthesis and Characterization of Semiconductor Heterojunctions Based on $Zr_6Nb_2O_{17}$ Nanoparticles. *Mater. Sci. Semicond. Process* **2020**, *112*, 105010. [CrossRef]
233. Lam, S.M.; Sin, J.C.; Mohamed, A.R. Fabrication of ZnO Nanorods via a Green Hydrothermal Method and Their Light Driven Catalytic Activity towards the Erasure of Phenol Compounds. *Mater. Lett.* **2016**, *167*, 141–144. [CrossRef]
234. Ma, J.; Wei, W.; Qin, G.T.; Jiang, L.; Wong, N.H.; Sunarso, J.; Liu, S.M. Electrochemical Oxidation of Phenol in a PtRu/NbC Membrane-Based Catalytic Nanoreactor. *J. Environ. Chem. Eng.* **2023**, *11*, 111128. [CrossRef]
235. Gargouri, O.D.; Samet, Y.; Abdelhedi, R. Electrocatalytic Performance of PbO_2 Films in the Degradation of Dimethoate Insecticide. *Water SA* **2013**, *39*, 31–37. [CrossRef]
236. Reddy, G.R.; Balasubramanian, S.; Chennakesavulu, K. Zeolite Encapsulated Active Metal Composites and Their Photocatalytic Studies for Rhodamine-B, Reactive Red-198 and Chloro-Phenols. *RSC Adv.* **2015**, *5*, 81013–81023. [CrossRef]
237. Tsai, S.J.; Cheng, S.F. Physico-Chemical Properties of Nb/Ti Binary Oxides and Their Photo-Catalytic Activities. *J. Chin. Chem. Soc.* **2001**, *48*, 1009–1016. [CrossRef]
238. Zhang, D.F.; Meng, X.; Meng, Y.; Pu, X.P.; Ge, B.; Li, W.Z.; Dou, J.M. One-Pot Molten Salt Synthesis of $CdNb_2O_6$/$Cd_2Nb_2O_7$ Heterojunction Photocatalysts with Enhanced Photocatalytic Properties. *Sep. Purif. Technol.* **2017**, *186*, 282–289. [CrossRef]
239. Grzegorzek, M.; Wartalska, K.; Kowalik, R. Occurrence and Sources of Hormones in Water Resources—Environmental and Health Impact. *Environ. Sci. Pollut. Res.* **2024**, *31*, 37907–37922. [CrossRef]
240. Brocenschi, R.F.; Rocha-Filho, R.C.; Bocchi, N.; Biaggio, S.R. Electrochemical Degradation of Estrone Using a Boron-Doped Diamond Anode in a Filter-Press Reactor. *Electrochim. Acta* **2016**, *197*, 186–193. [CrossRef]
241. Nippes, R.P.; Gomes, A.D.; Macruz, P.D.; de Souza, M. Photocatalytic Removal of 17β-Estradiol from Water Using a Novel Bimetallic NiCu/Nb_2O_5 Catalyst. *Environ. Sci. Pollut. Res.* **2023**, *30*, 103731–103742. [CrossRef] [PubMed]
242. Leal, G.F.; Barrett, D.H.; Carrer, H.; Figueroa, S.J.A.; Teixeira-Neto, E.; Curvelo, A.A.S.; Rodella, C.B. Morphological, Structural, and Chemical Properties of Thermally Stable Ni-Nb_2O_5 for Catalytic Applications. *J. Phys. Chem. C* **2019**, *123*, 3130–3143. [CrossRef]
243. Ko, J.S.; Le, N.Q.; Schlesinger, D.R.; Johnson, J.K.; Xia, Z. Novel Niobium-Doped Titanium Oxide Towards Electrochemical Destruction of Forever Chemicals. *Sci. Rep.* **2021**, *11*, 18020. [CrossRef] [PubMed]
244. Troncoso, F.D.; Tonetto, G.M. Nb_2O_5 Monolith as an Efficient and Reusable Catalyst for Textile Wastewater Treatment. *Sustain. Environ. Res.* **2021**, *31*, 35. [CrossRef]